

# Plasticity and dynamics of central synapses in mouse ES cell-derived neurons and cortical neurons

Inaugural-Dissertation

zur

Erlangung des Doktorgrades der  
Mathematisch-Naturwissenschaftlichen Fakultät  
der Heinrich-Heine-Universität Düsseldorf

vorgelegt von

Adriana Stan

aus Bukarest

Oktober 2008

Aus dem Institut für Neuro- und Sinnesphysiologie  
der Heinrich-Heine-Universität Düsseldorf

Gedruckt mit der Genehmigung der  
Mathematisch-Naturwissenschaftlichen Fakultät der  
Heinrich-Heine-Universität Düsseldorf

Referent: Prof. Dr. K. Gottmann

Koreferent: Prof. Dr. C. Rose

Tag der mündlichen Prüfung:

## Abstract

During brain development, formation and functional maturation of synapses between neurons are highly coordinated processes that ensure the correct wiring and functioning of neuronal networks. The accumulation of neurotransmitter-filled vesicles at presynaptic release sites is a decisive step in the formation and early functional maturation of central glutamatergic synapses. Trans-synaptic signaling through cell adhesion molecules has been proposed to regulate vesicle clustering at active zones, however, the underlying molecular mechanisms are incompletely understood.

In this study, the role of the cell adhesion molecule N-cadherin in synapse formation and maturation was addressed. Specific deletion of the N-cadherin gene in mice leads to early embryonic lethality around day 10 of gestation before the brain forms. To circumvent this problem, N-cadherin deficient neurons were obtained by *in vitro* differentiation from mouse embryonic stem (ES) cells genetically null for N-cadherin. ES cell-derived neurons were grown in a glial microisland culture system, in which the fraction of autapses is very high as confirmed by labeling pre- and postsynaptic specializations of glutamatergic synapses. Using a live imaging approach, it was shown that the recruitment of fluorescently labeled (by expression of DsRed2-VAMP2) presynaptic vesicles at nascent synapses is strongly impaired in the absence of N-cadherin. This in addition led to a lower density of presynaptic vesicle clusters in immature neurons. However, the density of active zones, as visualized by EGFP-Bassoon, was not affected in N-cadherin deficient neurons indicating that N-cadherin is specifically involved in the recruitment of vesicles to synaptic sites. To study vesicle accumulation in a more quantitative manner, fluorescence recovery after photobleaching (FRAP) was used, demonstrating that the recruitment of synaptic vesicles at individual synaptic sites is much slower in immature N-cadherin deficient neurons as compared to controls. Furthermore, time lapse studies indicated that the general dynamics of synaptic vesicle clusters is increased in the absence of N-cadherin, which might destabilize synapses. Together, these findings demonstrate that N-cadherin plays an important role in the formation and stabilization of vesicle pools at nascent synaptic sites. At more mature synapses, the role of N-cadherin became less significant, as at a morphological level presynaptic specializations (density

of presynaptic vesicles clusters and active zones) in N-cadherin deficient neurons were similar to control neurons. At this later maturational stage, accumulation of synaptic vesicles at synapses has largely ceased and appears to be no more an N-cadherin dependent process, indicating that other cell adhesion molecules may compensate for the loss of N-cadherin.

To study the molecular mechanisms that N-cadherin uses for regulating the accumulation of synaptic vesicles at nascent synaptic sites, synapse formation was induced in immature neurons by expression of neuroligin1. Neuroligin1 is a postsynaptic transmembrane protein well known for its ability to trigger *de novo* accumulation of presynaptic vesicles when overexpressed in neurons. Intriguingly, neuroligin's vesicle cluster-inducing effect was blocked in the absence of N-cadherin. In addition, N-cadherin was found to influence clustering and proper synaptic localization of neuroligin1. These studies suggested that there is a cooperative interaction between two cell adhesion systems: the N-cadherin/ $\beta$ -catenin and the neuroligin/neurexin system in trans-synaptically regulating the accumulation of vesicles. To gain further insight into the molecular mechanism underlying this functional cooperation, the postsynaptic scaffolding protein S-SCAM was chosen as a candidate linker protein. Previously, it was shown that S-SCAM, a multi-PDZ domain containing protein, can bind to neuroligin1 via its 1<sup>st</sup> PDZ domain and to  $\beta$ -catenin via its 5<sup>th</sup> PDZ domain. To test if S-SCAM could provide the molecular link between the N-cadherin/ $\beta$ -catenin and the neuroligin/neurexin adhesion systems, mutant S-SCAM constructs with either the PDZ1 domain or the PDZ5 domain deleted were expressed in cortical neurons and neuroligin's function was assessed. As expected, upon overexpression of mutated S-SCAMs the functional interaction between N-cadherin and neuroligin1 was impaired and the formation of presynaptic vesicle clusters under neuroligin1 overexpression was blocked. Similarly, clustering of neuroligin1 and its synaptic localization were impaired, indicating that S-SCAM provides a molecular link between the two cell adhesion systems. In summary, the present study provides first evidence for a novel mechanism for coupling bidirectional synapse maturation mediated by neuroligins/neurexins to cell type recognition processes mediated by classical cadherins.

## **Zusammenfassung**

Die Bildung und die funktionelle Ausreifung von neuronalen Synapsen sind hochkomplexe Prozesse, die die korrekte Verschaltung und Funktionsweise neuronaler Netzwerke im Verlauf der Entwicklung des Gehirns sicherstellen. Die Akkumulation von Neurotransmitter-haltigen Vesikeln an präsynaptischen Freisetzungstellen ist dabei ein entscheidender Schritt in der Bildung und frühen funktionellen Reifung zentraler glutamaterger Synapsen. Die Regulation der Vesikelakkumulation an aktiven Zonen erfolgt vermutlich durch transsynaptische Signalleitung über Zelladhäsionsmoleküle. Allerdings sind die zugrundeliegenden molekularen Mechanismen noch unvollständig bekannt.

In der vorliegenden Arbeit wurde die Rolle des Zelladhäsionsmoleküls N-Cadherin in der Synapsenbildung und –ausreifung untersucht. Die selektive Deletion des N-Cadheringens in Mäusen führt um den 10. Tag der Schwangerschaft, noch bevor das Gehirn ausgebildet ist, zu einer früh embryonalen Lethalität. Um dieses Problem zu umgehen, wurden N-Cadherin defiziente Neurone *in vitro* aus gentechnisch veränderten embryonalen Stammzellen (ES Zellen) der Maus, die kein intaktes N-Cadherin mehr besitzen („knockout“), differenziert. Diese neuronal differenzierten ES Zellen wurden in einem glialen „Insel“-Kultursystem, das die Ausbildung eines hohen Anteils von Autapsen ermöglicht, kultiviert. Dies konnte durch Darstellung der prä- und postsynaptischen Spezialisierungen bestätigt werden. Mit Hilfe von „live-cell imaging“ an gerade entstehenden Synapsen konnte weiter gezeigt werden, dass die Rekrutierung Fluoreszenz-markierter synaptischer Vesikel (durch Expression von DsRed2-VAMP2) in der Abwesenheit von N-Cadherin stark gestört ist. Dies führte in unreifen Neuronen zusätzlich zu einer verringerten Dichte präsynaptischer Vesikelcluster. Die Dichte der aktiven Zonen, die mittels EGFP-Bassoon dargestellt wurden, war jedoch in N-Cadherin defizienten Neuronen nicht verändert. Dies deutet darauf hin, dass N-Cadherin spezifisch an der Rekrutierung von Vesikeln an die Präsynapsen beteiligt ist. Um die Vesikelakkumulation quantitativ zu untersuchen, wurden „fluorescence recovery after photobleaching (FRAP)“ Experimente durchgeführt. Es zeigte sich, dass die Rekrutierung von synaptischen Vesikeln an einzelne Präsynapsen in N-Cadherin

defizienten Neuronen deutlich langsamer erfolgt als in Kontrollneuronen. Darüber hinaus ergaben Zeitrafferstudien, dass die allgemeine Mobilität der synaptischen Vesikelcluster in Abwesenheit von N-Cadherin erhöht ist. Dies könnte zu einer Destabilisierung von Synapsen führen. Zusammenfassend zeigen diese Ergebnisse, dass N-Cadherin eine wichtige Rolle bei der Ausbildung und Stabilisierung des Vesikelpools an entstehenden Synapsen zukommt. An weiter ausgereiften Synapsen scheint N-Cadherin eine weniger wichtige Rolle zu spielen, da in solchen Synapsen die präsynaptischen Spezialisierungen (Dichte der präsynaptischen Vesikelcluster und aktiven Zonen) morphologisch relativ zu Kontrollneuronen nicht unterschiedlich waren. In späteren Reifungsstadien war die Akkumulation synaptischer Vesikel weitgehend abgeschlossen und nicht mehr von N-Cadherin abhängig. Dies deutet darauf hin, dass andere Zelladhäsionsmoleküle den Verlust von N-Cadherin kompensieren können.

Um die molekularen Mechanismen, die der Regulation der Akkumulation synaptischer Vesikel an entstehenden Synapsen durch N-Cadherin zugrundeliegen, zu untersuchen, wurde Synapsenneubildung in unreifen Neuronen durch Expression von Neuroligin1 induziert. Neuroligin1 ist ein postsynaptisches Membranprotein, das die *de novo* Akkumulation präsynaptischer Vesikel nach Überexpression in Neuronen auslösen kann. Interessanterweise war der Vesikelcluster induzierende Effekt von Neuroligin1 in der Abwesenheit von N-Cadherin blockiert. Zusätzlich zeigte sich, dass N-Cadherin die Akkumulation und synaptische Lokalisation von Neuroligin1 beeinflusst. Diese Ergebnisse legten eine kooperative Interaktion zwischen zwei Zelladhäsionssystemen, dem N-Cadherin/ $\beta$ -catenin und dem Neuroligin/Neurexin System, in der transsynaptischen Regulation der Vesikelakkumulation nahe. Um den molekularen Mechanismus dieser funktionellen Kooperation näher zu untersuchen, wurde analysiert, ob das postsynaptische „Gerüstprotein“ S-SCAM als Verbindungsprotein („linker“) fungiert. S-SCAM ist ein Protein, das mehrere PDZ Domänen enthält und an Neuroligin1 über seine erste PDZ Domäne und weiter an  $\beta$ -catenin über seine 5. PDZ Domäne bindet. Um zu überprüfen, ob S-SCAM einen molekularen „linker“ zwischen dem N-Cadherin/ $\beta$ -catenin und dem Neuroligin/Neurexin System darstellt, wurden mutierte S-SCAM Konstrukte, die entweder eine Deletion der 1. oder der 5. PDZ Domäne aufwiesen, in kortikalen Neuronen exprimiert und es wurde der Effekt einer Neuroligin1

Überexpression analysiert. Die Expression mutierter S-SCAM Proteine führte zu einer Inhibition der funktionellen Interaktion zwischen N-Cadherin und Neuroligin1, was sich in einer Blockade der Induktion von präsynaptischen Vesikelclustern durch Neuroligin1 äusserte. Ebenso war die Akkumulation von Neuroligin1 und seine synaptische Lokalisation reduziert, was dafür spricht, dass S-SCAM eine molekulare Verbindung zwischen den beiden Adhäsionssystemen ermöglicht. Zusammenfassend konnten in der vorliegenden Arbeit erste Evidenzen für einen noch unbeschriebenen Mechanismus der Kopplung von bidirektionalen synaptischen Reifungsprozessen, die durch Neuroligine/Neurexine vermittelt sind, und Zellerkennungsprozessen, die durch klassische Cadherine vermittelt sind, erbracht werden.

# Contents

## 1. Introduction

1.1.	Organization of glutamatergic synapses .....	5
1.1.1.	Organization of presynaptic specializations .....	6
1.1.2.	Organization of postsynaptic densities .....	7
1.2	Glutamatergic synapse formation during brain development .....	8
1.2.1.	Recruitment of presynaptic proteins .....	8
1.2.2.	Recruitment of postsynaptic proteins .....	10
1.2.3.	Standard model of the stepwise assembly of glutamatergic synapses .....	10
1.3.	Synaptic cell adhesion molecules .....	13
1.3.1.	N-cadherin/ $\beta$ -catenin cell adhesion system .....	14
1.3.2.	Neurologin/neurexin cell adhesion system .....	17
1.4.	PDZ domain-containing proteins .....	20
1.4.1.	Synaptic scaffolding molecules of the MAGI family (S-SCAMs) .....	20
1.5.	Aims of the study.....	21

## 2. Materials and methods .....

23

2.1.	Solutions and Chemicals .....	23
2.1.1.	Chemicals .....	23
2.1.2.	Cell culture media .....	23
2.1.3.	Media for growing bacteria .....	24
2.2.	Plasmids .....	25
2.3.	Generation of mutant S-SCAM constructs .....	26
2.3.1.	Transformation of bacteria with pDEST53-MAGI2 full vector .....	26
2.3.2.	Plasmid isolation from 3 ml cultures (Minipreps) .....	26
2.3.3.	Plasmid isolation from 500ml cultures (Maxipreps) .....	27
2.3.4.	Primer design .....	27



2.3.5.	Polymerase chain reaction (PCR) .....	30
2.3.6.	DNA gel electrophoresis .....	30
2.3.7.	Digestion of PCR fragments and the pcDNA3 vector to get sticky ends .....	31
2.3.8.	Dephosphorylation of plasmid DNA .....	31
2.3.9.	Ligation of DNA fragments .....	31
2.3.10.	DNA sequencing .....	33
2.3.11.	Determination of DNA concentrations .....	33
2.4.	Proliferation and differentiation of mouse ES-cells .....	33
2.4.1.	Generation of mouse N-cadherin deficient ES cell lines .....	33
2.4.2.	Preparation and culturing of embryonic mouse fibroblasts (feeder cells) .....	35
2.4.3.	Proliferation of mouse ES cells .....	36
2.4.4.	In vitro differentiation of mouse ES cells .....	36
2.5.	L1-immunoisolation and glial microisland culture .....	37
2.5.1.	Purification of neurons by L1-immunoisolation .....	37
2.5.2.	Culture of ES cell-derived neurons on glial microislands .....	38
2.6.	Transfection of ES cell-derived neurons and cortical neurons .....	40
2.7.	Time lapse imaging of living cells .....	40
2.8.	Fluorescence Recovery After Photobleaching (FRAP) .....	42
2.9.	Digital image processing .....	43
2.9.1.	Deconvolution .....	43
2.9.2.	Maximum operation in MetaMorph .....	45
2.9.3.	Autothreshold operation in MetaMorph .....	45
2.9.4.	Low pass filter operation .....	46
2.9.5.	Integrated morphometry analysis .....	47
2.9.6.	Background subtraction .....	47
2.9.7.	Colocalization of clusters .....	47
2.10.	Data analysis and statistics .....	47

<b>3. Results</b>	<b>48</b>
3.1. Role of N-cadherin in the formation of presynaptic specializations in immature neurons	48
3.1.1. Co-transfection of individual ES cell-derived neurons	48
3.1.2. Role of N-cadherin in the accumulation of presynaptic vesicles at nascent synapses	50
3.1.2.1. Digital image processing of the DsRed2-VAMP2 signal	50
3.1.2.2. Analysis of the density of presynaptic vesicle clusters in immature neurons	52
3.1.2.3. Quantitative analysis of fluorescence intensity of DsRed2-labeled presynaptic vesicle clusters in immature neurons	53
3.1.2.4. Time lapse analysis of presynaptic vesicle accumulation at immature synapses	55
3.1.2.5. FRAP (fluorescence recovery after photobleaching) analysis of mobility and accumulation of presynaptic vesicles at immature synapses	57
3.1.2.6. Analysis of the dynamics of presynaptic vesicle clusters in immature neurons	59
3.1.3. Role of N-cadherin in the formation of active zones in immature neurons	61
3.1.3.1. Digital image processing of the EGFP-Bassoon signal	62
3.1.3.2. Analysis of the density of Bassoon clusters in immature neurons	63
3.1.3.3. Quantitative analysis of the fluorescence intensity of EGFP-Bassoon labeled active zones in immature neurons	64

3.2.	Role of N-cadherin in late phase maturation and maintenance of presynaptic specializations .....	66
3.2.1.	Role of N-cadherin in the accumulation of presynaptic vesicles at mature synapses .....	66
3.2.1.1.	Analysis of the density of presynaptic vesicle clusters in mature neurons .....	66
3.2.1.2.	Quantitative analysis of the fluorescence intensity of DsRed2-labeled presynaptic vesicle clusters in mature neurons .....	68
3.2.1.3.	Time lapse analysis of the accumulation of presynaptic vesicles at mature synapses .....	69
3.2.1.4.	Analysis of the dynamics of presynaptic vesicle clusters in mature neurons .....	70
3.2.2.	Role of N-cadherin in maintenance of active zones at mature synapses .....	72
3.2.2.1.	Analysis of the density of Bassoon clusters in mature neurons .....	72
3.2.2.2.	Quantitative analysis of the fluorescence intensity of EGFP-Bassoon labeled active zones in mature neurons .....	74
3.3.	Co-localization of presynaptic specializations with the postsynaptic marker protein PSD-95 in cultured ES-cell derived neurons .....	75
3.3.1.	Digital image processing of the PSD95-EGFP signal .....	75
3.3.2.	Analysis of colocalization between presynaptic vesicles and postsynaptic PSD-95 in N-cadherin deficient neurons .....	77
3.3.3.	Analysis of fluorescence intensity and area of PSD95-EGFP postsynaptic specializations .....	79

3.4.	Essential cooperation of N-cadherin and neuroligin1 during synapse formation in immature neurons .....	80
3.4.1.	Comparison of N-cadherin and neuroligin function in inducing presynaptic vesicle accumulation .....	80
3.4.2.	Vesicle-clustering activity of neuroligin1 requires N-cadherin expression .....	84
3.4.3.	Role of N-cadherin in synaptic localization of neuroligin1 .....	86
3.4.3.1.	Digital image processing of neuroligin1-EGFP clusters .....	86
3.4.3.2.	Analysis of the density and colocalization of postsynaptic neuroligin accumulations with presynaptic vesicles clusters .....	88
3.4.4.	Role of the postsynaptic scaffolding molecule S-SCAM in mediating the interaction of N-cadherin and neuroligin1 .....	89
3.4.5.	Role of S-SCAM in synaptic localization of neuroligin1 .....	92
3.4.6.	Role of N-cadherin and neuroligin1 in filopodia formation .....	94
<b>4.</b>	<b>Discussion .....</b>	<b>96</b>
4.1.	Characterization of presynaptic specializations of ES-cell derived neurons grown in glial microisland cultures .....	97
4.2.	Role of N-cadherin in the formation of presynaptic specializations in immature neurons .....	98
4.3.	Role of N-cadherin in maturation and maintenance of presynaptic specializations .....	101
4.4.	Cooperation of N-cadherin and neuroligin1 during synapse formation in immature neurons .....	102
4.5.	Role of N-cadherin in postsynaptic maturation: filopodia and spine formation, AMPA receptor regulation and LTP .....	111

<b>5. References .....</b>	<b>114</b>
<b>6. Appendix .....</b>	<b>126</b>
6.1. Abbreviations .....	126
6.2. List of figures .....	127
6.3. Curriculum vitae .....	131
6.4. Publications and conferences attended.....	131
<b>7. Acknowledgements .....</b>	<b>133</b>

## 1. Introduction

Synapses are highly organized connections between neurons, specialized for transfer of information from one neuron to another. The human brain has  $10^{11}$  neurons interconnected into functional networks through  $10^{14}$  synapses. In order to function properly, network formation during brain development is a tightly controlled process. During the initial wiring period, the number, location and function of synapses are established according to predetermined, largely genetically encoded algorithms that allow precise connectivity. In recent years, special interest was attributed to cell adhesion molecules for trans-synaptically regulating various aspects of synapse differentiation in the central nervous system. It has been hypothesized that the functional cooperation between different adhesion systems is required for proper formation and functioning of the nervous system.

### 1.1. Organization of glutamatergic synapses

Excitatory synapses are asymmetric junctions composed of a presynaptic terminal and a postsynaptic density (PSD). The presynaptic bouton of the axon is packed with hundreds to thousand of neurotransmitter-filled vesicles. Upon arrival of an action potential, the docked vesicles fuse with the plasma membrane at specific sites called active zones (Phillips et al., 2001). Synaptic vesicle fusion leads to the release of neurotransmitter (glutamate) into the synaptic cleft. Once in the synaptic cleft, glutamate binds to glutamate receptors in the postsynaptic membrane that are part of the postsynaptic density (PSD) of the dendrite. The PSD contains cytoplasmic protein scaffolds that form an electron-dense meshwork (Kennedy, 2000). Here, two major classes of ionotropic glutamate receptors (NMDA and AMPA receptors) are clustered (Hollmann et al., 1994). Binding of glutamate to these receptors leads to the opening of the intrinsic channels and influx of ions, which triggers local depolarization and activation of voltage-gated ion channels. In addition, metabotropic receptors activate a number of intracellular signaling cascades. This series of events represents a simplified model of synaptic transmission between neurons.

### 1.1.1. Organization of presynaptic specializations

Presynaptic boutons include the active zones where synaptic vesicles dock, fuse and recycle as well as a large accumulation of synaptic vesicles that can be functionally divided into three distinct pools: the resting pool, the recycling pool and the readily releasable pool (RRP) (for review see Rizzoli and Betz, 2005). The RRP contains vesicles that are docked and primed for release at the active zones and can easily undergo exocytosis upon stimulation. The reserve pool (resting + recycling pool) which represents up to 80-90% of the total pool contains vesicles which are released only in response to intense or prolonged stimulation. The recycling pool is intermediate between the two and its release precedes resting pool mobilization but follows the RRP. Synaptic vesicles are tethered to the matrix of fine filaments present at the active zones by synapsin molecules. Mutation of the different synapsin genes in mice has been shown to reduce dramatically the number of synaptic vesicles present in the reserve pool (Hilfiker et al., 1999). Synaptic vesicles dock at active zones, where they undergo a priming step to prepare them for fusion in response to calcium influx. During priming, a trimeric SNARE (soluble *N*-ethylmaleimide sensitive factor attachment receptor) complex is formed between the integral synaptic vesicle protein synaptobrevin/VAMP, the integral plasma membrane protein syntaxin and the plasma membrane associated protein SNAP-25 (soluble *N*-ethylmaleimide sensitive factor attachment protein 25). The stable assembly of this core complex is believed to drive membrane fusion and neurotransmitter release together with the triggering  $\text{Ca}^{2+}$  sensor proteins like the synaptic vesicle protein synaptotagmin. Following fusion, vesicle components are retrieved via endocytosis of vesicles.

The cytomatrix assembled at active zones is referred to as CAZ. Piccolo, Bassoon, RIMs (Rab3-interacting molecules), Munc13 and Munc18 are components of the CAZ. Bassoon-like proteins have a multidomain structure and are tightly anchored with the actin/spectrin cytoskeleton, suggesting that they play an important role in the organization of active zones (Fenster et al., 2000). Other cytoskeletal proteins associated with the active zones are members of the membrane-associated guanylate kinase (MAGUK) superfamily. They contain multiple PDZ domains, each of which functions as a protein-protein interaction module, being involved in the localization of presynaptic

membrane-associated signaling machineries (Craven and Bredt, 1998). Three MAGUKs are found at presynaptic boutons (but also in the PSD): SAP90, SAP97 and CASK. Of these, CASK has been shown to interact with the cell-adhesion molecule  $\beta$ -neurexin (Hata et al., 1996; Hsueh et al., 1998), which participates in the clustering of synaptic vesicle induced by neuroligins, the postsynaptic  $\beta$ -neurexin binding partners (Ichtchenko et al., 1995; Ichtchenko et al., 1996).

### 1.1.2. Organization of postsynaptic densities

Glutamatergic synapses, when viewed on electron micrographs, are characterized by an electron-dense thickening of the postsynaptic membrane representing the postsynaptic density (PSD). The PSD is a proteinaceous lattice composed of several large multimolecular complexes like: glutamate receptors, scaffolding and adapter proteins, cytoskeletal molecules, protein kinases/phosphatases and other signaling molecules. The major postsynaptic glutamate receptors are ionotropic AMPA, kainate and NMDA receptors together with metabotropic glutamate receptors (mGluRs), which are coupled to G protein signaling pathways. NMDA receptors have been shown to interact with the PDZ domains of the PSD95/SAP90 scaffolding protein (Niethammer et al., 1996). PSD95, a member of the MAGUK superfamily of proteins, is required for the specific targeting of NMDA receptors at PSDs and for the coupling of NMDA receptors to cytoplasmic signaling pathways (Sprengel et al., 1998). In addition to NMDA receptors, numerous other proteins, such as AMPA receptors, adhesion molecules, receptor tyrosine kinases, and other ion channels, can bind to the MAGUK proteins. PSD-95-like membrane-associated guanylate kinases (PSD-MAGUKs) were shown to mediate synaptic targeting of AMPA receptor subunits (Elias et al., 2006). The cell-adhesion molecule neuroligins has been shown to interact with PSD95 (Irie et al., 1997) and S-SCAM (another multiple PDZ domains-containing protein) (Iida et al., 2004). Interestingly, the extracellular domain of neuroligins is known to trans-synaptically interact with  $\beta$ -neurexin (Comoletti et al., 2007; Ichtchenko et al., 1995), a presynaptic membrane protein involved in the assembly of presynaptic specializations (Dean et al., 2003). This complex may provide a bridge between pre- and postsynaptic elements to regulate protein sorting and localization at nascent synapses. AMPA receptors are also



concentrated at postsynaptic sites of excitatory synapses, although the synaptic levels of AMPA receptors are much more heterogeneous than those of NMDA receptors. Some excitatory synapses contain NMDA receptors but no AMPA receptors, especially early in development (Takumi et al., 1999). AMPA receptors seem to be inserted into the membrane from intracellular compartments upon strong synaptic activity (Shi et al., 1999). The C-terminal cytoplasmic tails of AMPA receptor subunits interact with a distinct set of cytoplasmic proteins than do NMDA receptors. AMPA receptors bind to GRIP (glutamate receptor interacting protein) another multi-PDZ domain containing protein (Dong et al., 1997) and to SAP97 (a PSD95-related protein) ((Leonard et al., 1998) . Recently it has been shown that transmembrane AMPA receptor regulatory proteins (TARPs) like stargazin regulate many aspects of AMPA receptor activity. TARPs augment AMPA receptor plasma membrane trafficking, enhance synaptic clustering and increase glutamate affinity (Menuz et al., 2008; Tomita et al., 2005). Beside scaffolding proteins, the PSDs contain filamentous proteins like tubulins, actins and spectrins (Adam and Matus, 1996). The quantitatively largest amount of protein at the PSD is represented by  $\text{Ca}^{2+}$ -calmodulin dependent protein kinase II (Elgersma and Silva, 1999), which is involved in long-term synaptic plasticity.

### **1.2. Glutamatergic synapse formation during brain development**

For glutamatergic synapses to function properly, the pre- and postsynaptic components must accumulate at the initial axodendritic contacts with precise timing. This process is called synaptogenesis and is controlled by a series of hierarchical signals that assure the stabilization of the initial synaptic contact, the recruitment of pre- and postsynaptic proteins, the maturation and activity-dependent plasticity of synapses. There appear to be multiple mechanisms for synapse formation with different temporal orders of pre- and postsynaptic protein recruitment (for review see McAllister, 2007 and references therein), depending on the type of synaptic contact formation (axonal growth cone- or dendritic filopodia-initiated synapse formation) and on the state of differentiation of the neurons.

#### **1.2.1. Recruitment of presynaptic proteins**

Presynaptic specializations are formed from preassembled presynaptic protein/membrane complexes that are transported in packages before and during synaptogenesis (Vaughn,

## INTRODUCTION

1989; Ziv and Garner, 2004). In the axoplasm of immature neurons two different types of presynaptic precursor vesicles have been detected: PTVs (Piccolo transport vesicles) and STVs (synaptic vesicle transport protein vesicles) (Sabo et al., 2006; Zhai et al., 2001).

PTVs consist of active zone components like Piccolo and Bassoon, proteins that mediate synaptic vesicle exocytosis like Munc13 and Munc18, syntaxin and SNAP25, as well as N-cadherin, a cell adhesion molecule (Zhai et al., 2001). PTVs are assembled and transported via the trans-Golgi network and can exhibit saltatory movements in the axon, splitting into smaller clusters or fusion with other PTVs (Shapira et al., 2003). Active zones are ultimately assembled by fusion of a small number of PTVs (typically two to three) into the presynaptic plasma membrane (Shapira et al., 2003). Consistent with this mode of assembly, it has been shown that functional neurotransmitter release sites can form as soon as 30 minutes after the initial axodendritic contact has been established (Ahmari et al., 2000; Friedman et al., 2000). Bassoon is among the first active zone proteins to be detected at functional nascent synapses in cultured neurons (Shapira et al., 2003; Zhai et al., 2001), thereby representing a good molecular marker for active zone detection.

Synaptic vesicles are transported as heterogeneous organelles called STVs that differ in their morphology and protein content from PTVs (Zhai et al., 2001). STVs carry small clusters of synaptic vesicle-like vesicles together with many synaptic vesicles-associated proteins and other proteins critical for the vesicle cycle (Ahmari et al., 2000; Kraszewski et al., 1995). STVs are highly mobile within axons of immature neurons (Ahmari et al., 2000; Sabo et al., 2006), and they have been reported to fuse with other STVs or to split into smaller clusters (Bresler et al., 2004; Sytnyk et al., 2002).

Furthermore, there appear to be two distinct mechanisms for accumulation of presynaptic proteins at new synapses. In immature neurons, *de novo* accumulation of presynaptic components occurs via rapid recruitment of PTVs and STVs as described above. In more mature neurons, however, portions of mature presynaptic compartments have been shown to split off and become mobilized to form new presynaptic terminals (Krueger et al., 2003).

In cell culture assays, presynaptic differentiation seems to be triggered by heterophilic interactions between the axon and the dendrite, like binding of of presynaptic  $\beta$ -neurexin

to postsynaptic neuroligin (Scheifele et al., 2000), and/or by trans-synaptic binding of different SynCAM isoforms (Biederer et al., 2002).  $\beta$ -neurexin and SynCAMs can bind intracellularly to the PDZ domains of CASK. CASK, a multi-domain scaffolding protein has been shown to support the polymerization of actin at the neuroligin sites (Biederer and Sudhof, 2001), but also to form a tripartite complex with the presynaptic adaptor proteins Veli and Mint, thus coupling the synaptic vesicle exocytosis machinery to cell adhesion systems (Butz et al., 1998). Furthermore, this tripartite complex may also functionally interact with the cadherin/ $\beta$ -catenin cell adhesion system (Bamji et al., 2003)

### 1.2.2. Recruitment of postsynaptic proteins

One of the most critical events in the formation of the postsynaptic compartment is the recruitment of ionotropic glutamate receptors. Similar to the STVs it has been suggested that NMDARs are transported to the postsynaptic membrane via preassembled transport packets (Washbourne et al., 2002). Although the exact molecular composition of these packets has not been determined biochemically, retrospective immunostainings have suggested that they may contain also AMPARs but no PSD95. However, other studies have indicated that PSD assembly is fundamentally different from the presynaptic active zone assembly (Bresler et al., 2004). These authors have found that NMDARs are recruited to the synaptic sites in a gradual manner. Similarly, the mechanisms of accumulation of postsynaptic scaffolding proteins has remain largely under debate, as some studies have shown that PSD95 and Shank proteins accumulate at discrete, immobile clusters present in the dendrites before synapses have formed (Bresler et al., 2004; Friedman et al., 2000; Okabe et al., 2001a), whereas other studies have described a modular transport of PSD95 and preformed scaffolding complexes containing PSD95, GKAP and Shank (Gerrow et al., 2006; Prange and Murphy, 2001).

### 1.2.3. Standard model of the stepwise assembly of glutamatergic synapses

Although formation of synapses represents a continuous process from the time of initial axo-dendritic contact to the emergence of a fully functional synapse, it is useful to divide it into five different steps, as shown in Fig. 1.1 (Garner et al., 2006).

1. *Formation of axo-dendritic contacts.* For a synapse to form, contact must first be made between the axon and the dendrite (Fig. 1.1a). A number of possible types

of contacts have been described. Axodendritic contacts can be initiated either from the filopodia of an axonal growth cone or from dendritic growth cones. In addition, contacts may form between filopodia from the axons or dendrites to form en passant synapses. Finally, synaptic contacts can form between axons and dendritic shafts. In either case, most of these contacts are fleeting and transitory and become stabilized only after a still hypothetical recognition process between membrane signaling molecules present on the axon and on the dendrite. Cell adhesion molecules including integrins, classical cadherins, protocadherins, and members of the Ig superfamily are thought to govern this initial step of synaptogenesis by providing a mechanism of recognition between neuronal processes (axon and dendrite). These molecules, through their adhesion and signaling capabilities, are also important in bidirectional signaling to coordinate the differentiation of pre- and postsynaptic compartments at later stages.

2. *Induction of pre- and postsynaptic differentiation.* The presence of general “synptogenic” factors like SynCAMs,  $\beta$ -neurexin/neuroligin, EphrinB and Ephrin receptors is thought to induce the formation of presynaptic active zones and postsynaptic densities after recognition has occurred (Fig.1.1b). Neuroligins were the first to be shown to trigger the formation of functional presynaptic terminals when expressed in heterologous cells and in neurons (Chih et al., 2005; Scheiffele et al., 2000). Neuroligin function appears to require  $\beta$ -neurexin on the presynaptic site (Dean et al., 2003). Furthermore, neuroligins can also specify (validate) the type of synapse (excitatory or inhibitory) and control the ratio of excitatory and inhibitory synapse formation (Chubykin et al., 2007). Similarly, postsynaptic differentiation has been shown to be triggered by presynaptic  $\beta$ -neurexin (Graf et al., 2004).
3. *Synapse assembly.* Induction is followed by a differentiation step (Fig.1.1c), which lasts 1-2 hours and is characterized by accumulation of vesicles and synaptic proteins at the nascent contact site (Ahmari et al., 2000; Bresler et al., 2004; Friedman et al., 2000). At this stage synapses are already functional (Ziv and Garner, 2001), but rather immature and still missing their final molecular composition. Synaptic differentiation has been suggested to be regulated by

molecules like BDNF secreted into the extracellular space by axons or dendrites (O'Brien et al., 1999).

4. *Maturation of synaptic contacts.* Over the course of hours to days, the synapses undergo structural and functional maturation. At the presynaptic terminal a large, well defined pool of synaptic vesicles is emerging (Mozhayeva et al., 2002), while the postsynaptic dendrite takes a mushroom-shaped spine morphology (Fig. 1.1d). Functional maturation involves mainly the presynaptic release probability, and the type and subunit composition of postsynaptic glutamate receptors. This stage is associated with an increase in stability of the synaptic junction and a resistance to disassembly. It has been shown that mature synapses acquire resistance to actin depolymerizing drugs like latrunculin A (Zhang and Benson, 2001) and appear to be stable for days, weeks and even months (Zuo et al., 2005). In contrast, immature synapses are sensitive to latrunculin A (Zhang and Benson, 2001) and may only last for hours or even less (Jontes and Phillips, 2006).
5. *Maintenance of synaptic structure.* During the life time of a synapse (days, weeks, months and even years) the overall organization and function of its pre- and postsynaptic apparatus are kept stable. However, synaptic molecules seem to be in a dynamic equilibrium with the extrasynaptic pools (Fig. 1.1e). It has been shown that synaptic vesicles and even their release machinery are exchanged between adjacent presynaptic boutons (Darcy et al., 2006; Krueger et al., 2003; Matteoli et al., 2004), probably contributing to the formation of new synapses and/or to coordinate regulation of neighboring recycling pools (Darcy et al., 2006). Similarly, many postsynaptic molecules (PSD95, Homer, actin, Shank, AMPA and NMDA receptor subunits) have been shown to be continuously exchanged between the synaptic compartment and the extrasynaptic pools (Bresler et al., 2004; Okabe et al., 2001b; Sharma et al., 2006).

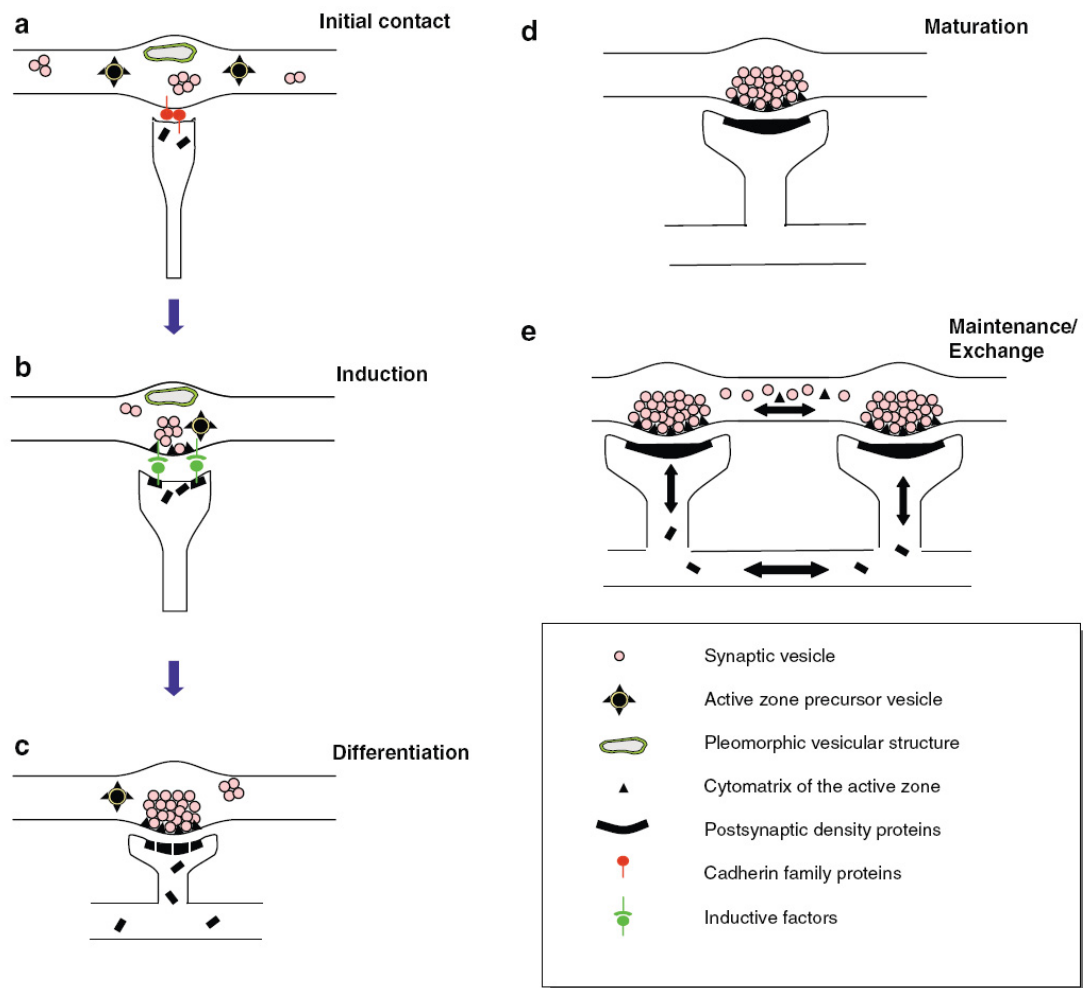


**Figure 1.1. Model of excitatory synapse formation** (modified after Garner et al., 2006).

(a) Axodendritic contact seems to be mediated by cell adhesion molecules, including members of the cadherin family. (b) Recruitment at the contact sites of inductive factors like SynCAM,  $\beta$ -neurexin/neuroligin, EphrinB/EphR triggers the formation of presynaptic active zones and postsynaptic densities, by recruiting pre- and postsynaptic components. (c) During the differentiation period, the nascent synaptic sites are stabilized by the cooperative action of different cell-adhesion molecules, and pre- and postsynaptic elements are further recruited to form (d) a fully functional, mature synapse. (e) Finally, the replacement and exchange of pre- and postsynaptic proteins enable synapses to be maintained over long periods of time.

### 1.3. Synaptic cell adhesion molecules

Neuronal interaction and recognition are thought to be mediated, at least in part, by cell-adhesion molecules. Cell adhesion molecules (CAMs) are transmembrane glycoproteins involved in binding with other CAMs present on the surface of other cells or with extracellular matrix molecules. Several classes of CAMs were reported to be

concentrated at glutamatergic synapses: cadherins (classic cadherins and protocadherins), members of the immunoglobulin (Ig) superfamily (NCAM, L1, nectins, SynCAMs), integrins, Ephrin receptors and their Ephrin ligands and the  $\beta$ -neurexin/neurologin adhesion system. Extracellularly, synaptic CAMs are involved in homophilic and/or heterophilic trans-synaptic interactions, while intracellularly they are linked with cytoplasmic signaling networks thus coordinating the functional organization of the pre- and postsynaptic specializations.

### 1.3.1. N-cadherin/ $\beta$ -catenin cell adhesion system

Cadherins are calcium-dependent cell adhesion molecules that have been shown to play important roles in establishing the embryonic subdivisions of the nervous system, in organizing cell groups into distinct nuclei, in axon outgrowth and target selection, and in synapse targeting, formation and maintenance. There are about 80 different cadherins expressed in the nervous system and they are grouped depending on their molecular structure into classic cadherins and protocadherins. Classic cadherins have about 20 members, which include among others N-, E-, P-cadherin, cadherin-8, and cadherin-11. Their molecular organization includes five characteristic extracellular cadherin repeats (EC1 - EC5), one transmembrane domain and a relatively short intracellular domain. The EC1-EC1 domain interaction is thought to mediate the *trans* homophilic binding of cadherins from opposing cell membranes (Fig. 1.2a), whereas the EC1-EC2 interaction is involved in *cis* interaction between adjacent cadherin molecules present on the same cell surface (Fig. 1.2b) (Pokutta and Weis, 2007). Dimerization has been shown to increase the adhesive strength of cadherins and activity is thought to augment levels of N-cadherin dimers (Bozdagi et al., 2000; Tanaka et al., 2000). The EC domains are delimited from each other by calcium binding domains. The formation of cadherin dimers has been shown to be a calcium dependent process. The main structural difference between different types of classic cadherins resides in the amino acid sequence of the EC1 domain thus controlling binding specificity.



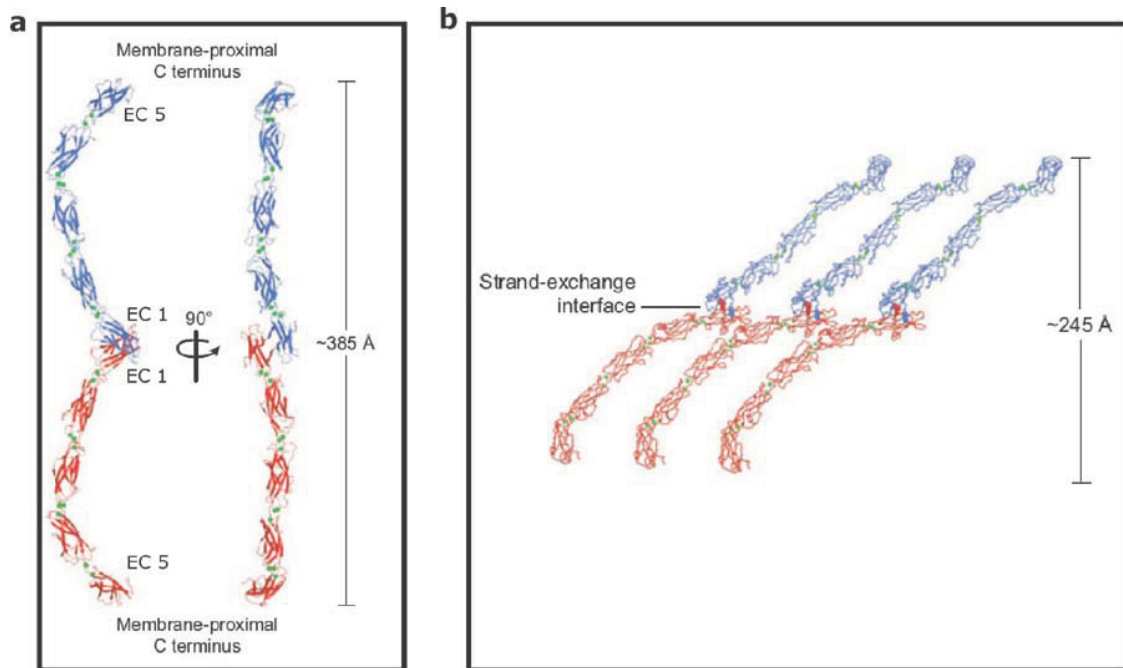


**Figure 1.2. Model of the homophilic N-cadherin complex at the synapse** (modified after Pokutta and Weis, 2007)

(a) Cadherin *trans*-dimers as seen in the crystal structure of cadherin full-length extracellular region. (b) Crystal structure of packed cadherin ectodomains in multimers showing *cis* and *trans*-interactions. In (a) and (b) individual cadherin monomers are colored in blue and red and individual  $\text{Ca}^{2+}$  are indicated as green small spheres. In (a) and (b) the approximate sizes of complexes are shown

The expression of different types of cadherins in the central nervous system has been shown to be restricted to subsets of fiber tracts and fascicles (for review see Redies, 1997 and references therein). Each cadherin shows a different expression pattern characteristic of the molecule but there is also a partial overlap. Interestingly, a given cadherin is often not only expressed by a subset of nerve fascicles but also by their target area. In this way, grey matter regions and the fiber tracts connecting them form neuronal circuits characterized by the expression of a particular cadherin. Cadherins have therefore been proposed to provide an adhesive code for the high degree of specificity and selectivity of in neural circuit formation (Redies, 1997).

N-cadherin was first identified in neural tissue, hence the name neural (N)-cadherin, but later it was shown to be expressed also in other tissues. Especially, expression of N-cadherin in the myocardial tissue seems to be of extraordinary importance as the



## INTRODUCTION

homozygous N-cadherin mutant embryos die by day 10 of gestation because of abnormal heart development (Radice et al., 1997). In the cerebral cortex, N-cadherin has been shown to be essential for maintaining the normal cytoarchitecture, as conditional deletion of the N-cadherin gene has been described to completely randomize the intracortical structures (Kadowaki et al., 2007). Expression of N-cadherin at synapses has been shown to depend on the maturational stage of the synapse. Early during development, N-cadherin is present at all synapses between hippocampal neurons, but at later maturational stages becomes restricted to excitatory synapses. Within the active zone, the pattern of N-cadherin expression also varies with the maturational stage of the synapse. At immature synapses N-cadherin molecules are distributed at the synaptic cleft throughout the active zone, whereas at mature excitatory synapses they cluster perisynaptically and border the active zone and the postsynaptic density (Benson and Tanaka, 1998; Elste and Benson, 2006). Extracellularly, N-cadherin engages in homophilic interaction with other N-cadherin molecules. Intracellularly, N-cadherin associates with different molecules that regulate the adhesive properties or mediate downstream signaling. Catenins ( $\alpha$ ,  $\beta$ ,  $\gamma$ ) are well known binding partners of cadherins and are mainly involved in linking the N-cadherin molecules to the actin cytoskeleton. However, the cadherin-catenin-actin cytoskeleton complex has been shown to be a very dynamic one, as  $\alpha$ -catenin seems to bind either to  $\beta$ -catenin or to F-actin in a mutually exclusive manner, with the monomeric form preferentially binding  $\beta$ -catenin and the dimeric form preferentially binding F-actin (Drees et al., 2005). Binding of  $\beta$ -catenin to N-cadherin has been shown to be regulated by protein-tyrosine phosphatase PTP-1B, which dephosphorylates  $\beta$ -catenin, thereby allowing its interaction with N-cadherin. Knockout studies have indicated that  $\beta$ -catenin regulates the reserve pool of synaptic vesicles through binding to cadherin and recruitment of PDZ-containing proteins to the complex (Bamji et al., 2003). Thereby, N-cadherin's role in organization of presynaptic specializations is thought to be mediated by its interaction with  $\beta$ -catenin. Postsynaptically, N-cadherin has been shown to play an important role in regulating spine morphology and spine density. Block of function studies or siRNA knockdown of N-cadherin have shown that in the absence of N-cadherin spines acquire a filopodia-like morphology and the number of spines is decreased (Saglietti et al., 2007; Togashi et al.,

2002). Similarly,  $\alpha$ (N)-catenin knockout mice show an enhanced spine motility suggesting that  $\alpha$ -catenin may mediate the postsynaptic effects of N-cadherin (Abe et al., 2004). However, conditional N-cadherin knockout neurons did not present any alterations in spines (Kadowaki et al., 2007). Interaction with other intracellular proteins (p120catenin,  $\delta$ -catenin and presenilin) is thought to regulate cell surface expression, turnover and *cis*-strand interaction, thereby modulating the adhesive strength of cadherins.

N-cadherin has also been suggested to regulate functional aspects of synaptic plasticity at mature synapses. Blocking N-cadherin adhesion by specific antibodies in hippocampal slices had no effect on normal synaptic transmission at Schaffer collateral-CA1 synapses, but the induction of L-LTP was completely abolished (Bozdagi et al., 2004; Tang et al., 1998).

### 1.3.2. Neuroligin/neurexin cell adhesion system

Neuroligins are encoded by at least four different genes in vertebrates and are restricted to the postsynaptic membrane (Ichtchenko et al., 1996). Neuroligins engage in heterophilic interactions with members of the neurexin family localized on the presynaptic membrane (Fig. 1.3). Neuroligins have a large extracellular domain, a transmembrane domain and a short cytoplasmic tail, which contains a PDZ-recognition motif. The extracellular region mediates the binding to neurexin's LNS domain. Neuroligins form dimers through their cholinesterase-like domains (for review see Dean and Dresbach, 2006 and references therein). The intracellular regions show little sequence identity among different neuroligin family members, suggesting that they are responsible for different localizations and functions. Neuroligin1 is specifically localized to glutamatergic postsynaptic specializations, whereas neuroligin 2 is exclusively localized to inhibitory synapses in the brain (Song et al., 1999; Varoqueaux et al., 2004). Neurexins may be expressed as thousands of different isoforms generated by alternative splicing of mRNA transcripts from six promoters in three genes (Ushkaryov et al., 1994). Two classes of mature proteins exist:  $\alpha$ -neurexins and  $\beta$ -neurexins (Ushkaryov et al., 1992).  $\alpha$ - and  $\beta$ -neurexins are single transmembrane proteins with different extracellular domains.  $\alpha$ -neurexins contain six extracellular LNS domains, whereas  $\beta$ -neurexins

contain only one LNS domain. The intracellular regions of both neuroligins contain a PDZ-recognition motif (Missler et al., 1998). Neuroligins appear to form a trans-synaptic complex mainly with  $\beta$ -neuroligins, with the binding of neuroligins to  $\beta$ - or  $\alpha$ -neuroligins regulated by alternative splicing at two sites in the extracellular region of neuroligins (Boucard et al., 2005; Chih et al., 2006)

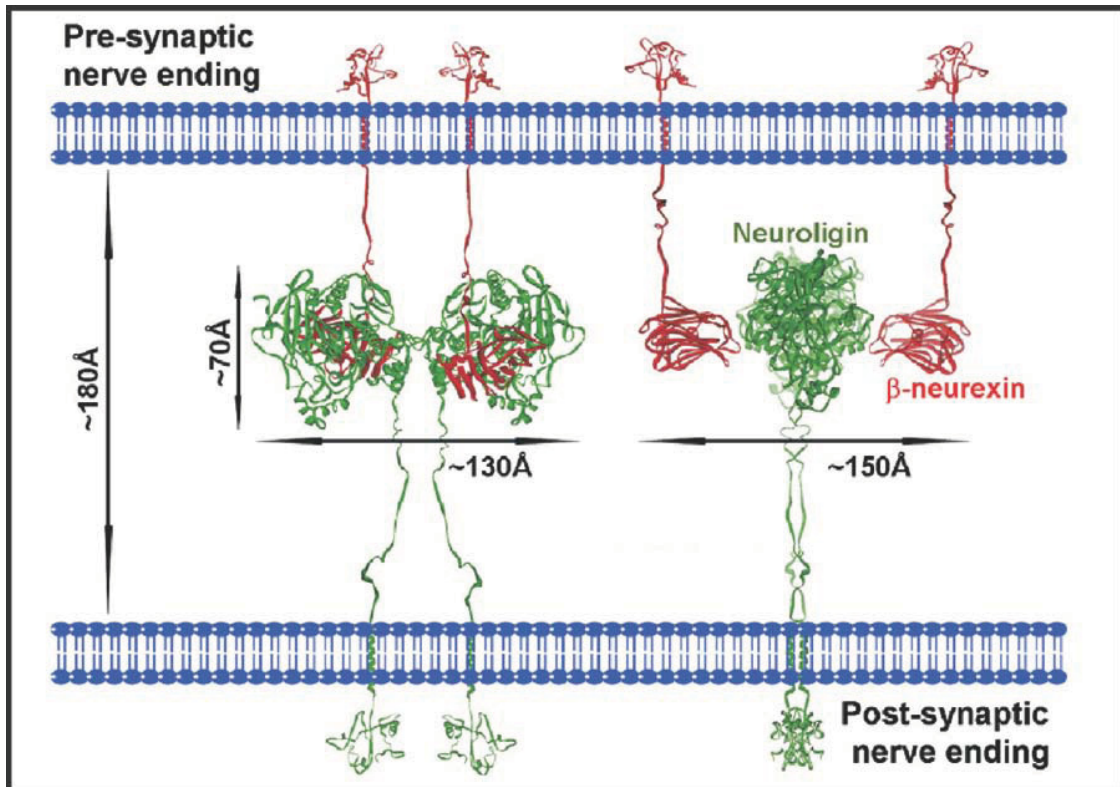


**Figure 1.3. Model of the heterophilic neuroligin1/ $\beta$ -neurexin complex at the synapse** (modified after Comoletti et al., 2007)

Model of the neuroligin1/ $\beta$ -neurexin complex. Neuroligin dimmer are indicated in green, whereas neurexin is red. The approximate sizes of complexes and synaptic cleft are shown

The neuroligin/neurexin adhesion system has recently received a lot of attention because of pioneering studies done by Scheiffele et al., 2000, which used an assay involving co-culture of neuronal and non-neuronal cells to study the minimum molecular requirements for synapse induction. In these experiments, presentation of neuroligin1 or neuroligin2 on non-neuronal cells was sufficient to induce functional synaptic terminals in axons contacting these cells. This inductive effect was also present when neuroligin was

## INTRODUCTION

expressed in neurons (Chih et al., 2005; Sara et al., 2005; Scheiffele et al., 2000). Similar to neuroligin, another molecule, SynCAM, was also shown to be able to trigger the formation and differentiation of new synapses (Biederer et al., 2002; Sara et al., 2005). Hence, SynCAMs and neuroligins were referred to as synaptogenic molecules. The synaptogenic effects of neuroligin1 were demonstrated to be dependent on neuroligin's oligomerization and its interaction with  $\beta$ -neurexin. At presynaptic terminals, neuroligins interact with CASK, which forms a tripartite complex with the adaptor proteins Veli and Mint (Butz et al., 1998), and might act as a scaffold for the assembly of the synaptic vesicle release machinery (Dean et al., 2003).

In line with the synaptogenic effects of neuroligin,  $\beta$ -neurexin expression was able to induce postsynaptic differentiation of both GABAergic and glutamatergic synapses via neuroligin (Graf et al., 2004). It has been shown that neuroligins bind to PSD95, a postsynaptic scaffolding molecule (Irie et al., 1997). Thus, coupling of neuroligins to PSD95 may coordinate the recruitment and assembly of several postsynaptic partners, including NMDA and AMPA receptors, intracellular signaling proteins and the actin cytoskeleton. Neuroligin1 has also been shown to associate with several other PDZ-domain containing proteins including SAP102, PSD93, S-SCAM, MAGI1, MAGI3, Shank, and Pick1. S-SCAM but not PSD95 has been described to induce synaptic clustering of neuroligin1 (Iida et al., 2004). However, this study is in contradiction with others, which have shown that PSD95 enhances synaptic clustering of neuroligin, thereby augmenting the size of excitatory presynaptic terminals (Prange et al., 2004).

Contrary to the synaptogenic property attributed to neuroligins in a large number of studies done *in vitro* including an siRNA knockdown approach (Chih et al., 2005), data from a knockout study suggest that neuroligins may be not required for generation of synapses *in vivo* (Varoqueaux et al., 2006). A recent knockout study has suggested that neuroligin1 and neuroligin2 are required for specification and validation of excitatory and inhibitory synapses, respectively. Furthermore, neuroligin seems to validate transitory synapses in an activity-dependent manner that involves postsynaptic signaling pathways (Chubykin et al., 2007).

## 1.4. PDZ domain-containing proteins

PDZ domains are protein-protein interaction domains mainly found in multidomain scaffolding proteins. PDZ domains are specialized for binding small PDZ binding motifs present at the C terminal regions of more than 400 proteins (Kornau and Seeburg, 1997). By their modular interaction with different proteins, PDZ-domain containing proteins assemble large molecular complexes at different sites in the cell, where they usually perform a specialized local function. The best characterized member of the synaptic PDZ domain containing protein family is the postsynaptic density protein 95 (PSD95). PSD95 is an abundant scaffold component at excitatory postsynaptic densities, and belongs to the MAGUK (membrane-associated guanylate kinase) family of PDZ domain proteins. However, PDZ domains are also found in many other non-MAGUK scaffold or adaptor proteins like Veli, Mint, Pick, and GRIP adaptor proteins (for review see Kim and Sheng, 2004 and references therein).

### 1.4.1. Synaptic scaffolding molecules of the MAGI family (S-SCAMs)

Using a yeast two hybrid screening system, S-SCAM was first identified as a binding partner of synaptic associated protein SAPAP (Hirao et al., 1998). S-SCAM belongs to the MAGI (MAGUK with inverted domain structure) family of MAGUKs. As all MAGUK proteins, S-SCAM has one guanylate kinase (GK) domain, two domains with conserved Trp (W) residues (WW domains) and depending on isoform type, five to six PDZ domains. S-SCAM  $\alpha$  has six PDZ domains, numbered from PDZ0 to PDZ6, whereas S-SCAM  $\beta$  and  $\gamma$  contain five PDZ domains, numbered from PDZ1 to PDZ5 (Hirao et al., 2000).

Neurologin1 has been shown to interact with the WW domains and the PDZ1 domain of S-SCAM. This interaction seems to be important for neurologin clustering at synapses, because deletion mutants of S-SCAM without WW and PDZ1 domains interfere with neurologin localization (Iida et al., 2004). However, these results are in contradiction with studies that have indicated PSD95 as the scaffolding protein required for neurologin's activity at synapses (Prange et al., 2004). Synaptic localization of S-SCAM in turn was shown to be dependent on  $\beta$ -catenin binding. S-SCAM interacts with  $\beta$ -catenin through its PDZ5 domain and this interaction was suggested to mediate the recruitment of S-

SCAM to synapses (Nishimura et al., 2002). However, this seems not to be the only possibility of S-SCAM targeting at synapses, as another study has shown that S-SCAM can be recruited to cadherin based adhesion sites through a nectin dependent mechanism (Yamada et al., 2003). The 5<sup>th</sup> PDZ domain of S-SCAM can also interact with PSD95, NMDA receptors and  $\delta$ -catenin. Consistent with its role as a scaffolding molecule, S-SCAM has been shown to form multimers through its PDZ4 and PDZ5 domains and can also interact with the GK domains of PSD95, however, it is not clear whether these bindings take place simultaneously (Hirao et al., 2000). Thus, it has been suggested that S-SCAM, as PSD95, may play a central role for the assembly of synaptic junctions, but its function in organization of synapses may be different compared to PSD95.

### 1.5. Aims of the study

The major goal of this study was to investigate the role of the cell adhesion molecule N-cadherin in synaptogenesis and early synapse maturation. Moreover, the molecular mechanisms through which N-cadherin participates in these processes were extensively addressed.

Deletion of the N-cadherin gene in mice leads to early embryonic lethality around day 10 of gestation, long before the brain has formed. Therefore, research concerning the role of N-cadherin in synapse formation and function was greatly hindered and the main findings about N-cadherin's function were indirectly obtained from overexpression of dominant-negative constructs or application of binding-blocking antibodies. However, the specific function of N-cadherin at synapses has remained largely elusive. In this study, homozygous N-cadherin knockout neurons were obtained by differentiation from mouse embryonic stem cells, thereby circumventing the early embryonic lethality of mice genetically null for N-cadherin. These neurons were investigated *in vitro* by time lapse imaging to study synapse formation and maturation and by fluorescence recovery after photobleaching (FRAP) to quantify the dynamics of synaptic vesicles at single synaptic sites. For visualization of synapses, neurons were co-transfected with constructs coding

## INTRODUCTION

for fluorescently tagged pre- and postsynaptic proteins. For visualization of neuronal processes EGFP or DsRed2, respectively were co-expressed in these neurons.

The first part of this study investigates the role of N-cadherin in the formation of nascent synapses and their further maturation. Presynaptic vesicle accumulation is a crucial step in the formation and early functional maturation of central glutamatergic synapses. The time course of presynaptic vesicle recruitment at nascent synaptic sites and at mature synapses was investigated in control and N-cadherin deficient neurons in order to study how fast the synapses are assembled and how they mature in the absence of N-cadherin compared to control conditions. To further investigate whether N-cadherin is involved in the stabilization of immature synapses and in the maintenance of mature synapses, the dynamics of vesicle pools in immature and more mature N-cadherin control and knockout neurons was analyzed. Additionally, the formation of active zones and postsynaptic densities was studied in immature and more mature control and N-cadherin deficient neurons.

The second part of the study focuses on the cooperation between two cell adhesion systems, the N-cadherin/ $\beta$ -catenin and the neuroligin/neurexin system, in trans-synaptically controlling the formation of presynaptic vesicle accumulations. This project was instigated by previous studies which have demonstrated that neuroligin, but not N-cadherin, when expressed on the surface of heterologous cells has the capacity to trigger presynaptic vesicle accumulation in axons that come into contact with these cells. The functional interaction between N-cadherin and neuroligin in respect to presynaptic vesicle clustering was analyzed by overexpression of neuroligin1 in N-cadherin control and N-cadherin deficient neurons. The potential role of the synaptic scaffolding protein S-SCAM as a link between these two cell adhesion systems was also investigated by expression of mutant S-SCAM proteins in primary cortical neurons. In summary, this study provides a molecular mechanism that may potentially be involved in mediating N-cadherin and neuroligin functional interaction in respect to presynaptic vesicle clustering.



## 2. Materials and methods

### 2.1. Solutions and Chemicals

#### 2.1.1. Chemicals

Restriction enzymes and DNA length standards (DNA ladder) were obtained from Promega. DNA purification kits were purchased from Qiagen. Molecular cloning reagents were obtained from Biotech, Clontech and Stratagene.

#### 2.1.2. Cell culture media

(all solutions were obtained from Invitrogen if not stated otherwise)

##### EF (“embryonic feeder” cells) media

DMEM	500 ml
Fetal Calf Serum (FCS)	50 ml
L-Glutamin 200mM	5 ml
Penicillin-Streptomycin solution 100X	5 ml

##### KO ES (knock out embryonic stem cell) media

Knock out DMEM	425 ml
FCS	75 ml
MEM Non Essential Amino-acids	5 ml
Penicillin-Streptomycin solution 100X	5 ml
2-mercaptoethanol 50 mM	0.5 ml
LIF (ESG1107) fresh added	0.7 µl/5 ml KO ES medium

##### SR (“serum replacement”) media

Serum Replacement	75 ml
L-Glutamin 200 mM	5 ml
2-mercaptoethanol 50 mM	0.5 ml
Penicillin-Streptomycin solution 100X	5 ml

##### Differentiation Media

DMEM	200 ml
FCS	50 ml
L-Glutamin 200 mM	2,5 ml



## MATERIALS AND METHODS

MEM	2.5 ml
Non-essential Aminoacid-Solution	2.5 ml
$\beta$ -Mercaptoethanol solution* (Serva)	2.5 ml
Penicillin-Streptomycin solution 100X	2.5 ml
Retinoic acid solution**	5 $\mu$ l/ml

\*  $\beta$ -Mercaptoethanol solution: 3.4  $\mu$ l  $\beta$ -Mercaptoethanol (Serva) in 10 ml DMEM

\*\* Retinoic acid solution: 3mg retinoic acid (Serva) in 10 ml; 1:9 dilution in differentiation media

### Neurobasal (NB) media

Neurobasal media	100 ml
B27-Supplement 50 X	2 ml
GlutaMAX-I Supplement	0.5 ml
Penicillin-Streptomycin solution 100X	1 ml

### BME media

BME Basal Media	500 ml
FCS	50 ml
L-Glutamin 200 mM	5ml
Glucose	20 mM
Insulin-Transferrin-Selenium solution	5 ml
Penicillin-Streptomycin solution	5 ml

### HEPES buffered extracellular solution

NaCl	130 mM
KCl	5 mM
CaCl <sub>2</sub>	2.5 mM
MgCl <sub>2</sub>	1 mM
HEPES	20 mM
pH 7.3 (adjusted with NaOH)	

### 2.1.3. Media for growing bacteria

(Media were autoclaved for 20 min and antibiotics were supplemented prior to use)

### LB-medium

Bacto-tryptone, pH 7.5	10 g/l
NaCl	5 g/l
Yeast extract	5 g/l
Glucose (w/v)	2 %
MgSO <sub>4</sub>	1 mM

## MATERIALS AND METHODS

### **LB/Amp-medium** (same for LB/Kan-medium)

Ampicillin in LB-medium	100 mg/l
-------------------------	----------

### **LB/Amp-plates** (same for LB/Kan-plates)

Agar in LB-medium	20 g/l
Ampicillin	100 mg/l

## **2.2. Plasmids**

<b>pEGFP-N1</b>	Clontech. Kanamycin resistance
-----------------	--------------------------------

<b>pDsRed2-N1</b>	Clontech. Kanamycin resistance
-------------------	--------------------------------

<b>DsRed2-VAMP2</b>	VAMP2 (Synaptobrevin II) from <i>Rattus norvegicus</i> inserted into the MCS of pDsRed2-C1 (Clontech). Kanamycin resistance. Gift from Dr. V. Lessmann, University of Mainz, Germany
---------------------	--

<b>EGFP-VAMP2</b>	VAMP2 (Synaptobrevin II) from <i>Rattus norvegicus</i> inserted into the MCS of pEGFP-C1 (Clontech). Kanamycin resistance. Gift from Dr. T. Dresbach, University of Heidelberg, Germany
-------------------	---

<b>EGFP-Bassoon</b>	Bassoon (amino-acids 95-3938) from <i>Rattus norvegicus</i> was inserted into pCSM. Ampicillin resistance. Gift from Dr. A. Fejtova and E. Gundelfinger, Leibniz Institute for Neurobiology, Magdeburg, Germany
---------------------	---

<b>PSD95-GFP</b>	PSD95 from <i>Rattus norvegicus</i> inserted into GW1 vector (British Biotechnology). Ampicillin resistance. Gift from Dr. V. Lessmann, University of Mainz, Germany
------------------	--

<b>Neurologin 1-GFP</b>	Neurologin 1 from <i>Rattus norvegicus</i> inserted into MCS of pEGFP-N1 (Clontech). Kanamycin resistance. Gift from Dr. T. Dresbach, University of Heidelberg, Germany
-------------------------	---

## MATERIALS AND METHODS

<b>pDEST53-MAGI2 full</b>	MAGI2 $\beta$ /S-SCAM from <i>Mus musculus</i> inserted into pcDNA-DEST53 (Gateway Technology). Ampicillin resistance. Gift from Dr. M.G. Price and D. L. Burgess, Baylor College of Medicine, Houston, Texas, USA
<b>pcDNA3</b>	Invitrogen. Ampicillin resistance
<b>N-cad-EGFP</b>	Full murine N-cadherin inserted into pEGFP-N1 (Clontech). Kanamycin resistance. Gift from Dr. C. Gauthier-Rouviere, CNRS, Montpellier, France

### 2.3. Generation of mutant S-SCAM constructs

#### 2.3.1. Transformation of bacteria with pDEST53-MAGI2 full vector

The pDEST53-MAGI2 full vector was provided by Dr. M.G. Price and Dr. D.L. Burgess (Baylor College of Medicine, Houston, Texas, USA). OneShot *ccdB* Survival T1 Phage-Resistant Cells (Catalog no.C7510-03 from Invitrogen) were used to propagate and maintain the pcDNA-DEST 53 vector. The *ccdB* Survival *E. coli* strain is resistant to *CcdB* effects and can support the propagation of plasmids containing the *ccdB* gene without deleting repeated domains.

All the other vectors used in this study were propagated and maintained in TOP10 competent bacteria (Invitrogen). To 100 $\mu$ l of TOP10 competent bacteria 1 $\mu$ g of plasmid DNA or 20 $\mu$ l of ligation mixture were added and incubated for 30min on ice. After a heat shock (2min, 42°C) and successive incubation on ice (3min), 800 $\mu$ l of LB-medium were added to the bacteria and incubated at 37°C for 30min. Cells were then centrifuged (10000rpm, 1min, RT) and the supernatant removed. Cells were resuspended in 100 $\mu$ l LB medium and plated on LB plates containing the appropriate antibiotics. Plates were incubated at 37°C overnight. (Sambrook and Russell, 2000)

#### 2.3.2. Plasmid isolation from 3 ml cultures (Minipreps)

(Sambrook and Russell, 2000 and Amersham Pharmacia Miniprep preparation kit)

3ml LB/Antibiotic-Medium were inoculated with a single colony and incubated overnight at 37°C with constant agitation. Cultures were transferred into 2ml Eppendorf tubes and cells were pelleted by centrifugation (12000rpm, 1min, RT). Plasmids were isolated from

## MATERIALS AND METHODS

the bacteria according to the manufactures protocol. The DNA was eluted from the columns by addition of 50µl Tris-HCl (10mM, pH 8.0) with subsequent centrifugation (12000rpm, 2min, RT)

### 2.3.3. Plasmid isolation from 500ml cultures (Maxipreps)

(Qiagen Maxiprep kit)

For preparation of large quantities of DNA, the Qiagen Maxiprep kit was used. A single colony was inoculated in 2ml LB-Antibiotic medium and grown at 37°C for 8 hours with constant agitation. Afterwards, this culture was added to 500ml LB-Antibiotic medium and the culture was incubated at 37°C with constant agitation overnight. Cells were pelleted in a Beckmann centrifuge (6000rpm, 15min, 4°C) and the DNA was isolated as described in the manufactures protocol. Finally, the DNA pellet was resuspended in TE buffer and the DNA concentration was determined.

### 2.3.4. Primer design

The vector contained a full-length mouse MAGI-2β/S-SCAM cDNA clone (GenBank accession number BC059005).

The coding sequence (CDS) DNA 1-3339 codes for S-SCAM (amino-acids 1-1112): GKW [amino-acids 1-233, containing both the guanylate kinase (GK) and WW domains], PDZ1 (amino-acids 245-393), PDZ2 (amino-acids 404-556), PDZ3 (amino-acids 583-732), PDZ4 (amino-acids 723-963), PDZ5 (amino-acids 922-1112).

For designing the PCR primers, several variables were taken into account ([www.eppendorf.de](http://www.eppendorf.de)):

- primer length – between 18 and 25 bases
- melting temperature ( $T_m$ ) – both primers should have similar melting temperatures (between 55°C and 72°C)
- specificity – primers must be chosen so that they have a unique sequence within the template DNA that is to be amplified
- G/C content

The  $T_m$  can be calculated using the formula:

## MATERIALS AND METHODS

$$T_m = 69.3 + (\text{NGC}/L) \times 41 - 650/L,$$

Where NGC represents the number of C and G bases, and L represents the total number of bases.

The designed primers were:

- **FP-start:** G ACC AAG CTT **ATG** GAA TTG GAG AAA AGT GGT GC  
 $T_m = 58.9$
- **FP-PDZ2:** GAC CAA GCT **TAT** **GTC** TTT GCA CTC CAT GCC AGC  
 $T_m = 59.3$
- **RP-end:** GCC TCT AGA **CTA** CTT CCG GCA GGC CTG  
 $T_m = 58.2$
- **RP-PDZ4:** GCC TCT AGA CAG AGG GTA CTG CCT GGT  
 $T_m = 58.2$

The start codon ATG is indicated in red and the stop codon CTA in blue. The HindIII and XbaI restriction sites are underlined. FP stands for Forward Primer, while RP stands for Reverse Primer.

## MATERIALS AND METHODS

1 atggaattgg agaaaagtgg tgctctccta gaaagcggga cctatgaaga caactactac  
 61 ggtaccccgga agcctccagc tgaaccagca ccattattaa atgtaacaga ccagatactt  
 121 ccgggagcta ctccaagtgc tgaggggaag cggaaaagaa ataagtcagt gaccaacatg  
 181 gagaaagcaa gtatagagcc tccagaggag gaagaagaag aaaggcctgt agtcaatgga  
 241 aacggcggtg tcataacccc agaatccagt gaacatgaag acaaaaagtgc aggtgcctca  
 301 ggggagacac cctcccagcc ttaccctgca cccgtgtaca gccagcccgga agagctcaag  
 361 gaccagatgg acgatacaaa gccacaacaa cctgaggaga acgaggactc tgatccattg  
 421 cctgataact gggaaatggc ctacacagag aagggggaag tctacttcat tgaccataac  
 481 acaaagacaa catcatggct ggatccgcga cttgcgaaaa aggctaacc tccagaagag  
 541 tgcaaagaaa atgagcttcc atatggctgg gaaaaaatcg atgatccctat atatggcact  
 601 tactatgttg accacataaa tagaagaaca cagtttgaaa accctgtcct ggaagcaaaa  
 661 aggaagctac agcaacataa catgccccac acagaacttg gagcaaagcc cctgcaggcc  
 721 ccagggtttcc gagaaaagcc actcttcacc cgggatgcat cccagttgaa gggaaacgttc  
 781 ctacagacca ccctcaaaaa gagcaacatg ggctttgggt ttaccatcat tgggtggagac  
 841 gagccggatg agtttctaca ggtgaaaagt gtgatcccg atgggcctgc cgcacaggat  
 901 gggaaaatgg agacaggtga tgtcattgtc tatattaatg aagtttgtgt ccttggacac  
 961 actctatgca atgttgtcaa acttttccag tctgttccta ttggtcagag tgtcaacttg  
 1021 gtgttgtgtc gtggctaccc tttgcccttt gaccctgaag atcctgtcaa cagcatggtg  
 1081 ccaccctttg caataatgga gaggccacct ccggtgatgg tcaatggaag acataactat  
 1141 gaaacatact tggataacat ttctcgacc tcacagtcgg tcccagatat tacagaccgg  
 1201 ccacctcatt ctttgcactc catgccagct gacggccagc tagatggcac gtatccacca  
 1261 cccgtccatg acgacaatgt gtctatggct tcgtctggag ccactcaagc tgaacttatg  
 1321 accttaacca ttgtgaaagg tgcccaggga tttggcttta ctattgccga cagtcccacg  
 1381 ggacagcggg tgaacaaaat ccttgacatt cagggatgcc ctgggctgtg tgaaggagac  
 1441 ctcatgttg agatcaacca acagaatgta cagaacctga gccatacaga agtagtggat  
 1501 atacttaagg actgccccgt tggaaagtga acttctttaa tcatccatcg aggaggtttc  
 1561 ttttctccat ggaaaactcc aaagcctatg atggaccgat gggagaacca aggcagtcca  
 1621 caaacaagtt tatctgctcc ggccgtccca cagaacctgc cttcccacc tgcccttcac  
 1681 aggagctcct ttcttgattc aacagaggcc tttgaccac ggaagcctga cccatatgag  
 1741 ctctacgaga aatcgagagc catttatgaa agtaggcaac aagtgccacc caggaccagt  
 1801 tttcgaatgg attcctctgg tccagattat aaggaactgg atgttcacct tcggaggatg  
 1861 gagtctggat ttggctttag aatccttggg ggagatgaac ctggacagcc tattttgatc  
 1921 ggagccgtca ttgccatggg ctacagtgac agagacggcc gtctacaccc aggagatgag  
 1981 cttgtctatg tcgatgggat cccagtggtt ggcaagacc accgctatgt catcgacctc  
 2041 atgaccacg cggcccgcga tgggcagggtt aacctcactg tgagaagaaa ggtgctatgt  
 2101 ggaggggagc cctgcccaga gaatgggagg agtccagggt ctgtatcaac tcaccacagc  
 2161 tctccgcgca gtgactatgc cactactcc aacagcaacc acgcccgcac cagcagcaat  
 2221 gcctcacctc ctgaaggctt tgccctcac agcttgcaag ccaagtgtgt ggtcattcac  
 2281 cgcaaagaaa acgaagggtt tggtctcgtc atcatcagct ctctgaacag gcctgagtct  
 2341 ggagccacca taactgtgcc ccataaaatt ggacgaatca ttgatgggag ccttgcagat  
 2401 cgctgtgcca aactcaaagt gggcgaccgt atcttagcag tcaacggcca gtctatcatc  
 2461 aacatgcctc acgctgacat tgtgaagctc atcaaggac ccggtctcag tgtcaccctt  
 2521 cgcacatctc ctacaggagga gctcaacagc ccaacatcag caccagttc agagaaacag  
 2581 agccccatgg cccagcagca cagccctctg gccagcaga gtcctctggc ccagccaagc  
 2641 cccgccaccc ccaacagccc agtcgcacag ccagctctc cccaacctct ccagctgcaa  
 2701 ggacacgaaa atagttacag gtcagaagtt aaagcgaggc aagatgtgaa gccagacatc  
 2761 cggcagcctc cttcacaga ctacaggcag ccccgcctgg actacaggca gccccggga  
 2821 ggagactact cacagcccc acccttggac tacaggcagc actctccaga caccaggcag  
 2881 tacctctgt cagactacag gcagccacag gattttgatt atttactgt ggacatggag  
 2941 aaaggagcca aaggatttgg attcagcatt cgtggaggaa gggaatacaa gatggatctg  
 3001 tatgtgttga gattggcaga ggatgggcca gccataagga acggcaggat gagggttagga  
 3061 gatcagatca ttgaaataaa tggggaaagc acacgagaca tgaccacgc cagagcaata  
 3121 gaactcatca agtctggagg aagaagagt cggtctgtgc tgaagagagg cacggggcag  
 3181 gtcccggagt atggaatggt accttcagc ctctccatgt gcatgaaaag tgacaagcat  
 3241 ggggtcccat atttctactt actgggccac cctaaagaca cgacgaacct cacgcctgga  
 3301 gtgctgcccgc tgcgcgcgc caggcctgc cggaagtag

## MATERIALS AND METHODS

### Figure 2.1. Full-length mouse MAGI-2 $\beta$ /S-SCAM cDNA sequence

The unique binding sequences for the primers are shown in color (red corresponds to **FP-start**, green to **FP-PDZ1**, blue to **RP-PDZ4** and yellow **RP-end**, respectively).

### 2.3.5. Polymerase chain reaction (PCR)

Amplification of DNA fragments was performed in a 50 $\mu$ l reaction mix with thin-walled PCR tubes in a MWG PCR cycler. *Pfu*-Polymerase and the appropriate reaction buffer were obtained from Stratagene. The following reaction mixture was used:

pDEST53-MAGI 2 full	100ng
Primer 1 (100 $\mu$ M)	0.5 $\mu$ l
Primer 2 (100 $\mu$ M)	0.5 $\mu$ l
dNTP (10mM)	1 $\mu$ l
PCR-buffer (10x)	5 $\mu$ l
<i>Pfu</i> -Polymerase	1 $\mu$ l
ddH <sub>2</sub> O	as 50 $\mu$ l

The primer combination was as follows:

S-SCAM full	Primer 1 = FP-start	Primer 2 = RP-end
S-SCAM PDZ1 del	Primer 1 = FP-PDZ2	Primer 2 = RP-end
S-SCAM PDZ5 del	Primer 1 = FP-start	Primer 2 = RP-PDZ4

The PCR was performed with the following step gradient:

1. Initial denaturing	94°C	1min
2. Denaturing	94°C	1min
3. Annealing	$T_m$ -4°C	1min
4. Synthesis	72°C	1min/ 1kb DNA
5. Termination	72°C	10min
6. Cooling	4°C	

The amplification procedure (steps 2-4) was repeated 30 times.

### 2.3.6. DNA gel electrophoresis

(Sambrook and Russell, 2000)

DNA fragments were separated by horizontal electrophoresis chamber (BioRad) using agarose gels. Agarose gels were prepared by heating 1% (w/v) agarose (Gibco) in 1xTAE buffer. The gel was covered with 1xTAE buffer containing etidiumbromide and the DNA samples were pipetted in the sample pockets. DNA sample buffer was added to the probes and the gel was run at constant voltage (10V/cm gel length) until the

## MATERIALS AND METHODS

indicating dye had reached the end of the gel. Finally gels were documented using E.A.S.Y Light UV-light documentation system.

### **2.3.7. Digestion of PCR fragments and the pcDNA3 vector to get sticky ends**

For restriction, the DNA was incubated with 0.15µl HindIII (10U/µl) and 0.15µl XbaI (12U/µl), 2µl Buffer Y++, 2.5µl DNA obtained from miniprep. in 20µl end volume.

### **2.3.8. Dephosphorylation of plasmid DNA**

After restriction the plasmid DNA was purified using MinElute PCR Purification Kit (Qiagen) and 1U *SAP* (scrims alkine phosphatase) per 100ng plasmid DNA were added. The reaction was incubated at 37°C for 2 hours and terminated by incubation at 70°C for 10 min. The plasmid DNA was used for ligation without further purification.

### **2.3.9. Ligation of DNA fragments**

Ligation of DNA fragments was performed by mixing 50ng vector DNA with the fivefold molar excess of insert DNA. 1µl of T4 Ligase and 2µl of ligation buffer were added and the reaction mix was brought to a final volume of 20µl. The reaction was incubated for 2 hours at room temperature. The reaction mixture was used directly for transformation without any further purification.

After ligation, TOP10 competent bacteria were transformed with the ligation product and incubated overnight on LB with Ampicilin plates. The second day 2 colonies for each ligation construct were picked and grown in 3 ml LB/Amp medium. The plasmids were purified using the Miniprep kit and were subject to enzymatic restriction (*HindIII* and *XbaI*) to check for the insert DNA in each colony.



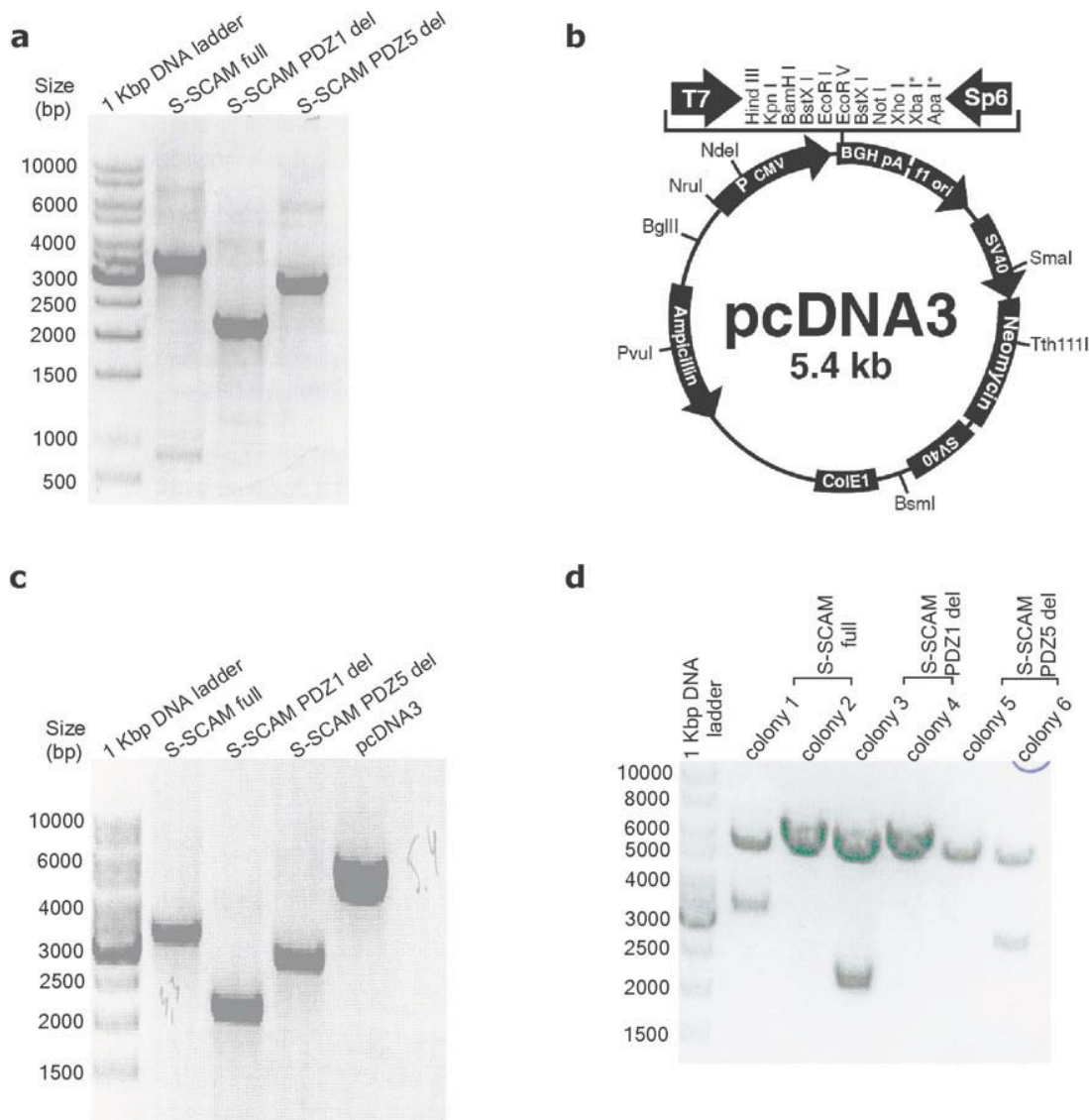


**Figure 2.2. Generation of mutant S-SCAM constructs**

**(a)** PCR amplification of the different S-SCAM sequences. PCR amplification of full length S-SCAM (3.3kb), S-SCAM PDZ1 deleted (2.1kb) and S-SCAM PDZ5 deleted (2.9kb) using the pDEST53-MAGI 2 full as template. **(b)** Restriction map of the pcDNA3 vector (Invitrogen). **(c)** Enzymatic restriction of the different S-SCAM amplicons and the pcDNA3 vector. The PCR fragments (S-SCAM full - 3.3kb, S-SCAM PDZ1 del - 2.1kb, S-SCAM PDZ5 del - 2.9kb) and the pcDNA3 (5.4kb) vector were subject to enzymatic digestion and gel electrophoresis **(d)** Enzymatic restriction of plasmids isolated from 6 different colonies transformed with S-SCAM full, S-SCAM PDZ1 del and S-SCAM PDZ5 del. Plasmids of 2 colonies for each ligation construct were digested with *HindIII* and *XbaI*. Colonies 1, 3, and 6 contain the DNA insert corresponding to S-SCAM full, S-SCAM PDZ1 del and S-SCAM PDZ5 del, respectively. The other colonies contain only the plasmid without any insert.

### 2.3.10. DNA sequencing

Plasmids for colonies 1, 3 and 6 were sent for sequencing at GATC Company (www.gatc.de). For preparation, 1 µg of DNA was diluted in 30 µl water and 1 µl of the appropriate sequencing primer (10 pM) was added.

### 2.3.11. Determination of DNA concentrations

DNA concentrations were determined spectroscopically using an Amersham-Pharmacia spectrometer. The absolute volume necessary for measurement was 50 µl. For determining the concentration of DNA preparations, the eluate was diluted 1:50 with water and the solution was pipetted into a 50 µl cuvette. Concentration was determined by measuring the absorbance at 260 nm and 280 nm. Absorbance at 260 nm had to be higher than 0.1 but less than 0.6 for reliable determinations. A ratio of  $A_{260}/A_{280}$  between 1.8 and 2 indicated a sufficient purity of DNA preparation.

## 2.4. Proliferation and differentiation of mouse ES-cells

### 2.4.1. Generation of mouse N-cadherin deficient ES cell lines

(Moore et al., 1999)

The mouse N-cadherin gene consists of 16 exons that spread over >200 kb of genomic DNA. This large size of the N-cadherin gene, compared with its cDNA (4.3 kb) is ascribed to the fact that the first and second intron are 34.2 kilobases and >100 kilobases long, respectively. The N-cadherin gene is localized on the mouse chromosome 18 (Miyatani et al., 1992). For targeted disruption of the N-cadherin gene, homologous recombination between a targeting vector and the wild-type allele of D3 ES-cells has been employed (Radice et al., 1997). The targeting vector contained a neomycin phosphotransferase (neo) expression cassette inserted in exon 10. This disrupts the open reading frame of the N-cadherin gene in the extracellular domain of the protein. The vector included also genomic sequences 5' and 3' of the neo gene and a flanking herpes simplex virus thymidine kinase expression cassette (HSV tk) as a promoter and for negative selection.

## MATERIALS AND METHODS

The linearized targeting vector has been electroporated into D3 ES cells, and the electroporated cells were subjected to positive/negative selection using G418 and ganciclovir (Radice et al., 1997). The double resistant clones were analyzed by Southern blot and enzymatic restriction to confirm that the homologous recombination took place at the N-cadherin locus and no rearrangements had occurred. The targeted clones were injected into host C57Bl/6 blastocysts, and the blastocysts were transferred to the uteri of pseudopregnant females. In order to generate N-cadherin  $-/-$  ES cells, mice heterozygous for the N-cadherin mutation were mated *inter se* and blastocysts from embryonic day 3.5 were isolated and the inner cell mass was expanded in culture by repeated passages. The N-cadherin genotype of ES cells was assigned by Southern blot analysis (Moore et al., 1999).

Homozygous N-cadherin knockout and littermate heterozygous N-cadherin control ES cell lines (Moore et al., 1999) were kindly provided for this study by Dr. R. Kemler, MPI Immunobiology, Freiburg.

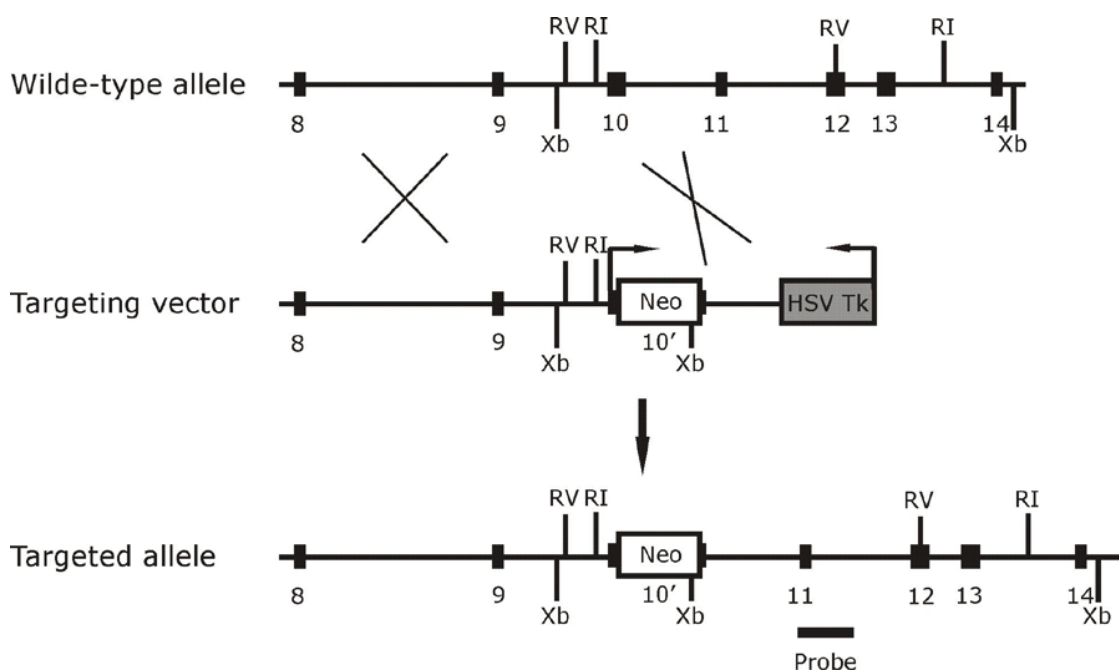


**Figure 2.3. Targeted disruption of the N-cadherin gene** (modified after Radice et al., 1997)  
Schematic representation of the wild-type allele, the targeting vector and the targeted allele of the N-cadherin gene. Exons are represented as black boxes and the restriction endonucleases sites are shown. The neomycine resistance cassette and thymidine kynase cassette are designated Neo and HSV tk, respectively. The probe used for screening ES cells clones and genotyping mice is shown (Probe).

### 2.4.2. Preparation and culturing of embryonic mouse fibroblasts (feeder cells)

Embryonic feeder (EF) cells serve as a basal layer for ES cells and supply important metabolites. For obtaining EF cells, a 13 to 14 embryonic day (ED) pregnant C57BL/6 mouse was sacrificed by CO<sub>2</sub> exposure and the uterus was dissected out by making an incision across the abdomen. The embryos were isolated from the uterus and released from their embryonic sacs. After removal of embryo's head, limbs, intestines, heart and spinal cord, the embryo carcass was finely minced using a scalpel and incubated for 5 minutes in 5 ml Trypsin/EDTA (Invitrogen) at 37°C and 5 % CO<sub>2</sub>. The enzymatic reaction was stopped by adding 5 ml EF-Medium. The Trypsin containing medium was removed and the tissue pieces were mechanically dissociated in 2 ml fresh EF-Medium. The cell suspension was then transferred to a 175 cm<sup>2</sup> Nunc culture flask with 40 ml EF-Medium and cultured in the incubator (37°C and 5 % CO<sub>2</sub> and 95% humidity). The medium was changed after 24 h and the cells were grown until confluency.

The confluent layer of EF-cells was washed with PBS<sup>-/-</sup> (PBS without Ca<sup>2+</sup> and Mg<sup>2+</sup>, Invitrogen) and then cells were incubated in 8 ml Trypsin for 5 min at 37°C. The enzymatic reaction was stopped with 5 ml EF-medium and the cell suspension was transferred into a 15 ml Falcon tube and centrifuged at 800 rpm for 5 minutes. The pellet was then resuspended in 1.5 ml EF-medium. This cell suspension was either used for further culturing, by splitting it into three 25 cm<sup>2</sup> gelatin treated culture flasks with 5 ml EF-medium, or was frozen in liquid nitrogen for later use. For storage purposes, 0.5 ml of cell suspension was aliquoted into cryovials with 0.5 ml Freezing medium (60% EF-medium + 20% FCS + 20% DMSO). The cells were then frozen immediately at -80° C and transferred to liquid nitrogen the next day.

The EF cells cultured in 25 cm<sup>2</sup> flasks were used after 3-4 days for ES-cell culturing. Before ES-cells are plated, feeder cells must be inhibited in their growth capacity by chemical treatment with Mitomycin C. For this, the cells were incubated for 2 h (37°C and 5 % CO<sub>2</sub>) with EF-medium containing Mitomycin C (1mg/5ml Mitomycin C in PBS added to 200 ml EF-medium). After incubation, the cells were washed 4 to 5 times with PBS and were ready to use for ES-cell culturing.

### 2.4.3. Proliferation of mouse ES cells

Proliferating mouse ES cells were cultured on mouse embryonic feeder cells (inactivated with mitomycin C) in the presence of Leukemia Inhibitory Factor (LIF). LIF acts to inhibit spontaneous differentiation and therefore maintains the pluripotent phenotype of murine ES cells.

$1 \times 10^6$  ES cells/culture flask ( $25\text{cm}^2$ , Nunc) were plated on a monolayer of EF cells in 5 ml ES medium and incubated at  $37^\circ\text{C}$ , 5 %  $\text{CO}_2$  and 95 % humidity. 24 hours after plating the medium was changed to fresh ES medium. After 2-3 days, ES cell cultures became crowded with large colonies. At this point, the ES cells were passaged at 1:2 ratio without feeders, on gelatin coated flasks ( $25\text{cm}^2$ , Nunc). To passage ES cells, the ES cell medium was removed and plates were washed twice with PBS -/- and then the cells were incubated for 5 min at  $37^\circ\text{C}$  with 3 ml Trypsin-EDTA. The enzymatic reaction was stopped by adding 5 ml ES medium. The ES cell aggregates were dislodged from the bottom of the flask and dissociated to a single cell suspension. This cell suspension was centrifuged for 1 minute at 2000 rpm and then the cell pellet was resuspended in 1 ml ES medium containing LIF. 0.5 ml were added to each gelatinized culture flask containing 5 ml ES cell medium. The ES cells were then transferred into the incubator.

### 2.4.4. In vitro differentiation of mouse ES cells

The generation of neurons from ES cells was done using an embryoid body (EB) system. ES cells cultured without feeders (as in the previous paragraph) were further deprived of feeder cells by incubating 2 times, 20 minutes,  $3 \times 10^6$  cells in one tissue culture dish (100 mm diameter, Sarstedt Inc, Newton, NC) containing 10 ml ES medium with LIF. During the 20 minutes incubation only the feeders attached to the dish, while the ES cells remained in suspension. After this feeder deprivation treatment, the ES cell suspension was cultured on a gelatine coated petri dish. After the cells had reached confluency, they were used to form EBs. For this, the ES cells were dissociated with Trypsin-EDTA and a defined number ( $0.75 \times 10^6$ ) of cells was incubated in nonadhesive bacterial dishes (92 mm, Sarstedt, Germany) for 6-8 days in serum replacement (SR) medium. During this time ES cells form cellular aggregates (embryoid bodies) that grow in suspension. These EBs were then collected and redistributed in 4 Falcon dishes (35 mm, Falcon) with 2 ml

differentiation medium containing retinoic acid ( $5 \times 10^{-7} \text{M}$ , Serva) which triggers neuronal differentiation. After 2-3 days incubation the EBs from each Falcon dish were redistributed in 5 Falcon dishes containing NB+ medium and incubated for further 2-3 weeks.

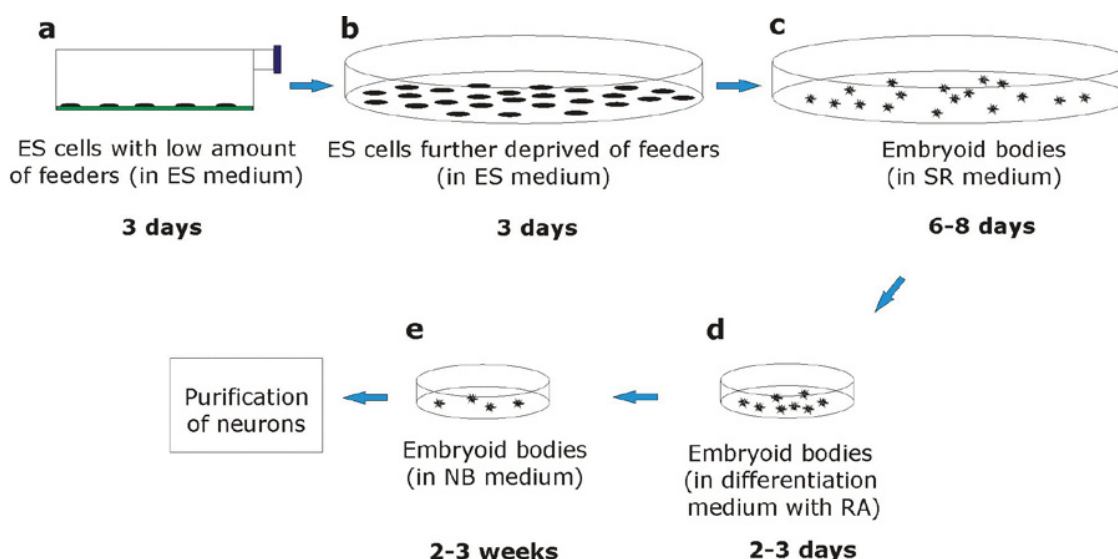


**Figure 2.4. Schematic representation of the neuronal differentiation procedure**

ES cells cultured on (a) low amount of feeders are further (b) deprived of feeders. (c) ES cells on non-adherent bacterial dishes form cellular aggregates (EBs) that grow in suspension. (d) EBs are cultured for 2-3 days in the presence of RA. (e) EBs are redistributed and allowed to attach by culturing them in NB medium. After 2-3 weeks EBs were used for immunoisolation of neurons.

## 2.5. L1-immunoisolation and glial microisland culture

### 2.5.1. Purification of neurons by L1-immunoisolation

In vitro differentiation of ES cells within the EBs can partly be controlled by specific cultivation protocols to yield preferentially neurons. However, in vitro differentiation produces heterogeneous cell populations and does not lead to the desired pure population of a single cell type. The L1-immunoisolation technique is a purification procedure for ES cell-derived neurons based on the neuron specific expression of the cell adhesion molecule L1 (Jüngling et al., 2003).

## MATERIALS AND METHODS

For L1-immunoisolation, a non-adherent bacterial dish was coated with a goat anti-rat IgG (80 µl antibody, 1.3 mg/ml – Jackson Immunoresearch Laboratories, West Grove, PA) in 10 ml Tris/HCl pH 9.5 and incubated overnight at 4 °C. The dish was then 3 times rinsed with PBS and incubated overnight at 4 °C with 10 ml of supernatant from a rat anti-L1 antibody (1 µg/ml) producing hybridoma cell line.

EBs from NB medium were collected in 15 ml Falcon tubes and incubated in 10 ml EBSS medium (+ 1.5 mM CaCl<sub>2</sub>, + 1 mM MgCl<sub>2</sub>, + 1 ml EDTA) containing 120 µl Papain (Worthington, Cell Systems, Germany) and 200 µl Desoxyribonuclease I (1 mg/ml in H<sub>2</sub>O, stock solution – Sigma, Germany) for 50 minutes at 37 °C, 5% CO<sub>2</sub>. The EB solution was then shortly centrifuged and the enzymatic reaction was stopped with 4 ml 0.15 % trypsin inhibitor /ovomucoid (Roche, Germany) in PBS and EBs were mechanically dissociated in 0.15 % trypsin inhibitor /ovomucoid in PBS plus DNaseI. After centrifugation (2000 rpm, 1 minute), cells were resuspended in 1 % trypsin inhibitor /ovomucoid in PBS. After another centrifugation step, cells were resuspended in 0.02 % bovine serum albumine (BSA) solution in PBS with 0.25 % FCS. The L1-coated dish was 5 times rinsed with PBS and the cell suspension in BSA solution was added. Immunoisolation was performed at room temperature for 1.5 h. Then, nonadherent cells were washed off with PBS (4-5 washing steps). Adherent cells were harvested using trypsin/EDTA for 3 minutes at 37 °C and were suspended in 25 % FBS in PBS to block trypsin activity. Cells were centrifuged and then resuspended in 1 ml NB medium and were seeded on glia microislands.

### **2.5.2. Culture of ES cell-derived neurons on glial microislands**

L1-selected ES cell-derived neurons were seeded on glial cells in a microisland system (Lessmann and Heumann, 1997) for obtaining a high percentage of autapses. Glial cells were obtained from C57BL/6 mice at postnatal day 0-2. After the mice had been decapitated, the brain was removed and placed in ice cold PBS. Under a binocular (Zeiss), both cortical hemispheres were separated and finely minced using a scalpel. The cortical pieces were then incubated with 0.1 % Trypsin in PBS at 37 °C for 5 minutes. The enzymatic reaction was stopped by adding serum-containing medium [BME<sup>+</sup> medium: Eagle's basal medium with addition of insulin, L-glutamine, glucose and 10% fetal



## MATERIALS AND METHODS

bovine serum (Invitrogen, Carlsbad, CA)]. After mechanical dissociation, the cell suspension was transferred into a 25 cm<sup>2</sup> culture flask with 5ml BME+ medium. The second day the medium was changed to fresh BME+ medium. The culturing of proliferating cells was done for several weeks, until the confluent glial cells were completely devoid of neurons.

To prepare glial microislands, the confluent glial cells were incubated in Trypsin/EDTA, dissociated to single cells and seeded at low density on uncoated glass bottom dishes (Willco Wells B.V., Amsterdam, The Netherlands) in BME<sup>+</sup> medium and cultured 4-6 days (DIV) in the presence of cytosine- $\beta$ -D-arabinofuranoside (10 $\mu$ M) to inhibit proliferation. ES cell-derived, L1 selected neurons were seeded on these glial microislands at a density of 2x10<sup>5</sup> cells/35mm<sup>2</sup> dish and were cultured in Neurobasal medium (Invitrogen) with additional B27 supplement, glutamax and penicillin/streptomycin, leading to the formation of neuronal networks of 10-15 neurons.

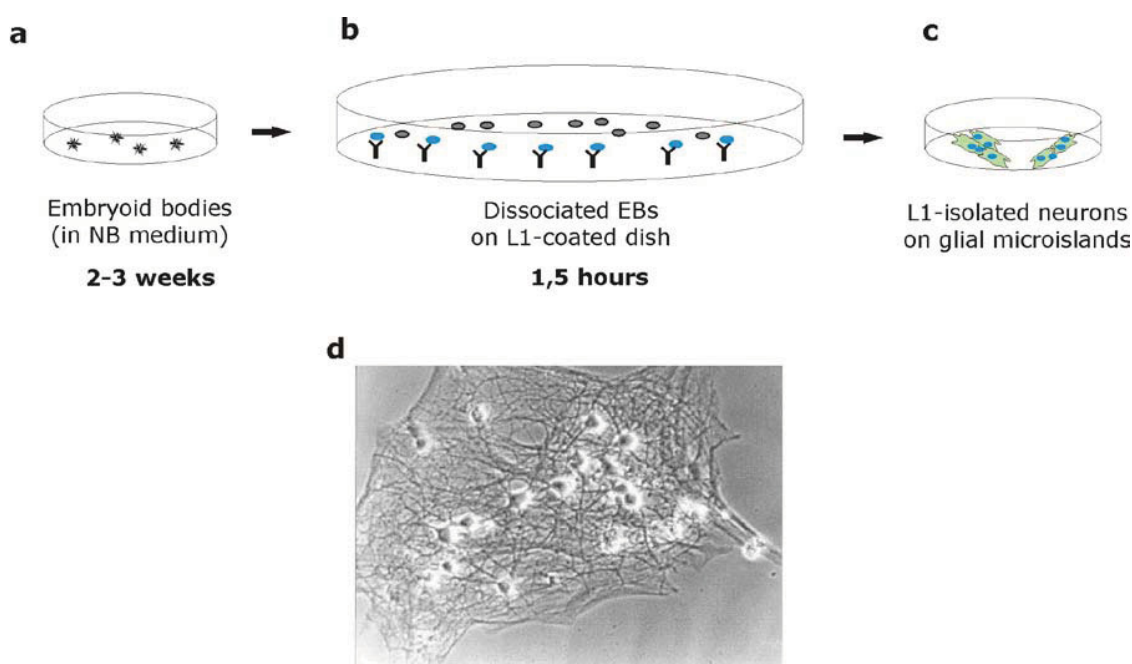


**Figure 2.5. Schematic representation of purification of ES cell-derived neurons**

(a) EBs were mechanically dissociated to a single cell suspension and incubated onto a L1 coated dish. (b) The neurons (blue circles) bind to the L1 antibody, while the other cell types (grey circles) remain in suspension and can be washed away. (c) The L1- isolated neurons were seeded on glial microislands. (d) Phase contrast image of a glial microisland on which several neurons had formed a synaptic network.



### 2.6. Transfection of ES cell-derived neurons and cortical neurons

Lipofectamine 2000 reagent is a cationic lipid-based transfection reagent. The cationic lipids interact with the DNA molecules in aqueous solution to form micelles or liposomes. These lipid-nucleic acid complexes fuse with the membrane, become internalized and subsequently expressed in the cell.

3µl Lipofectamine 2000 were mixed with 50µl Opti-MEM and incubated for 5 minutes at room temperature. The DNA for transfection (varying from 1.5 to 7.5µg for one glass bottom dish) was added to another 50µl Opti-MEM. After 5 minutes incubation the diluted DNA was combined with diluted Lipofectamine 2000 (total volume = 100µl), gently mixed and incubated for 20 minutes at room temperature. 800µl culturing medium from the cells (conditioned medium) were added to the DNA-Lipofectamine complexes while the rest of the culture medium (1200µl) was saved for later use. The DNA-Lipofectamine complex in medium was transferred to the cells and gently mixed by rocking the dish back and forth. The cells were incubated at 37 °C in a CO<sub>2</sub> incubator for 6-7 hours and then the medium was replaced with fresh 800µl NB-medium + 1200µl culture medium, which was previously saved and the cells were returned to the incubator. The cells were tested for transgene expression 2 days after transfection.

Two different maturational stages of cultured neurons were analyzed in this study: immature neurons – 4-5 days in vitro (DIV) at the time of transfection, and more mature neurons – 8-12 DIV at the time of transfection.

### 2.7. Time lapse imaging of living cells

For time lapse imaging, live cells in culture medium were mounted in an incubation chamber at 37°C through which a continuous flow of 5% CO<sub>2</sub> was passed. Images were obtained with an Axiovert 200M (Zeiss) deconvolution microscope using a 63X oil immersion objective with an objective heater and a 12bit monochrome *CoolSNAP ES* CCD camera (Visitron Systems). To correct for out-of-focus clusters in field of view, Z-stacked images at 1µm depth intervals were taken every 20min. The cells were allowed to equilibrate for a period of at least 30 minutes before they were subjected to imaging. Images were acquired automatically using a time lapse protocol (“journal”) written in MetaMorph with an exposure time of 0.2s having the UV lamp aperture minimum

## MATERIALS AND METHODS

opened and a binning of 2x2 for both the EGFP and the DsRed signal. With these settings the synapse dynamics could be observed for a time period of 2 hours without any significant bleaching.

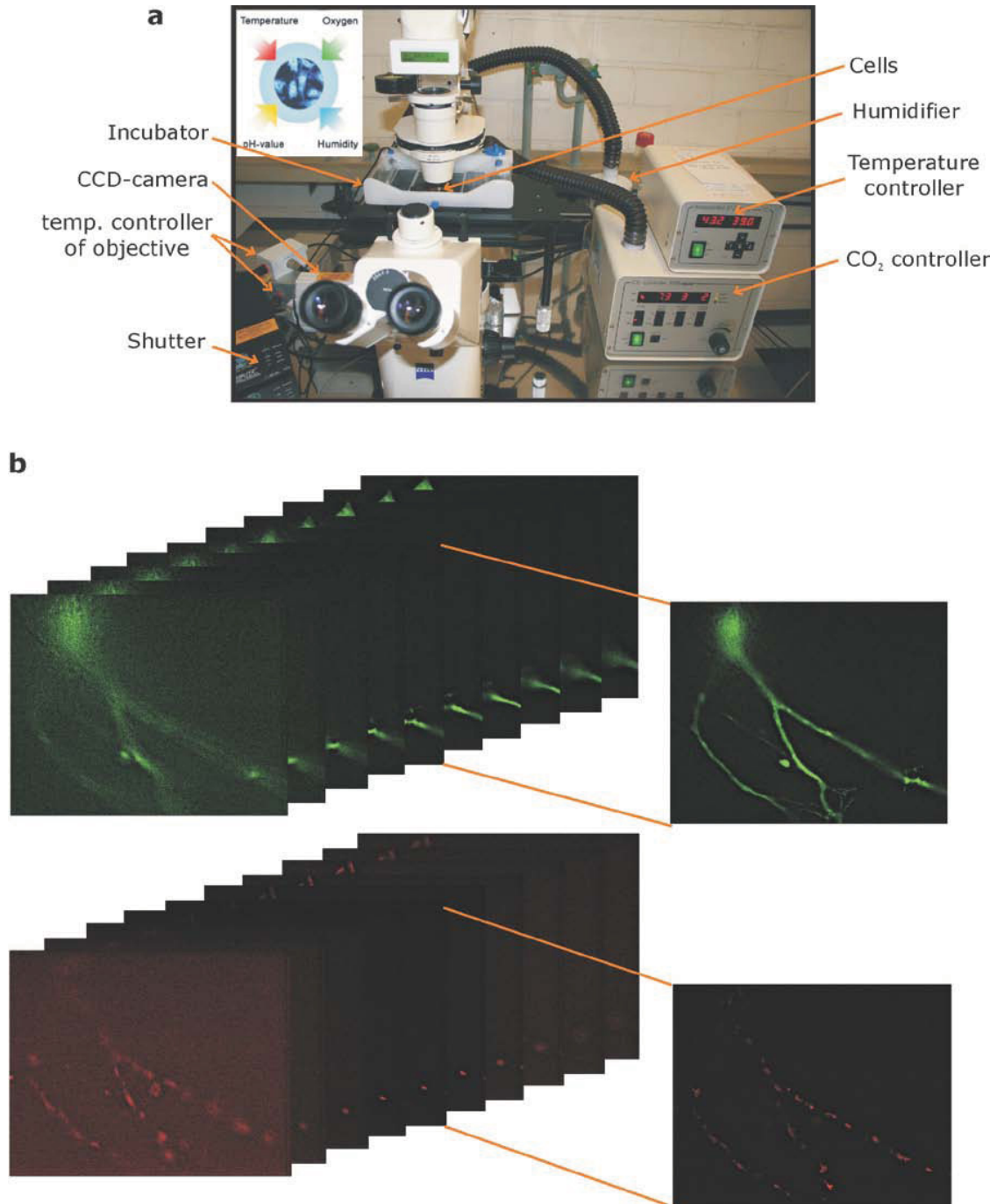


### **Figure 2.6. Time lapse imaging set-up and fluorescence image acquisition**

(a) An Axiovert 200M inverted Zeiss microscope equipped with a Charged-Coupled-Device (CCD) camera was connected to a computer and a small incubator for keeping the cells under constant levels of temperature, oxygen, pH value and humidity. (b) z-stacks of a co-transfected neuron were acquired simultaneously for the EGFP and the DsRed signal with 1  $\mu$ m distance between the adjacent planes. One plane from both the EGFP and the DsRed2 signal, located at the same z distance, is shown separately for better visualization.

### **2.8. Fluorescence Recovery After Photobleaching (FRAP)**

FRAP experiments consist of photobleaching a small region of interest and then observing the recovery of fluorescence in the bleached area. The observation of recovery indicates that the fluorescently labeled molecules or vesicles are mobile. The rate of recovery is an indication of the speed at which the molecules or vesicles are moving.

To perform a FRAP experiment a laser scanning microscope (LSM510 system consisting of an Zeiss Axiovert 200M inverted microscope equipped with a 488nm Argon laser) was used. During imaging the neuronal cultures were kept in a HEPES-buffered culture medium and the temperature was kept constant at 37°C by using an incubator chamber (Incubator XL, Zeiss, Germany) built on the microscope.

Neurons expressing EGFP-VAMP2 were visualized using the 488nm Argon laser line and a fluorescein filter set. To resolve synaptic structures a 63X oil immersion objective (Plan-Apochromat, Zeiss, Germany) was used with an additional electronic zoom factor of 2-4. Images were collected using a *CoolSNAP ES* CCD camera (Visitron Systems). To correct for out-of-focus clusters in field of view, Z-stacked images (10-15 optical sections with a 512x512 pixel array) at 1  $\mu$ m depth intervals were collected every 5 minutes using the LSM 510 software. Laser illumination was attenuated to 25% of the laser power and the detector pinhole was opened (1.5 Airy disc) to improve light collection. The detector gain was adjusted to permit detection of weak diffuse EGFP fluorescence as well as intensely fluorescent clusters.

For processing of time lapse images, optical sections were reconstructed off-line into single two-dimensional projection images for each time point using a maximum brightness operation of the MetaMorph software (Visitron Systems, Germany).

Photobleaching was performed by defining a region of interest around a single synaptic bouton and 150 frames were scanned with 100% of the laser power within the selected

bleaching area to effectively bleach the fluorescent molecules close to the background level.

FRAP data were normalized and corrected for ongoing photobleaching according to the following equation.

$$F_{cor_t} = (F_t / F_0) / (Fnb_t / Fnb_0)$$

Where  $F_t$  is the fluorescence at time  $t$ ,  $F_0$  is the prephotobleaching fluorescence,  $Fnb_t$  is the average fluorescence intensity of 2-4 nonbleached puncta at time  $t$  and  $Fnb_0$  is the average fluorescence intensity of the same nonbleached puncta at time  $t = 0$ .

## 2.9. Digital image processing

### 2.9.1. Deconvolution

(AutoDeblur Deconvolution Software, Visitron Systems)

Deconvolution is a computational method used to reduce out-of-focus fluorescence in three-dimensional (3D) microscope images. When it is applied to improve images from conventional fluorescence microscopes it has the advantage that it can be accomplished at very low light levels, thus enabling multiple focal-plane imaging of light sensitive living specimens over longer periods of time compared with confocal microscopy, where the amount of excitation light is very high.

Deconvolution methods determine how much out-of-focus light is expected for the optics in use and then seek to redistribute this light to its points of origin in the specimen. The characterization of out-of-focus light is based on the 3D image of a point source of light, the so called point-spread function (PSF). The image of a point source is never a point source, even if a perfect lens were used. The reason is that the aperture of any lens is finite and therefore fails to collect all the light emitted from the point source and consequently can not form a perfect image. Instead, a 3D image results in the form a double cone with tips meeting at the point source.

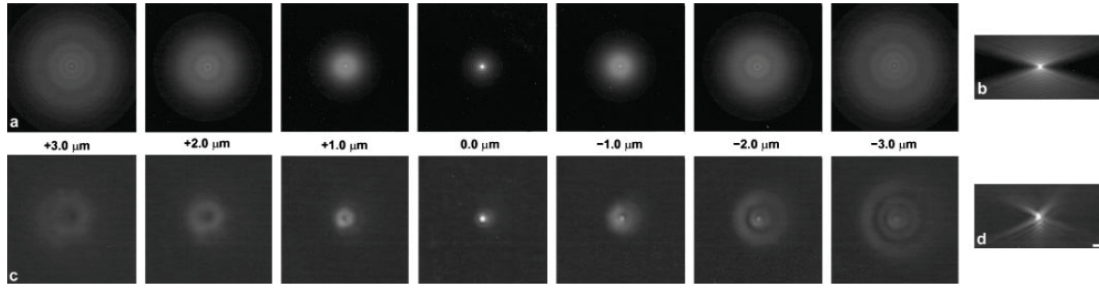


**Figure 2.7. Example of sequential focal planes through a theoretically or experimentally determined point-spread function of a 100X, 1.35 NA Olympus UplanApo objective (after . McNally et al., 1999).**

Distances above and below focus are shown for  $+3.0\mu\text{m}$  to  $-3.0\mu\text{m}$ . One can notice that for both the (a) theoretical and (c) experimental PSF rings increase in number and diameter as the microscope focal plane moves further away from the point source, a fluorescent microsphere ( $0.0\mu\text{m}$  corresponds to in focus). When viewed from the side (an XZ view) the PSF forms a double cone (b, theoretical PSF and d, experimental PSF). For the experimental PSF the asymmetry in ring patterns arises from spherical aberration of this objective

Deconvolution algorithms are derived from a mathematical formula, which describes the imaging process on a microscope. In the simplest form, the formula for microscope-image creation incorporates two known quantities, namely  $PSF(X,Y,Z)$  and the measured blurred 3D image,  $B(X,Y,Z)$  and one unknown quantity, namely the actual distribution of light in the 3D specimen,  $S(X,Y,Z)$ . These terms are related by the imaging equation

$$B(X,Y,Z) = S(X,Y,Z) \odot PSF(X,Y,Z),$$

where the symbol  $\odot$  represents the mathematical operation known as convolution. The convolution essentially shifts the PSF so that it is centered at each point in the specimen and then sums the contributions of all these shifted PSFs. Both the  $B(X,Y,Z)$  and  $PSF(X,Y,Z)$  can be determined, and so the process of solving  $S$  has become known as deconvolution.

The z-stacks acquired with MetaView were imported in the AutoDeblur software and were subject to 3D deconvolution, using the Blind Deconvolution Algorithm. In this algorithm the point spread function (PSF) is considered unknown and is estimated only by the optics in use and from the information within the data set,  $B(X,Y,Z)$ . This is done by first assuming a  $PSF(X,Y,Z)$ , then (1) estimating which  $S(X,Y,Z)$  could have caused

$B(X,Y,Z)$ . This calculation is followed by (2), estimating which  $PSF(X,Y,Z)$  could have caused  $B(X,Y,Z)$  from the estimated  $S(X,Y,Z)$ , and then steps (1) and (2) are repeated again and again. It is conceivable that the PSF information is in the data, because one often sees the light spreading from fine point structures in the data, and this spreading makes up the PSF.

### 2.9.2. Maximum operation in MetaMorph

Using the Maximum operation, a deconvolved image stack is projected along the axis perpendicular to the image plane (the so-called "z" axis). Maximum intensity projection creates an output image each of whose pixels contains the maximum value over all images in the stack at the particular pixel location.

### 2.9.3. Autothreshold operation in MetaMorph

Autothreshold uses the histogram data to heuristically (by trial-and-error) determine the optimum threshold value for the image. It assumes that there is a peak at the background intensity level, which has a width based on noise or other image variations. A 3-tier approach is taken. First the largest peak is found and assumed to be the background. A search is done for the local minimum. The minimum is assumed to be the trough between the background and the object level. If the local minimum is found then the number of pixels selected by the threshold is calculated. If no local minimum was found, or if less than 1% of the pixels are above the threshold then it is assumed that the major peak was actually the object data and the search is done for an earlier peak. If no early peak is found (one smooth curve) the code defaults to using the standard deviation from the image as an estimate for noise. Pixels beyond two times standard deviation from the peak are determined to be from object data.

For the Autothreshold operation to perform better, the soma of the neurons was always excluded from the image analysis. For this, regions located on the proximal dendrites were cut out from the original Maximum image and the Autothreshold function was applied.

#### 2.9.4. Low pass filter operation

A low pass filter operation was used to remove image components with high frequency. "High frequency" details are those where there is rapid change from pixel to pixel. The low pass filter operation attenuates the image noise and produces a smoothed image. A filter is a mathematical transformation (called a convolution product) which allows the value of a pixel to be modified according to the values of neighboring pixels, with coefficients, for each pixel of the region to which it is applied. This spatial convolution blurs the edges within an image or region of interest by using an averaging convolution operation to create a "moving average" of regional intensity values within the image data. The numerical average is calculated for the intensity of pixels in a region of a user-specified size and centered on the pixel being processed. This is done for each pixel in the image.

The Low Pass Filter operation was applied to remove individual pixels from the background noise left in the image after the Autothreshold operation has been applied.

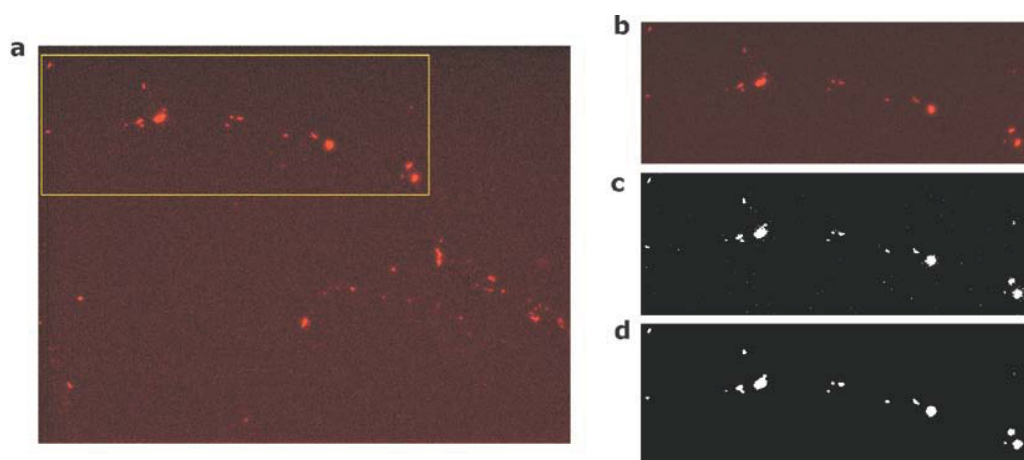


**Figure 2.8. Autothreshold and Low Pass Filter operation**

(a) Maximum projection image of a DsRed2-VAMP2 z-stack. The boxed area represents the region on the proximal dendrite that will be used for analysis. (b) Region cut from image in (a). (c) Thresholded image, after the autothreshold operation was applied on the region in (b). (d) Low Pass image, after the single pixel noise was removed using the low pass filter operation.



### **2.9.5. Integrated morphometry analysis**

The Integrated morphometry analysis command was used to perform automatic morphometric measurements of objects in the Low Pass images. The parameters selected for the measurements included area and mean intensity of the clusters. Additionally, classifier filters were defined, which restrict the measurements only to clusters which were bigger than 8 pixels in size. After measurements the data were logged in MS Excel files and then imported in Sigma Plot for further analysis.

### **2.9.6. Background subtraction**

For obtaining the mean fluorescence intensity of the background, a region of approximately 200 pixels was defined outside of the dendrite in the Low Pass image and the average fluorescence intensity was measured. In Sigma Plot, this value was subtracted from the individual pixels analyzed.

### **2.9.7. Colocalization of clusters**

For analyzing the colocalization of clusters, the function “Create regions around objects” was used with Low Pass images for the two different wavelengths. This operation traces the outlines of objects automatically in the current image by determining the edges of objects based on the distribution of the thresholding overlay and will draw a region of interest around each object. If the regions belonging to the two fluorescent signals were presenting overlapping pixels, then the objects were considered to be colocalized.

### **2.10. Data analysis and statistics**

For calculations and statistical analysis data were imported to the software “Excel” (Windows) or „SigmaPlot 9.0“ (Jandel Scientific). All data are given as mean  $\pm$  standard deviation (SD). Statistical analysis was carried out with the “Student’s t-test“. Illustration of images and figures was performed using the software “CorelDraw 12.0” (Corel, Unterschleißheim, Germany).



### 3. Results

#### 3.1. Role of N-cadherin in the formation of presynaptic specializations in immature neurons

Cadherins are among the first molecules to be detected at the axon-filopodial contact site and they persist in mature synapses (Jontes et al., 2004; Togashi et al., 2002), where they are thought to keep the pre- and postsynaptic specializations closely aligned (Bozdagi et al., 2004). This makes cadherins attractive candidate molecules in initiating and controlling synapse formation and maturation in mammalian central neurons. However, the potential role of N-cadherin in regulating synapse formation has remained elusive.

To study the role of N-cadherin in the formation of presynaptic specializations, immature homozygous N-cadherin deficient ES cell-derived neurons (N-cad<sup>-/-</sup>) and immature heterozygous N-cadherin (N-cad<sup>+/-</sup>) control ES cell-derived neurons were used. The neuronal differentiation from embryonic stem cells circumvented the early embryonic lethality of mice genetically null for N-cadherin (Radice et al., 1997). In this study N-cadherin heterozygous neurons were used as control because they have a similar N-cadherin expression level as the wild type (N-cad<sup>+/+</sup>) and have the advantage of a similar genetic background as N-cad<sup>-/-</sup> neurons, because they were isolated from littermate blastocysts (Moore et al., 1999; Jungling et al., 2006). The ES cell-derived neurons were grown for 6-7 days in vitro (DIV) on glial microislands (10-15 neurons on a glial island growing in complete separation from other islands) and were analyzed at this immature maturational stage which is characterized by intense *de novo* synaptogenesis.

##### 3.1.1. Co-transfection of individual ES cell-derived neurons

To investigate the role of N-cadherin in regulating presynaptic vesicle accumulation during synapse formation and maturation, vectors coding for the fusion protein DsRed2-VAMP2(synaptobrevin2; vesicle membrane protein) for labeling presynaptic vesicles and for EGFP for visualization of dendrites were co-transfected in individual N-cadherin knockout neurons and control neurons. Similarly, for studying active zone formation (see Chapter 3.1.3. and 3.2.2.) neurons were co-transfected with vectors coding for the fusion protein EGFP-Bassoon for labeling the active zones and for DsRed2 for visualization of dendrites. Using Lipofectamine 2000 reagent as a vehicle to deliver the constructs inside

## RESULTS

the neurons, commonly only one neuron per microisland was transfected and most DsRed2-labeled vesicle clusters were localized on EGFP-expressing dendrites of the same neuron in both mature (Fig. 3.1) and immature neurons [or EGFP-Bassoon clusters were localized on the DsRed2-labeled dendrites, respectively (not shown)]. For investigation of immature neurons the cells were co-transfected with the constructs at 4-5 DIV and were imaged two days later; for investigation of mature neurons (see 3.2) co-transfection was done at 8-12 DIV and imaging again two days later.

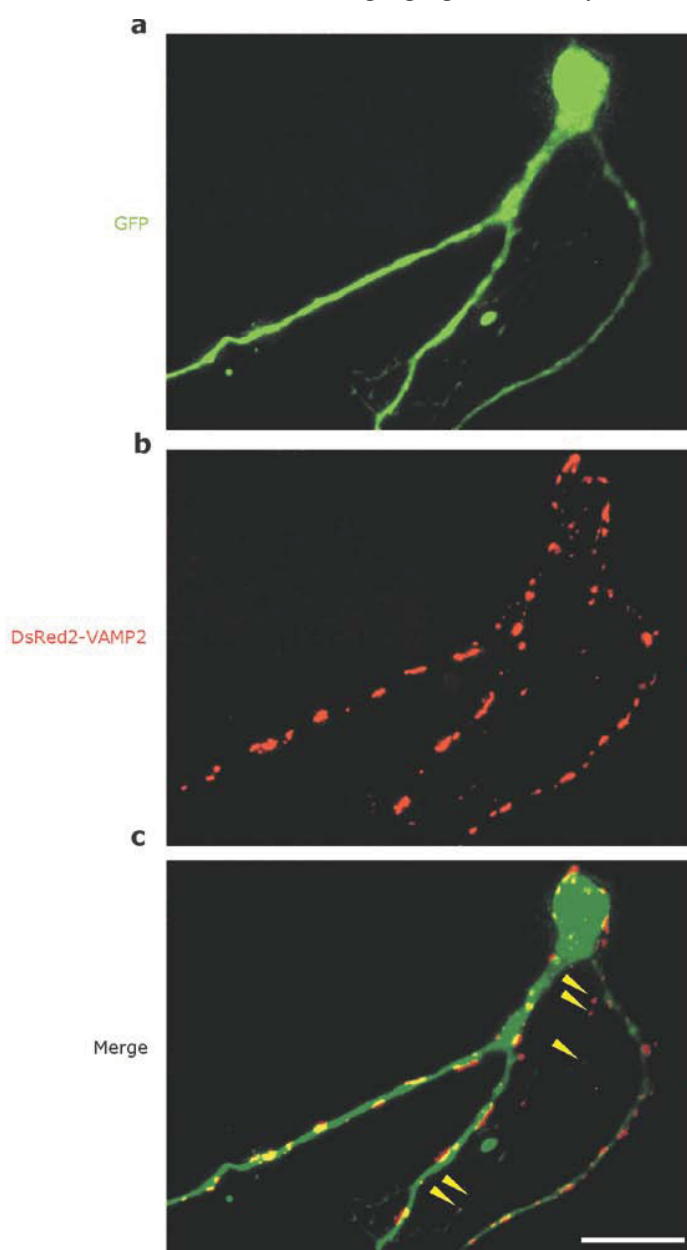


**Figure 3.1. Co-transfection of EGFP and DsRed2-VAMP2 in the same neuron**

Fluorescence images of a co-transfected ES cell-derived neuron (14 DIV). **(a)** EGFP (green) is expressed in the cytoplasm of the neuron, labeling soma and neuronal processes. **(b)** DsRed2-VAMP2 (synaptobrevin2) (red) has a punctate distribution corresponding to vesicle clusters. **(c)** Overlay image showing that the majority of the DsRed2-VAMP2 labeled vesicle clusters are localized on the neuron's dendrites expressing EGFP (yellow). Some DsRed2-VAMP2 puncta are localized on faintly fluorescent EGFP labeled axons (arrowheads) and represent either transport packages or presynaptic components of synapses made by the transfected neuron with dendrites of non-transfected neurons present on the same glial island. Scale bar represent 10 $\mu$ m.

**3.1.2. Role of N-cadherin in the accumulation of presynaptic vesicles at nascent synapses**

Previous studies have proposed that the formation of glutamatergic synapses follows a series of sequential steps that eventually lead to mature synapses. One of the first steps is the recruitment and accumulation of neurotransmitter-filled vesicles at presynaptic sites. Because the vesicle clusters formed during this accumulation process have sizes in the range of a few hundred nanometers (Ahmari and Smith, 2002) they can be easily identified microscopically. In this study, fluorescently labelled presynaptic vesicles were used as a morphological criterion to identify and study nascent synapses in N-cadherin deficient and control neurons.

**3.1.2.1. Digital image processing of the DsRed2-VAMP2 signal**

For the analysis of presynaptic vesicle clusters, DsRed2-VAMP2 and EGFP co-transfected N-cadherin deficient and control neurons in culture were imaged using an inverted widefield fluorescence microscope. Z-stack fluorescence images of living neurons were acquired using identical conditions for the two genotypes and offline, computer algorithms were performed on the digital images to remove the background noise and allow a quantitative analysis of the data.

DsRed2-VAMP2 expression had a punctate distribution (Fig. 3.2a) corresponding to the presynaptic vesicle clusters. In the microisland culture system used in this study, most of the DsRed2-VAMP2 labeled clusters were localized on GFP-expressing dendrites (Fig. 3.2c). To visualize the fluorescence intensity of DsRed2-labeled clusters, a colour coded image was used (Fig. 3.2a-middle), where high intensity pixels are depicted as hot colours whereas low intensity pixels are shown as cold colours. For simplification of the image presentation and for all the quantitative measurements done in this study, the

DsRed2-VAMP2 signal was thresholded. Regions on proximal dendrites were cut from the original image and an automatic threshold operation was applied using the software MetaMorph. This threshold operation takes into account the histogram distribution of all pixels in the image and the pixels which have a fluorescence intensity that is higher than two times the standard deviation of the background fluorescence intensity are shown in white whereas all the pixels whose fluorescence intensity is lower than this threshold value are shown in black (for more details see Threshold operation in Materials and Methods). In this way, presynaptic vesicle clusters appear as white puncta on a black background (Fig. 3.2-left). All punctate structures recognizable using this threshold algorithm were included into the analysis.

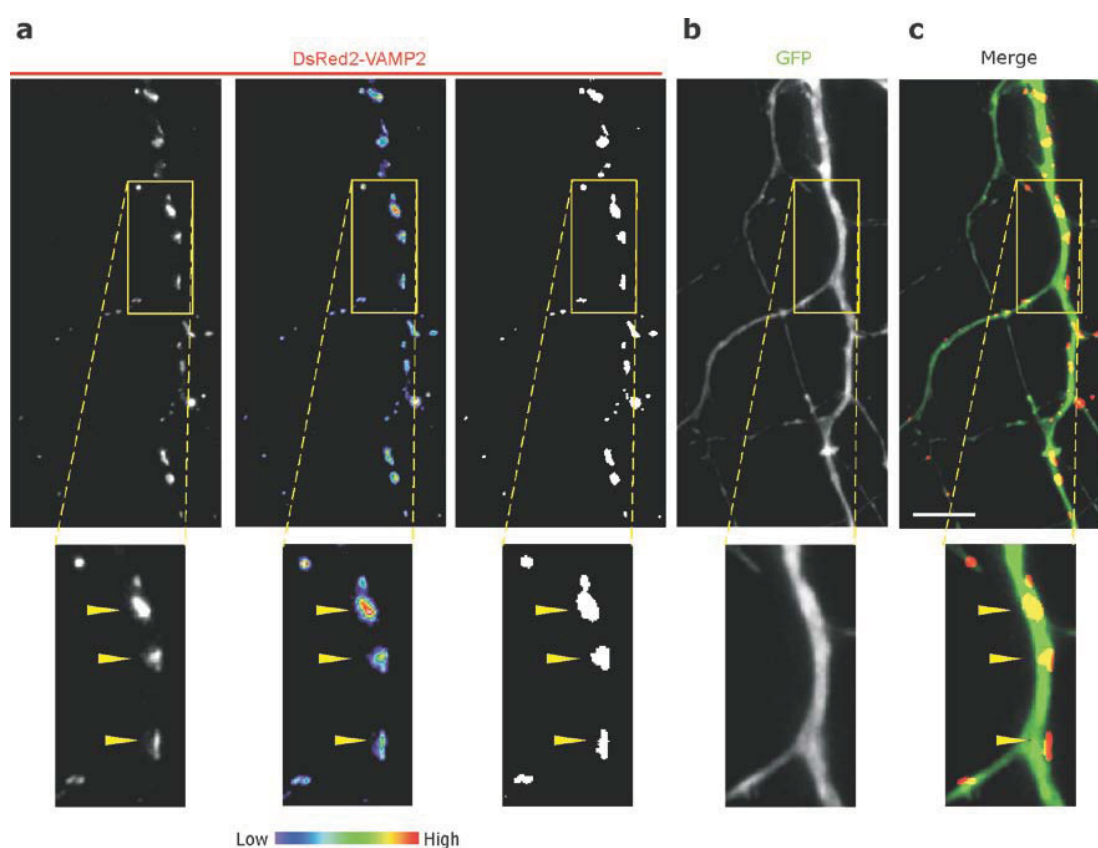


**Figure 3.2. Threshold operation used for analysis of the DsRed2-VAMP2 clusters in ES cell-derived neurons**

Fluorescence images of dendrites from mouse ES cell-derived neuron (14 DIV) co-transfected with (a) DsRed2-VAMP2 and (b) EGFP (co-transfection as in figure 3.1). Boxed areas in images a-c are magnified below the corresponding images for better visualization. (a) Left: Raw image showing that DsRed2-VAMP2 has a punctate distribution (arrows) corresponding to presynaptic vesicle clusters. Middle: Pseudocolor images of the same dendritic region indicating that vesicle

## RESULTS

clusters have high fluorescence intensity whereas the fluorescence outside of the clusters has low intensity close to background levels. DsRed2-VAMP2 fluorescence intensity is colour-coded. Right: Threshold images showing that after the threshold operation vesicle clusters appear as white puncta on a black background. **(b)** The corresponding region of the GFP expressing dendrite. **(c)** Overlay images showing that DsRed2-VAMP2 labeled presynaptic vesicle clusters are localized on the GFP expressing dendrite. Scale bar represents 5 $\mu$ m.

### 3.1.2.2. Analysis of the density of presynaptic vesicle clusters in immature neurons

To study the formation of presynaptic specializations in the absence of N-cadherin, first, the density of presynaptic vesicle clusters in immature neurons (6-7 DIV) was investigated. The density of DsRed2-labeled puncta along the GFP-expressing dendrites in cultures consisting of N-cadherin deficient (differentiated from homozygous N-cadherin knockout ES cells; N-cad<sup>-/-</sup>) or control neurons (differentiated from heterozygous ES cells; N-cad<sup>+/-</sup>) was determined by counting the number of DsRed2-VAMP2 clusters on proximal GFP-expressing dendrites of at least 10-15 $\mu$ m length (Fig. 3.3a). Intriguingly, in immature neurons at 6-7 DIV the density of presynaptic vesicle clusters was significantly ( $P=0.01$ ) reduced in N-cad<sup>-/-</sup> neurons ( $2.3\pm0.3$  puncta/20 $\mu$ m dendrite;  $n=20$ ) as compared to N-cad<sup>+/-</sup> controls ( $3.5\pm0.4$  puncta/20 $\mu$ m dendrite;  $n=26$ ; Fig. 3.3b).

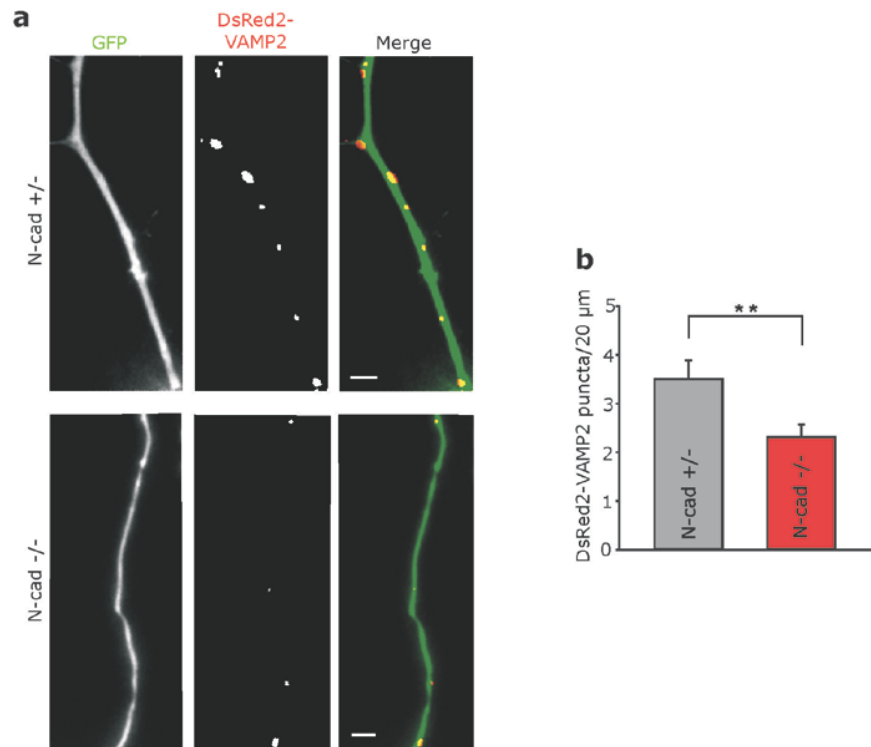


**Figure 3.3. The density of presynaptic vesicle clusters is reduced in the absence of N-cadherin in immature neurons**

(a) Fluorescence images of dendrites from ES cell-derived neurons at 7 days in microisland culture. Neurons were co-transfected with DsRed2-VAMP2 (red) and EGFP (green). N-cad<sup>+/-</sup>: N-cadherin heterozygous control neurons; N-cad<sup>-/-</sup>: homozygous N-cadherin knockout neurons. Scale bars represent 2 $\mu$ m. (b) Quantification of the density of DsRed2-VAMP2 puncta on dendrites at 6-7DIV (N-cad<sup>+/-</sup>:  $n=26$ ; N-cad<sup>-/-</sup>:  $n=20$ ,  $n$  represents number of neurons). Error bars, s.e.m.; \*\*  $P\leq 0.01$

This result may reflect a general defect in synapse formation in the absence of N-cadherin or may point to a smaller vesicle pool of N-cadherin deficient synapses. As described above, the DsRed2 signal was processed using a threshold operation so that only vesicle clusters which had fluorescence intensity higher than two times standard deviation of the background noise were included in the analysis. If N-cadherin deficient neurons have lower number of vesicles accumulated in the cluster and hence, lower DsRed2 fluorescence intensity compared with control, then by this threshold operation more of the low intensity vesicle clusters may have been omitted from the analysis in the N-cadherin knockout neurons than in the control neurons leading to a lower density of presynaptic vesicle clusters. To attempt to study whether N-cadherin deficient neurons have fewer vesicles accumulated in the clusters, the fluorescence intensity of DsRed2-VAMP2 clusters was analyzed.

**3.1.2.3. Quantitative analysis of fluorescence intensity of DsRed2-labeled presynaptic vesicle clusters in immature neurons**

To investigate the role of N-cadherin in the organization of the presynaptic vesicle pool more quantitatively, the mean fluorescence intensity and the size of the DsRed2-labeled clusters in immature N-cadherin heterozygous control and N-cadherin homozygous knock out neurons were analyzed. Mean fluorescence intensity represents a measure of the density of presynaptic vesicles present in a cluster whereas the area of the cluster indicates the spread (distribution) of vesicles in the presynaptic terminal. However, no significant difference in mean intensity between the two genotypes was detectable (Fig. 3.4 b, N-cad<sup>+/-</sup>:  $112.15\pm 11.94$  a.u.;  $n=26$  N-cad<sup>-/-</sup>:  $102.89\pm 8.61$  a.u.;  $n=20$ ). This may be due to a considerable intensity/vesicle variability caused by different expression levels of DsRed2-VAMP2 in different neurons, as shown in the individual neurons plot in Fig.

3.4b. Indeed, the correlation analysis between the DsRed2-VAMP2 signal and the GFP signal indicated that even in the same neuron the expression level of two different vectors (DsRed2-VAMP2 and EGFP, their expression both being under a similar CMV promoter) showed wide variability. Fig. 3.4a shows that there is no correlation in the expression levels of DsRed2-VAMP2 and GFP in individual N-cadherin heterozygous and N-cadherin knock out neurons. In addition, the analysis of the mean area occupied by DsRed2-labeled vesicles showed no difference between the genotypes (Fig. 3.4c, N-cad<sup>+/+</sup>:  $0.23 \pm 0.02 \mu\text{m}^2$ ,  $n=26$  N-cad<sup>-/-</sup>:  $0.27 \pm 0.03 \mu\text{m}^2$ ,  $n=20$ ).

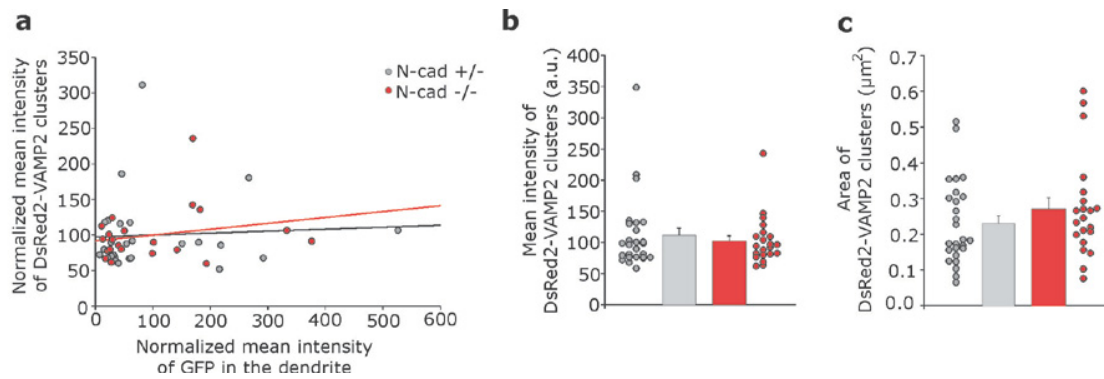


**Figure 3.4. Analysis of mean fluorescence intensity and size (area) of the DsRed2-VAMP2 clusters in immature neurons revealed no differences between the two genotypes**

(a) Correlation of normalized average fluorescence intensity of DsRed2-VAMP2 clusters versus normalized GFP fluorescence in the dendrites for individual immature 6-7DIV neurons (N-cad<sup>+/+</sup>: control neurons, grey symbols,  $n=26$ ; N-cad<sup>-/-</sup>: homozygous N-cadherin knockout neurons, red symbols,  $n=20$ ). Each circle represents one neuron for which the mean fluorescence intensity of its DsRed2-VAMP2 clusters was normalized to the mean fluorescence intensity of DsRed2-VAMP2 vesicle clusters in all neurons analyzed to illustrate variability. Similarly, the mean fluorescence intensity of the GFP signal in the dendrites of a neuron was normalized to the mean fluorescence intensity of the GFP signal in all neurons. (b, c) Quantification of (b) mean fluorescence intensity and (c) mean area of DsRed2-VAMP2 clusters in immature N-cad<sup>+/+</sup> and N-cad<sup>-/-</sup> neurons. Error bars represent s.e.m.

However, using FM4-64 staining (fluorescent dye that stains the membrane of recycled synaptic vesicles) it has been shown that the mean fluorescence intensity was reduced to 75.3% in homozygous N-cadherin knockout neurons as compared to N-cadherin heterozygous control neurons (Jüngling et al., 2006) and to a similar extent in hippocampal neurons transfected with a dominant negative N-cadherin construct (Bozdagi et al., 2004), indicating that N-cadherin deficient synapses have a smaller



vesicle pool. In summary, the quantitative analysis of the fluorescence intensity of DsRed2-VAMP2 transfected neurons does not represent a reliable method for calculating the density or number of vesicles in a synaptic cluster as the fluorescence intensity strongly depends on the expression level of the transfected vectors and this may vary widely from one cell to another.

#### **3.1.2.4. Time lapse analysis of presynaptic vesicle accumulation at immature synapses**

Accumulation of synaptic vesicles at presynaptic terminals represents a decisive step in the formation and maturation of synapses (Vaughn, 1989; Mozhayeva et al., 2002; Mohrmann et al., 2003; Goda and Davis, 2003; McAllister, 2007). To study presynaptic vesicle accumulation during synapse maturation more directly and thus quantitatively more reliable, live-imaging time-lapse analysis of DsRed2-VAMP2-labeled vesicle clusters on dendrites of transfected N-cadherin control and N-cadherin knockout neurons was performed. For this, images of labeled vesicle clusters on GFP-expressing dendrites were acquired every 20 minutes for a period of 2 hours (Fig. 3.5a). Offline, individual clusters fulfilling two criteria: *i*) to be localized on GFP-expressing dendrites and *ii*) to be stable during the recording time (no splitting or fusion with other vesicle clusters) from control (N-cad<sup>+/-</sup>) and N-cad<sup>-/-</sup> neurons were selected. The changes in total fluorescence intensity (the product between mean fluorescence intensity/pixel and area of a cluster) were calculated at different time points for each cluster analyzed and were plotted against time. Individual nascent synapses of control N-cadherin expressing neurons (6-7 DIV) showed a strong, continuous increase in DsRed2 fluorescence intensity during the 2 hours live-imaging period reflecting ongoing accumulation of synaptic vesicles (Fig. 3.5a, b). In sharp contrast, in the absence of N-cadherin from the synaptic sites no net increase in DsRed2 fluorescence intensity was detectable (Fig. 3.5a, b). Overall, a mean increase in total fluorescence intensity of  $144.5 \pm 10.7\%$  ( $n=18$  puncta from 10 cells) was found at individual labeled presynaptic vesicle clusters in control cells. This was significantly different ( $P=0.0001$ ) from the absence of a mean increase in fluorescence intensity ( $79.2 \pm 6.7\%$ ;  $n=13$  puncta from 11 cells) in N-cad<sup>-/-</sup> neurons (Fig. 3.5c). In summary,



live-imaging of individual vesicle clusters revealed that ongoing vesicle recruitment and accumulation at nascent synapses is strongly dependent on the expression of N-cadherin.

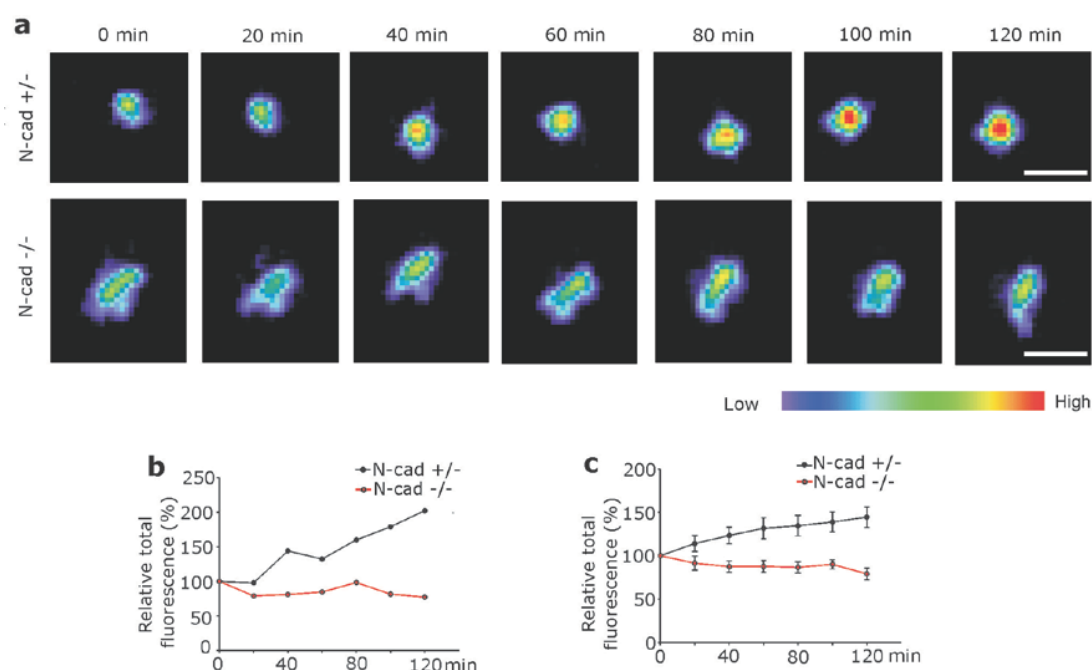


**Figure 3.5. Presynaptic vesicle accumulation during early synapse maturation requires N-cadherin expression**

(a) Pseudocolor images of individual vesicle clusters observed for a period of 2 hours (DsRed2-VAMP2 puncta on EGFP-expressing dendrites; co-transfection as in Fig. 1; 6 DIV). Time points of data acquisition are indicated above images. DsRed2-VAMP2 fluorescence intensity is colour-coded, so that low fluorescence intensity appears as blue whereas high fluorescence intensity appears as red. N-cad<sup>+/+</sup>: control heterozygous N-cadherin neurons. N-cad<sup>-/-</sup>: homozygous N-cadherin knockout neurons. Scale bars represent 1  $\mu$ m. (b,c) Quantification of DsRed2-VAMP2 fluorescence intensity versus observation time (b) for the individual vesicle clusters shown in (a) and (c) for all clusters studied (6-7 DIV; mean  $\pm$  s.e.m.). Total fluorescence intensity of all pixels representing a punctum was calculated and normalized to the intensity at 0 min. N-cad<sup>+/+</sup>:  $n=18$  puncta (from 10 cells); N-cad<sup>-/-</sup>:  $n=13$  puncta (from 11 cells). Error bars, s.e.m.

### 3.1.2.5. FRAP (fluorescence recovery after photobleaching) analysis of mobility and accumulation of presynaptic vesicles at immature synapses

To further study vesicle accumulation at nascent synapses in a quantitatively more controlled manner, fluorescence recovery after photobleaching (FRAP) experiments were performed at 6-7 DIV in N-cadherin control and N-cadherin knockout neurons transfected with a vector coding for a EGFP-VAMP2 fusion protein. FRAP measures the mobility of synaptic vesicles in the presynaptic terminals and along the axon by acutely inactivating the fluorescence in a single cluster of vesicles with strong illumination and then following the fluorescence recovery in time. The recovery of fluorescence will take place as mobile vesicles from neighbouring axon regions will start to repopulate the bleached area over time. The rate of recovery depends on the vesicle mobility between the clusters but also on the capacity of presynaptic terminals to retain the incoming vesicles at the synaptic site.

Individual EGFP-VAMP2 clusters on dendrites were locally photobleached using high intensity laser light until the fluorescence intensity was close to background levels and then the recovery of EGFP fluorescence was monitored with live-imaging for 45 minutes, acquiring pictures every 5 minutes (Fig. 3.6a). Boutons were bleached to an average of  $6.63 \pm 1.17$  % and  $4.47 \pm 1.57$  % of the initial fluorescence for N-cadherin control and N-cadherin knockout boutons, respectively (Fig. 3.6c). Ongoing photobleaching induced by imaging during recovery was subtracted from fluorescence recovery curves (Fig. 3.6b). In control neurons more than 60% recovery ( $64 \pm 11$ %,  $n=13$ ) was reached after 45 minutes, whereas in N-cad<sup>-/-</sup> neurons only about 30% recovery was observed ( $28 \pm 4$ %,  $n=11$ ; Fig. 3.6c, d). The difference in recovery after 45 minutes was statistically significant ( $P=0.017$ ) indicating that either the mobility or the capacity to retain incoming vesicles (accumulation of vesicles) is severely impaired in the absence of N-cadherin.

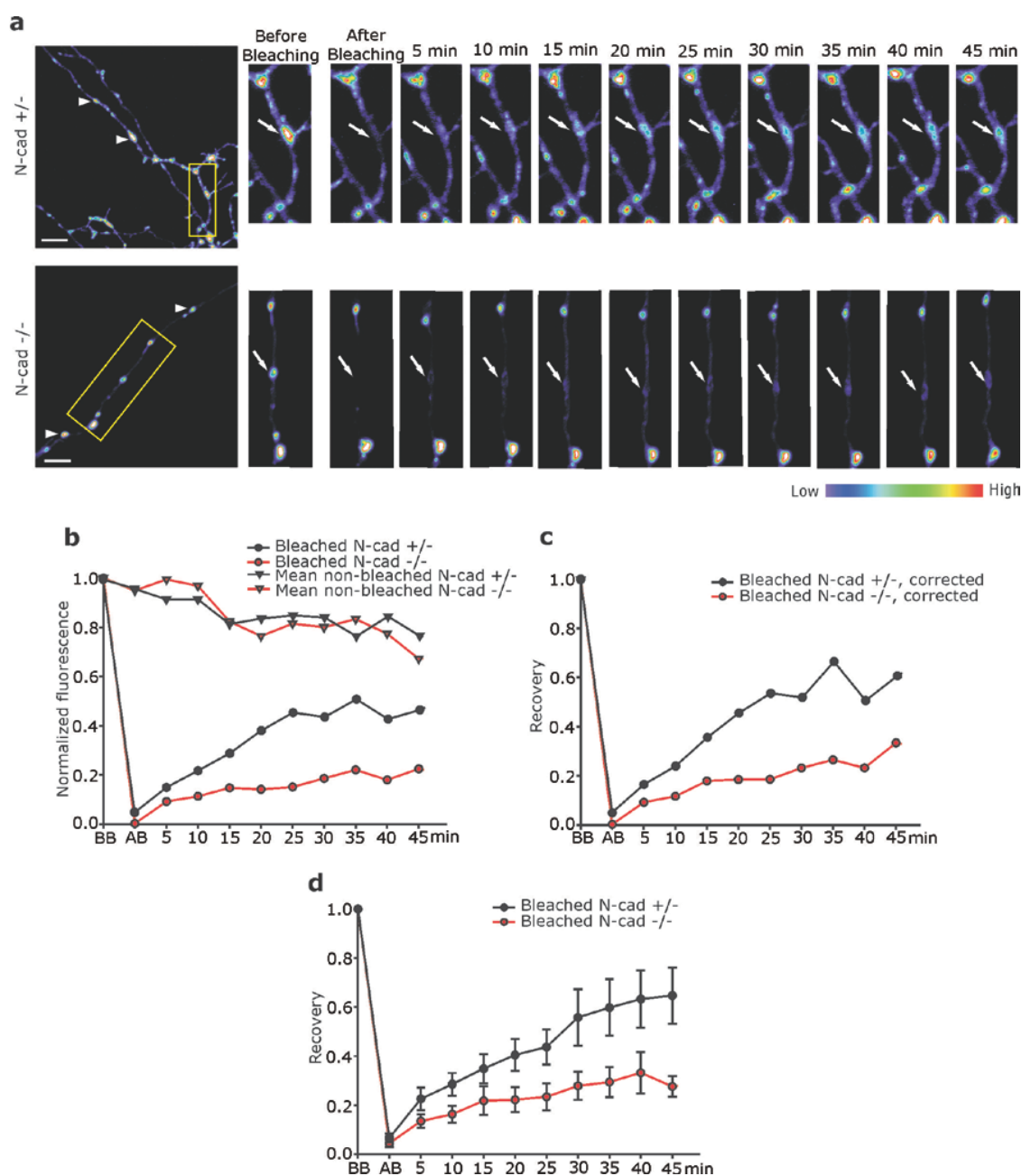


**Figure 3.6. FRAP experiments revealed slower recovery of vesicle cluster-associated fluorescence in the absence of N-cadherin**

(a) Examples of FRAP experiments in control neurons (N-cad<sup>+/+</sup>) and in N-cadherin deficient neurons (N-cad<sup>-/-</sup>) (6 DIV). The left image shows EGFP-VAMP2 fluorescence on dendrites. Boxed areas indicate the part of the dendrite where photobleaching experiments illustrated on the left were performed. Arrowheads indicate EGFP-VAMP2 clusters analyzed to estimate imaging-induced ongoing bleaching. In the images on the left the photobleached vesicle cluster is indicated by an arrow, time relative to bleaching is indicated above images and fluorescence intensity is colour-coded. Individual vesicle clusters were photobleached using high intensity laser light. Scale bars represent 5  $\mu$ m (b,c,d) Quantification of fluorescence recovery after

photobleaching. **(b)** Normalized fluorescence intensity of photobleached and non-bleached individual vesicle clusters shown in (a) versus observation time. BB: before photobleaching; AB: after photobleaching ( $t=0\text{min}$ ). **(c)** Recovery curves corrected for ongoing bleaching during imaging shown in (b) for individual vesicle clusters. **(d)** Mean recovery of normalized and corrected fluorescence intensity (6-7 DIV). N-cad $^{+/-}$ :  $n=13$ , N-cad $^{-/-}$ :  $n=11$ ,  $n$  represents number of neurons. Error bars, s.e.m.

To further test whether the presynaptic vesicle clusters exhibit an altered motility in the absence of N-cadherin, the dynamics of vesicle accumulations were investigated using time-lapse imaging.

### 3.1.2.6. Analysis of the dynamics of presynaptic vesicle clusters in immature neurons

Preassembled clusters of presynaptic and postsynaptic components may facilitate rapid synapse formation in developing neurons (Ahmari et al., 2000; Zhai et al., 2001). Previous studies have shown that many of the synaptic vesicle packages that undergo fast axonal transport actually constitute recycled vesicles from nearby synapses suggesting that vesicle mobility could represent a mechanism for sharing vesicles between synapses (Darcy et al., 2006; Krueger et al., 2003). Synaptic vesicle mobility in immature neurons is thought to be involved in presynaptic assembly or disassembly processes in developing neurons. During the time lapse imaging of immature N-cadherin heterozygous and N-cadherin knockout neurons described above (the same neurons as in Fig. 3.5), three different types of vesicle clusters were observed: *i*) clusters that were stable during the whole recording period (which were included in the analysis from Fig. 3.5), *ii*) clusters that were observed to be splitting and/or fusing and *iii*) clusters that traveled along an axon contacting the GFP-labeled dendrite without splitting or fusing (not analyzed in this study).

To address the mobility of vesicle clusters between presynaptic release sites, the frequency of budding (splitting) events of individual DsRed2-VAMP2 clusters on GFP expressing dendrites was analyzed (Fig. 3.7a). Interestingly, in the absence of N-cadherin the frequency of budding was significantly ( $P=0.034$ ) higher compared with control N-cad $^{+/-}$  neurons (Fig. 3.7b), (N-cad $^{+/-}$ :  $0.03\pm0.01$  budding events/synapse/20min,  $n=10$ ; N-cad $^{-/-}$ :  $0.06\pm0.01$  budding events/synapse/20min,  $n=11$ ).

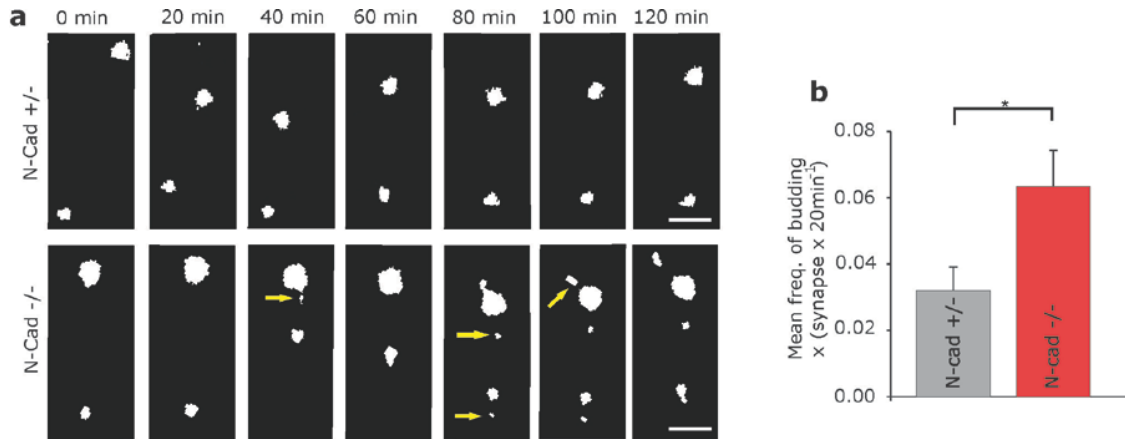


**Figure 3.7. Spontaneous splitting of vesicle clusters is increased in the absence of N-cadherin (7DIV)**

(a) Examples of live-imaging of vesicle clusters (DsRed2-VAMP2 puncta on EGFP-expressing dendrites; co-transfection as in Fig. 3.1). Fluorescence images were thresholded resulting in black-and-white images of DsRed2-VAMP2 puncta. Budding events observed during time-lapse recording are indicated by arrows (yellow). Time points of data acquisition are indicated above images. N-cad<sup>+/–</sup>: control neurons. N-cad<sup>–/–</sup>: homozygous N-cadherin knockout neurons. Scale bars represent 2  $\mu$ m. (b) Quantification of the frequency of budding events occurring at individual vesicle clusters during the observation time. Error bars, s.e.m.; \* $P < 0.05$ . N-cad<sup>+/–</sup>:  $n = 10$  cells; N-cad<sup>–/–</sup>:  $n = 11$  cells.

The mobility of vesicle clusters can be also inferred from the analysis of the total dynamics (all splitting and fusion events together) of vesicle clusters. The total dynamics was calculated by counting the absolute change in number of vesicle clusters between two adjacent time points and then normalizing the sum of changes to the length of the dendrite analyzed (see example Fig. 3.8a). The difference to the previous analysis (see Fig. 3.7) is that total dynamics reflects not only splitting, but also fusion of vesicle clusters and it includes a cluster density factor (density of DsRed2-VAMP2 clusters on the GFP-expressing dendrite). As expected, the total dynamics was significantly increased ( $P = 0.042$ ) in the absence of N-cadherin ( $4.42 \pm 0.81$  fusion and splitting events/ 20  $\mu$ m dendrite/120min,  $n = 11$ ) compared with N-cadherin control ( $1.91 \pm 0.78$  fusion and splitting events/ 20  $\mu$ m dendrite/120min,  $n = 10$ ; Fig. 3.8b). If the frequency of fusion and splitting events is interpreted as a measure of the stability of vesicle clusters, these results together with the results from FRAP analysis indicate that N-cadherin is important in maintaining the presynaptic vesicle pool integrity and that in the absence of N-cadherin vesicles can not be retained at immature synaptic sites.

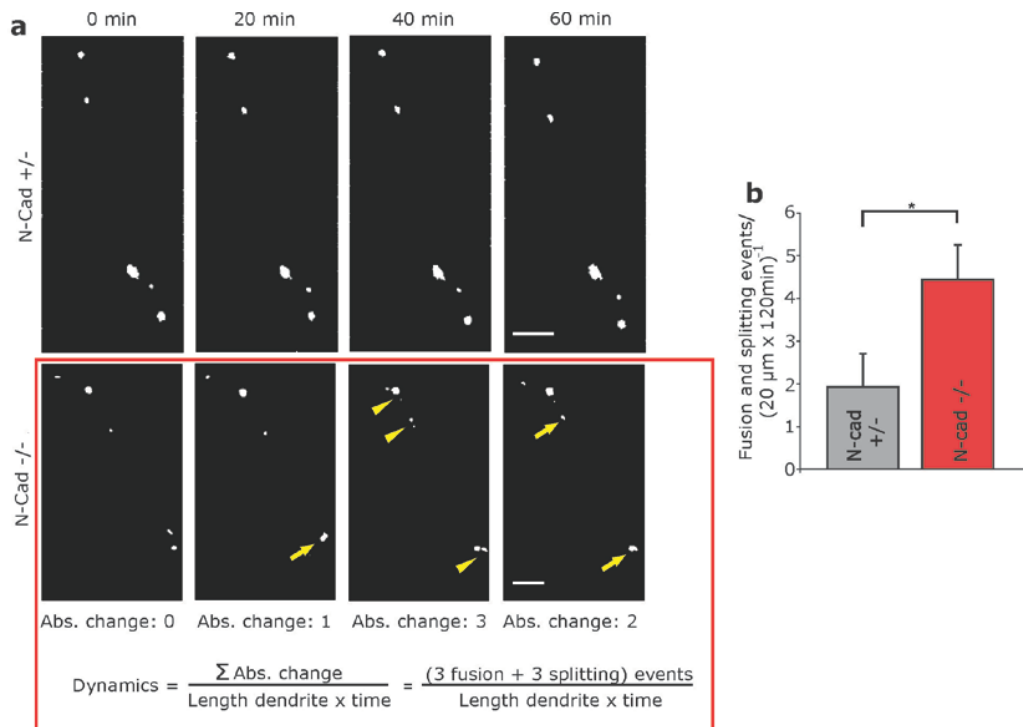


**Figure 3.8. The total dynamics (fusion and splitting) of vesicle clusters is increased in the absence of N-cadherin (6-7DIV)**

(a) Examples of live-imaging of vesicle clusters (DsRed2-VAMP2 puncta on EGFP-expressing dendrites; co-transfection as in Fig. 3.1; 7 DIV). Fluorescence images were thresholded resulting in black-and-white images of DsRed2-VAMP2 puncta area. Budding (splitting) events observed during time-lapse recording are indicated by arrowheads whereas fusion events are indicated by arrows. Time points of data acquisition are indicated above images. For simplicity only the first 60 minutes of the 120 minutes recording time are shown. N-cad<sup>+/+</sup>: control neurons. N-cad<sup>-/-</sup>: homozygous N-cadherin knockout neurons. For the N-cad<sup>-/-</sup> example it is shown how total dynamics was calculated. *Abs. change*: absolute change in number of puncta,  $\Sigma$ : sum. Scale bars represent 4 μm. (b) Quantification of the frequency of fusion and splitting events occurring on 20 μm dendritic length during the 120 minutes observation time. Error bars, s.e.m.; \* $P < 0.05$ . N-cad<sup>+/+</sup>:  $n = 10$  cells; N-cad<sup>-/-</sup>:  $n = 11$  cells.

### 3.1.3. Role of N-cadherin in the formation of active zones in immature neurons

Active zones are electron dense presynaptic specializations in neurons that play a pivotal role in providing sites for neurotransmitter release and synaptic vesicle recycling. During synaptogenesis, active zone proteins are the first to accumulate at developing synapses in cultured neurons. The above described major finding that the density of presynaptic vesicle clusters is reduced in immature N-cadherin deficient neurons might reflect a defect in synapse formation *per se* or a more specific defect in the accumulation of

synaptic vesicles at active zones. To further study, whether N-cadherin is also involved in the formation of active zones, Bassoon was chosen as a marker protein for active zones. Bassoon is a large multidomain protein found at active zones of nascent synapses and it has been shown to play an important role in the assembly of the cytomatrix at the active zone (CAZ) (Zhai et al., 2001; Shapira et al., 2003, Altrock et al., 2003; Dick et al., 2003).

### **3.1.3.1. Digital image processing of the EGFP-Bassoon signal**

EGFP-Bassoon for labeling active zones and DsRed2 for visualization of dendrites were co-transfected in control and N-cadherin deficient neurons using lipofectamine 2000. Images of living transfected neurons were acquired as described above for DsRed2-VAMP2, using identical conditions for the two genotypes. In order to quantitatively analyze the EGFP-Bassoon clusters, offline images were digitally processed for removing the background noise. EGFP-Bassoon had a punctate distribution (arrows, Fig. 3.9a- left) corresponding to active zones but there was also a diffuse EGFP-Bassoon signal outside of the clusters. The GFP-labeled presynaptic specializations were mostly localized on DsRed2-expressing dendrites (Fig. 3.9b, c). To visualize the fluorescence intensity, a colour-coded image was used (Fig. 3.9a- middle), where high intensity pixels are depicted as hot colours whereas the low intensity pixels are shown in cold colours. For simplification of image presentation but also for all the quantitative measurements done, the EGFP-Bassoon signal was thresholded. Because EGFP-Bassoon had in addition a diffuse signal outside of the active zone clusters, the threshold applied to EGFP-Bassoon signal was manually set, contrary to the autothreshold operation applied for the DsRed2-VAMP2 signal, because this algorithm could not distinguish efficiently the signal in clusters from the signal in the dendrite. The threshold value was set so that only the high intensity fluorescent clusters were above the threshold, whereas the EGFP-Bassoon signal in the dendrite (outside of the cluster) was below the threshold. In this way, active zones on transfected neurons appeared as white puncta on a black background (Fig. 3.9a-right).



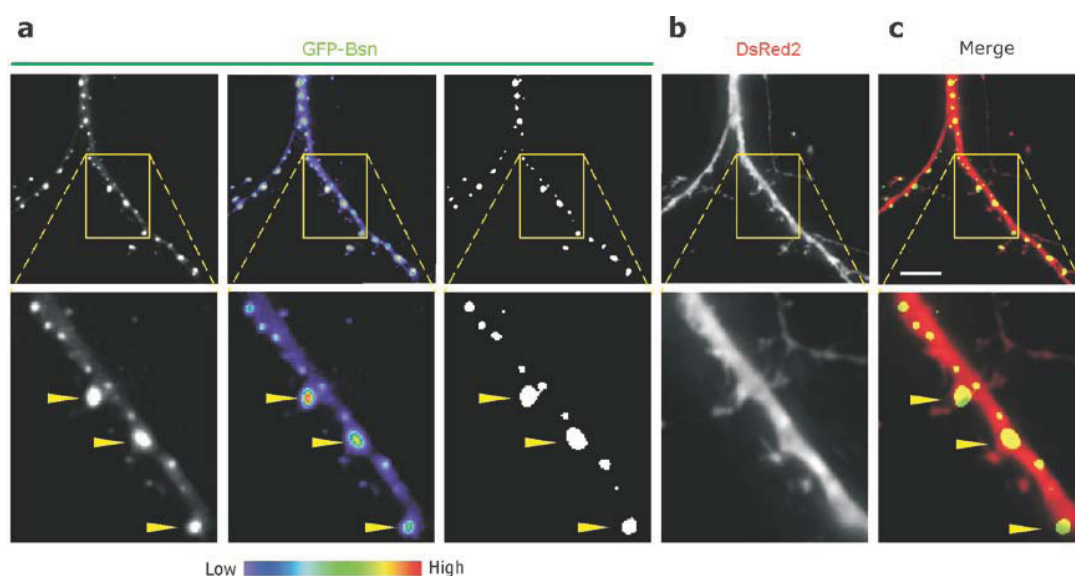


**Figure 3.9. Threshold operation used for the analysis of the EGFP-Bassoon clusters in ES cell-derived neurons**

Fluorescence images of dendrites from mouse ES cell-derived neuron (14 DIV) co-transfected with (a) EGFP-Bassoon and (b) DsRed2. Boxed areas in images a-c are magnified below the corresponding images for better visualization. (a) Left: Raw image showing that EGFP-Bassoon had a punctate distribution (arrows) corresponding to active zones but there is also a diffuse EGFP-Bassoon signal outside of the clusters. Middle: Pseudocolor images of the same dendritic region indicating that Bassoon clusters have high fluorescence intensity whereas the fluorescence outside of the clusters has lower intensity but still much above the background levels. EGFP-Bassoon fluorescence intensity is colour-coded. Right: Threshold images showing that after the threshold operation vesicle clusters appear as white puncta on a black background. (b) Corresponding image of the DsRed2 expressing dendrite. (c) Overlay images showing that EGFP-Bassoon labeled active zones are localized on the DsRed2 expressing dendrite. Scale bar represents 5 $\mu$ m.

### 3.1.3.2. Analysis of the density of Bassoon clusters in immature neurons

To study the formation of active zones in the absence of N-cadherin, first the density of Bassoon clusters in immature neurons (6-7 DIV) was investigated. The density of EGFP-labeled Bassoon clusters along the DsRed2-expressing dendrites in cultures consisting of N-cadherin-deficient (differentiated from homozygous N-cadherin knockout ES cells; N-cad<sup>-/-</sup>) or control neurons (differentiated from heterozygous ES cells; N-cad<sup>+/-</sup>) was determined by counting the number of EGFP-Bassoon clusters on proximal DsRed2-expressing dendrites of at least 10-15 $\mu$ m length (Fig. 3.10a). No significant difference was observed between the two genotypes (Fig. 3.10b; N-cad<sup>+/-</sup> controls:  $3.34 \pm 0.90$



puncta/20 $\mu$ m dendrite;  $n=11$ ; N-cad $^{-/-}$ :  $2.82 \pm 0.82$  puncta/20 $\mu$ m dendrite;  $n=11$ ), suggesting that active zone formation occurs in an N-cadherin independent manner.

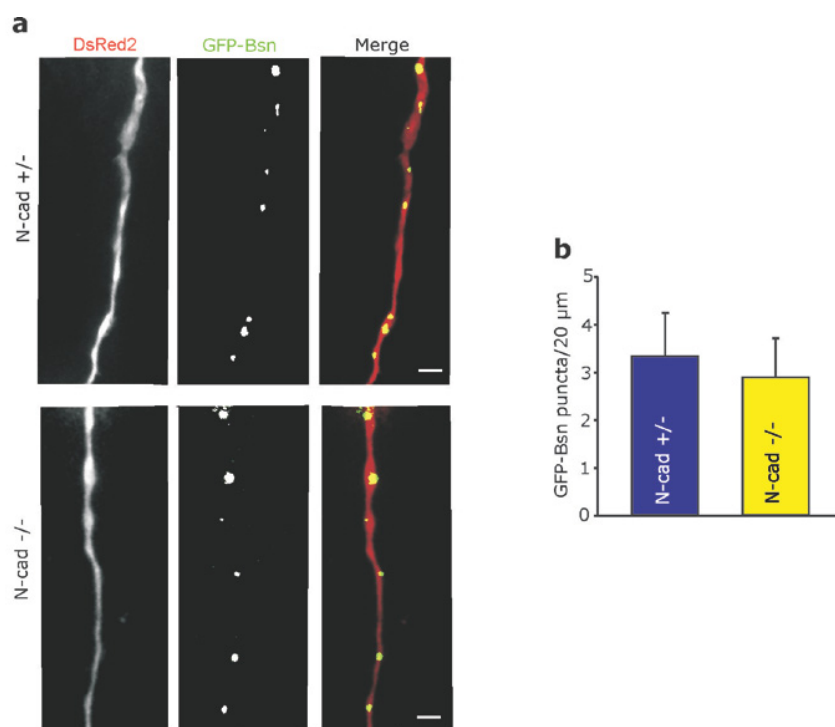


**Figure 3.10. Density of EGFP-Bassoon clusters is unaltered in N-cadherin deficient neurons indicating that formation of active zones does not require N-cadherin**

(a) Fluorescence images of dendrites from mouse ES cell-derived neurons at 7 days in microisland culture. Neurons were co-transfected with EGFP-Bassoon (green) and DsRed2 (red). N-cad $^{+/-}$ : control neurons; N-cad $^{-/-}$ : homozygous N-cadherin knockout neurons. Scale bars represent 2  $\mu$ m. (b) Quantification of the density of EGFP-Bassoon puncta on dendrites at 6-7DIV (N-cad $^{+/-}$ :  $n=11$ ; N-cad $^{-/-}$ :  $n=11$ ,  $n$  represents number of neurons).

### 3.1.3.3. Quantitative analysis of the fluorescence intensity of EGFP-Bassoon labeled active zones in immature neurons

To further investigate the role of N-cadherin in the organization of Bassoon molecules at the cytomatrix of the active zones, the mean fluorescence intensity and the size of the GFP-labeled Bassoon clusters in immature N-cadherin heterozygous control and N-cadherin homozygous knockout neurons were analyzed. Mean fluorescence intensity represents a measure of the density of presynaptic Bassoon molecules in a cluster

whereas the area of the cluster indicates the spread (distribution) of Bassoon protein at the cytomatrix of the active zone.

Intriguingly, the transfection of neurons with EGFP-Bassoon led to the expression of GFP-labeled Bassoon also in the dendrites, where normally Bassoon is not expressed (see Fig. 3.9). The quantitative analysis of EGFP-Bassoon fluorescence intensity in the clusters and in the dendrites of individual neurons showed a strong correlation for both genotypes, indicating that the dendritic expression of EGFP-Bassoon represents an overexpression artifact (Fig. 3.11a). Nevertheless, decreasing the amount of transfected DNA did not improve the EGFP-Bassoon expression pattern (data not shown). Mean fluorescence intensity of EGFP-Bassoon in the clusters (Fig. 3.11b) and also the size of the clusters (Fig. 3.11c) were not different between the two genotypes (Mean fluorescence intensity: N-cad<sup>+/-</sup>:  $526.09 \pm 80.21$  a.u.,  $n=11$ ; N-cad<sup>-/-</sup>:  $324.37 \pm 46.81$  a.u.,  $n=11$  Area: N-cad<sup>+/-</sup>:  $0.16 \pm 0.03 \mu\text{m}^2$ ,  $n=11$ ; N-cad<sup>-/-</sup>:  $0.15 \pm 0.02 \mu\text{m}^2$ ,  $n=11$ ).

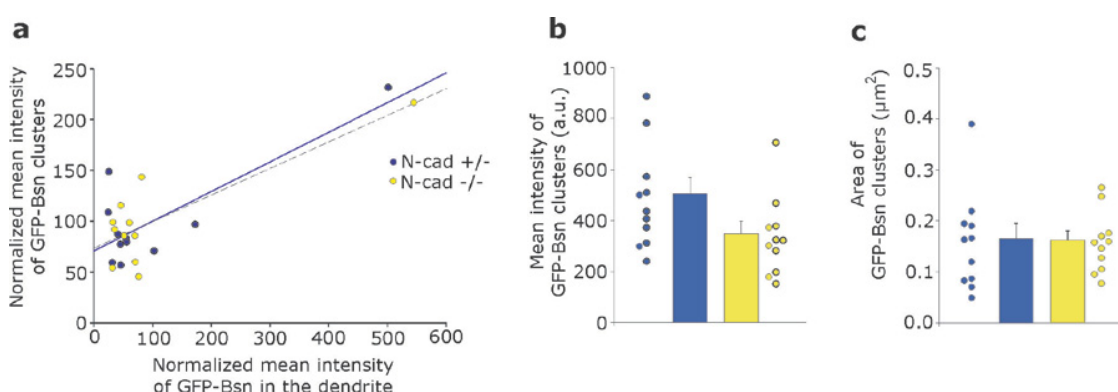


**Figure 3.11. Analysis of fluorescence intensity and area of the EGFP-Bassoon clusters in immature neurons shows no differences between the two genotypes**

(a) Correlation of normalized fluorescence intensity of EGFP-Bassoon clusters versus normalized EGFP-Bassoon fluorescence of diffusely distributed EGFP-Bassoon signal outside of the clusters for individual 6-7 DIV neurons. (N-cad<sup>+/-</sup>: control neurons, blue symbols,  $n=11$ ; N-cad<sup>-/-</sup>: homozygous N-cadherin knockout neurons, yellow symbols and dotted black line,  $n=11$ ). Each circle represents one neuron for which the mean fluorescence intensity of its EGFP-Bassoon signal in clusters was normalized to the mean fluorescence intensity of the EGFP-Bassoon clusters present in all neurons to visualize variability. Similarly, the mean fluorescence intensity of the EGFP-Bassoon signal outside of the clusters (in the dendrites) of a neuron was normalized to the mean fluorescence intensity of the EGFP-Bassoon signal in the dendrites of all neurons. (b, c) Quantification of (b) mean fluorescence intensity and (c) mean area of EGFP-Bassoon clusters in immature N-cad<sup>+/-</sup> and N-cad<sup>-/-</sup> neurons. Error bars, s.e.m.,  $n$  represents number of neurons.

### **3.2. Role of N-cadherin in late phase maturation and maintenance of presynaptic specializations**

To study the role of N-cadherin in the late phase maturation and maintenance of synapses, mature N-cadherin heterozygous (N-cad<sup>+/-</sup>) and homozygous, N-cadherin deficient ES cell-derived neurons (N-cad<sup>-/-</sup>) were investigated. The neurons were grown for 10-14 days in vitro (DIV) on glial microislands. At this time in culture, most of the synapses have already formed but late maturational processes are still taking place.

#### **3.2.1. Role of N-cadherin in the accumulation of presynaptic vesicles at mature synapses**

The clustering of synaptic vesicles around active zones is the initial structural sign of synapse formation. As shown in the previous chapters, N-cadherin plays an important role in the initial formation of synapses, specifically in controlling the accumulation of presynaptic vesicles at the nascent synaptic sites. During further synapse maturation the number of vesicles in the vesicle pools increases in parallel with changes in the architectural complexity of synaptic boutons (Vaughn, 1989). To investigate the role of N-cadherin in the accumulation of vesicles at mature synapses, control and N-cadherin deficient neurons were co-transfected with DsRed2-VAMP2 for visualizing the presynaptic vesicle clusters and EGFP for labeling the dendrites. Two days after transfection, the neurons were imaged and digitally processed as described in Chapter 3.1.2.

##### **3.2.1.1. Analysis of the density of presynaptic vesicle clusters in mature neurons**

Changes in the density of presynaptic vesicle clusters in mature N-cadherin control and N-cadherin deficient neurons were studied in order to clarify the effect of N-cadherin on long-term maintenance of synapses. Intriguingly, the analysis of the density of DsRed2-labeled presynaptic vesicle clusters on the GFP-expressing dendrites (Fig. 3.12a) led to no significant difference between the two genotypes (Fig. 3.12b, N-cad<sup>+/-</sup>:  $11.80 \pm 1.28/20\mu\text{m}$  dendrite,  $n=18$ ; N-cad<sup>-/-</sup>:  $11.59 \pm 0.95/20\mu\text{m}$  dendrite,  $n=20$ ). Considering that immature N-cadherin knockout neurons have a lower density of vesicle clusters compared to controls (see Fig. 3.3), this result may indicate that at later

## RESULTS

maturational stages either other mechanisms compensate for the loss of N-cadherin and thus eventually synaptic density reaches the control levels or that the synaptic defects become less evident in regard to the number of synapses but more prominent in respect to the maturational stage in which the synapses are. The latter has been previously shown in our lab by Jüngling et al. (2006) in a study where the authors have investigated mature N-cadherin heterozygous and N-cadherin knockout neurons in culture and found that N-cadherin is required for controlling the functional properties (vesicle recruitment to active zone) of glutamatergic synapses.

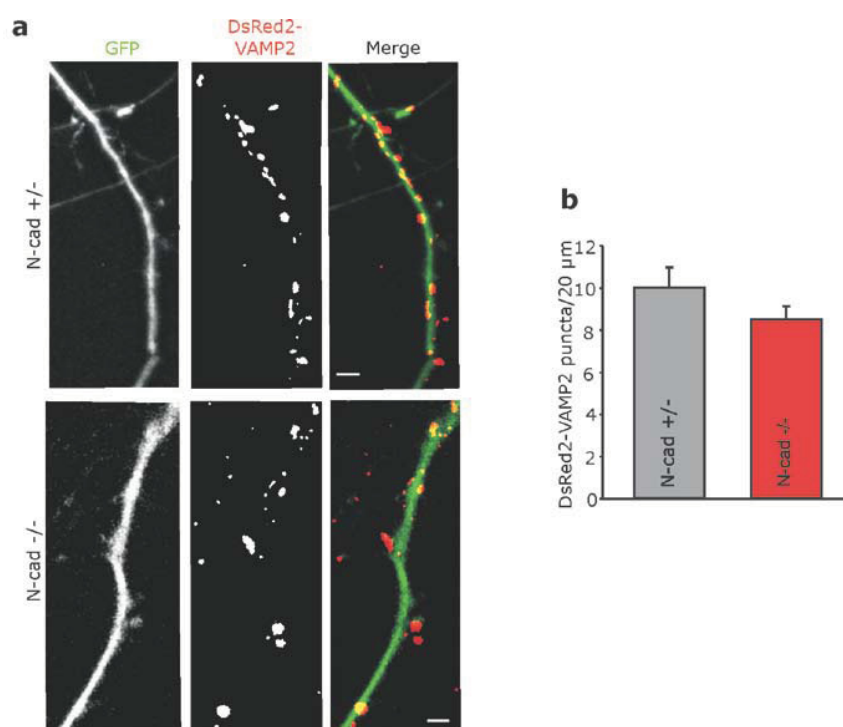


**Figure 3.12. The density of presynaptic vesicle clusters is not different between the two genotypes in mature ES cell-derived neurons**

(a) Fluorescence images of dendrites from ES cell-derived neurons at 14 days in microisland culture (DIV). Neurons were co-transfected with DsRed2-VAMP2(synaptobrevin2) (red) and EGFP (green) using the lipofectamine technique. N-cad+/ -: control neurons; N-cad-/-: homozygous N-cadherin knockout neurons. Scale bars represent 2 μm. (b) Quantification of the density of DsRed2-VAMP2 puncta on dendrites at 10-14 DIV (N-cad+/ -:  $n=18$ ; N-cad-/-:  $n=20$ ). Error bars, s.e.m.,  $n$  represents number of neurons

### 3.2.1.2. Quantitative analysis of the fluorescence intensity of DsRed2-labeled presynaptic vesicle clusters in mature neurons

As described for immature neurons, the transfection of DsRed2 tagged VAMP2, allows not only the visualization of vesicle clusters but also the quantification of fluorescence intensity and size of labeled clusters. These parameters are indicators of the vesicle pool organization. Mean fluorescence intensity and area of the DsRed2-VAMP2 clusters was analyzed in more mature N-cadherin heterozygous and N-cadherin homozygous knockout neurons at 10-14 DIV. The results were similar to the ones obtained in immature neurons. First, no correlation between the fluorescence intensity of DsRed2-labeled vesicle clusters and fluorescence intensity of GFP in the dendrite of individual neurons for the two genotypes was found (Fig. 3.13a), indicating that the expression levels of the two vectors vary widely. This large variability in expression might well explain the result of the analysis of the mean fluorescence intensity of DsRed2-VAMP2 clusters (Fig. 3.13b), in which no significant difference was observed between the two genotypes (N-cad<sup>+/-</sup>:  $160.00 \pm 13.27$  a.u.,  $n=18$ ; N-cad<sup>-/-</sup>:  $138.70 \pm 7.09$  a.u.,  $n=20$ ) although a previous study had indicated a slightly smaller recycling vesicle pool in mature N-cadherin knockout neurons (Jungling et al., 2006). Similarly, the area of DsRed2-VAMP2 clusters showed no significant difference between the two genotypes (Fig. 14c, N-cad<sup>+/-</sup>:  $0.26 \pm 0.03 \mu\text{m}^2$ ,  $n=18$ ; N-cad<sup>-/-</sup>:  $0.30 \pm 0.03 \mu\text{m}^2$ ,  $n=20$ ).

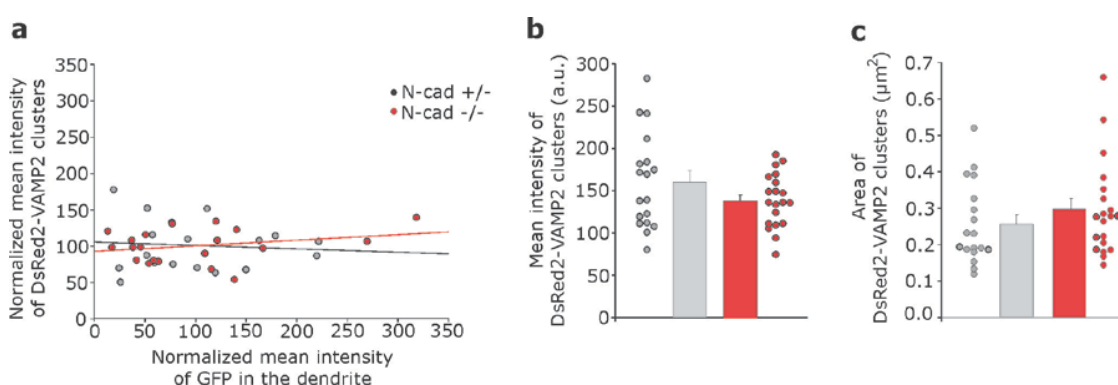


**Figure 3.13. Analysis of average fluorescence intensity and size of the DsRed2-VAMP2 clusters in more mature neurons revealed no differences between the two genotypes**

(a) Correlation of normalized fluorescence intensity of DsRed2-VAMP2 clusters versus normalized GFP fluorescence in the dendrites for individual 10-14 DIV neurons (N-cad<sup>+/-</sup>: control neurons, grey symbols,  $n=18$ ; N-cad<sup>-/-</sup>: homozygous N-cadherin knockout neurons, red

symbols,  $n=20$ ). Each circle represents one neuron for which the mean fluorescence intensity of its DsRed2-VAMP2 clusters was normalized to the mean fluorescence intensity of DsRed2-VAMP2 vesicle clusters of all neurons to visualize variability. Similarly, the mean fluorescence intensity of the GFP signal in the dendrites of a neuron was normalized to the mean fluorescence intensity of the GFP signal in all neurons. **(b, c)** Quantification of **(b)** mean fluorescence intensity and **(c)** mean area of DsRed2-VAMP2 clusters in mature N-cad<sup>+/+</sup> and N-cad<sup>-/-</sup> neurons. Error bars represent s.e.m,  $n$  represents number of neurons.

### 3.2.1.3. Time lapse analysis of the accumulation of presynaptic vesicles at mature synapses

The accumulation of presynaptic vesicles continues also at more mature synapses but at much slower rates compared with immature nascent synapses. The accumulation of vesicles at individual mature synaptic sites at 10-14 DIV was analyzed using time lapse-imaging as described in Chapter 3.1.2.4. N-cadherin heterozygous control and N-cadherin homozygous knockout neurons were co-transfected with DsRed2-VAMP2 and EGFP at 8-12 DIV and imaged 2 days after transfection. Offline, individual clusters of presynaptic vesicles from N-cad<sup>+/+</sup> and N-cad<sup>-/-</sup> neurons, again fulfilling two criteria: *i*) to be localized on EGFP-expressing dendrites and *ii*) to be stable during the recording time (no splitting or fusion with other vesicle clusters), were selected (Fig. 3.14a). The changes in total fluorescence intensity (the product between mean fluorescence intensity and area of a cluster) were calculated at different time points for each cluster (Fig. 3.14b). The summary of all neurons analyzed (Fig. 3.14c) indicated that the accumulation of vesicles at control mature synapses is strongly reduced as compared to immature N-cadherin control synapses (see Fig. 3.5). On the other hand a comparative analysis of vesicle accumulation at mature N-cadherin deficient synapses indicated that N-cadherin is not involved in this process anymore, as the residual rate of vesicle accumulation was similar for the two genotypes (percent fluorescence increase after 2 hours: N-cad<sup>+/+</sup>:  $122.43 \pm 7.86\%$ , 18 puncta from 18 cells; N-cad<sup>-/-</sup>:  $113.54 \pm 6.90\%$ , 18 puncta from 18 cells). This result indicates that N-cadherin plays a more important role at immature synapses whereas at later maturational stages other, compensatory mechanisms may come into play, partially rescuing the N-cadherin deficient synapses. Another plausible explanation for this result is that N-cadherin may still be important for the accumulation of vesicles at more mature synapses but a defect in accumulation in N-cadherin deficient synapses

becomes less evident as the accumulation of vesicles has largely ceased at this maturational stage.

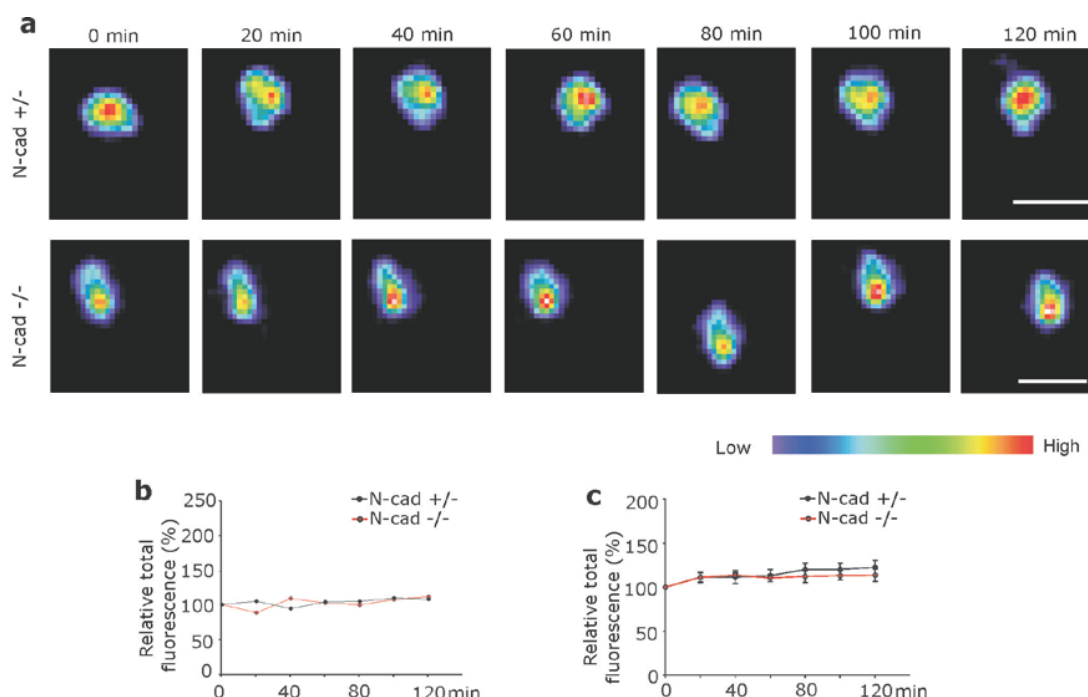


**Figure 3.14. Ongoing presynaptic vesicle accumulation is strongly reduced in more mature neurons (14 DIV) and is unaffected in N-cadherin knockout neurons**

(a) Examples of live-imaging of individual vesicle clusters (DsRed2-VAMP2 puncta on EGFP-expressing dendrites; co-transfection as in Fig. 3.1). Time points of data acquisition are indicated above images. DsRed2-VAMP2 fluorescence intensity is colour-coded. N-cad<sup>+/+</sup>: control neurons. N-cad<sup>-/-</sup>: homozygous N-cadherin knockout neurons. Scale bars represent 1 μm. (b,c) Quantification of DsRed2-VAMP2 fluorescence intensity versus observation time (b) for the individual vesicle clusters shown in (a) and (c) for all clusters studied (mean ± s.e.m.). Total fluorescence intensity of all pixels representing a punctum was calculated and normalized to the intensity at 0 min. N-cad<sup>+/+</sup>: *n*=18 puncta (from 18 cells); N-cad<sup>-/-</sup>: *n*=18 puncta (from 11 cells). Error bars, s.e.m.

### 3.2.1.4. Analysis of the dynamics of presynaptic vesicle clusters in mature neurons

Synaptic vesicle mobility between mature presynaptic terminals has been previously reported (Hopf et al., 2002; Krueger et al., 2003). Mobile synaptic vesicle clusters have been shown to represent not only a mechanism in the fast formation of new synapses or elimination of synapses in mature neurons (Ahmari and Smith, 2002; Kraszewski et al.,

1995; Matteoli et al., 1992), but also a modality of adjacent synapses to share their vesicle pools and in this way acquire similar release probabilities (Darcy et al., 2006).

The stability of the presynaptic vesicle clusters in mature neurons was analyzed in an identical manner as described in Chapter 3.1.2.6. For this, 10-14 DIV N-cadherin heterozygous control and homozygous N-cadherin knockout neurons were co-transfected with DsRed2-VAMP2 and EGFP and imaged for a period of 2 hours (Fig 3.15a; for simplicity only the first 60 minutes are shown). Offline, the absolute change in number of DsRed2-VAMP2 clusters on proximal GFP-expressing dendrites was determined (for more details see Chapter 3.1.2.6 and Fig 3.8) and used as a measure of total dynamics (fusion and splitting events). Surprisingly, the total dynamics was not significantly different in neurons from the two genotypes (Fig. 3.15b, N-cad<sup>+/-</sup>:  $8.93 \pm 1.10$  fusion and splitting events/  $20\mu\text{m}/120\text{min}$ ,  $n=18$ ; N-cad<sup>-/-</sup>:  $8.55 \pm 1.05$  fusion and splitting events/  $20\mu\text{m}/120\text{min}$ ,  $n=18$ ) but was increased compared with the total dynamics in immature neurons (see Fig. 3.8). This intriguing increase in total dynamics in more mature neurons does not mean an increased instability of vesicle clusters, but is explained by the increase in the density of presynaptic vesicle clusters in 10-14 DIV neurons compared to immature 6-7 DIV neurons (notice that total dynamics include a density factor). A higher number of clusters that can split and fuse leads to an increase in the number of events detected (and hence to an increase in total dynamics), even if individual clusters do not split or fuse more often. Unfortunately, because of the high density of DsRed2-labeled vesicle clusters in 10-14 DIV neurons, it was difficult to follow single clusters over the 2 hours recording time, making the analysis of the stability of individual clusters (as in Fig. 3.7) impossible.



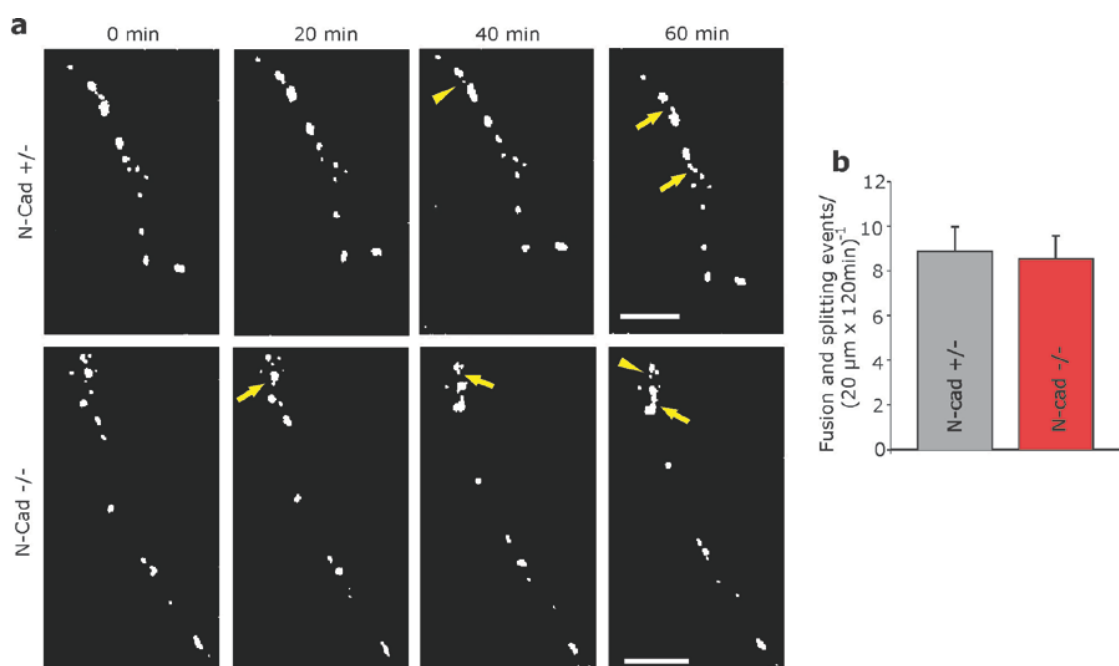


**Figure 3.15. At late maturational stages (10-14 DIV) the total dynamics (fusion and splitting) of vesicle clusters is similar in the absence of N-cadherin**

(a) Examples of live-imaging of vesicle clusters (DsRed2-VAMP2 puncta on EGFP-expressing dendrites; co-transfection as in Fig. 1; 14 DIV). Fluorescence images were thresholded resulting in black-and-white images of DsRed2-VAMP2 puncta area. Budding (splitting) events observed during time-lapse recording are indicated by arrowheads, whereas fusion events are indicated by arrows. Time points of data acquisition are indicated above images. For simplicity only the first 60 minutes of the 120 minutes recording time are shown. N-cad<sup>+/</sup>:- control neurons. N-cad<sup>-/-</sup>: homozygous N-cadherin knockout neurons. Scale bars represent 4 μm. (b) Quantification of the frequency of fusion and splitting events occurring on 20 μm length dendrites during observation time. Error bars, s.e.m.; N-cad<sup>+/</sup>:-  $n = 18$  cells; N-cad<sup>-/-</sup>:  $n = 18$  cells.

### 3.2.2. Role of N-cadherin in maintenance of active zones at mature synapses

The above results on EGFP-Bassoon clusters in immature neurons (see Chapter 3.1.3.2) had indicated that the formation of active zones is not altered in N-cadherin deficient neurons. To further study the role of N-cadherin in the formation and maintenance of active zones, individual mature 10-14 DIV N-cadherin control and N-cadherin deficient neurons were co-transfected with EGFP-Bassoon for visualization of active zones and DsRed2 for labeling the dendrites.

#### 3.2.2.1. Analysis of the density of Bassoon clusters in mature neurons

The density of active zones was determined by counting the EGFP-Bassoon labeled clusters on the DsRed2 expressing dendrites of mature N-cadherin heterozygous control

## RESULTS

and homozygous N-cadherin knockout neurons (Fig. 3.16a). The analysis of the density of Bassoon clusters for the two genotypes (Fig. 3.16b) indicated that in the absence of N-cadherin the formation and maintenance of active zones is not perturbed. The number of active zones per length of dendrite (N-cad<sup>-/-</sup>:  $5.29 \pm 1.29$  clusters/20 $\mu$ m dendrite,  $n=12$ ) was not significantly different between N-cadherin knockout and control neurons (N-cad<sup>+/-</sup>:  $5.83 \pm 1.43$  clusters/20 $\mu$ m dendrite,  $n=8$ ). This finding is in line with the above results that N-cadherin seems to play a more important role in the accumulation of vesicles at nascent synapses than in the maturation of presynaptic specializations at later maturational stages.

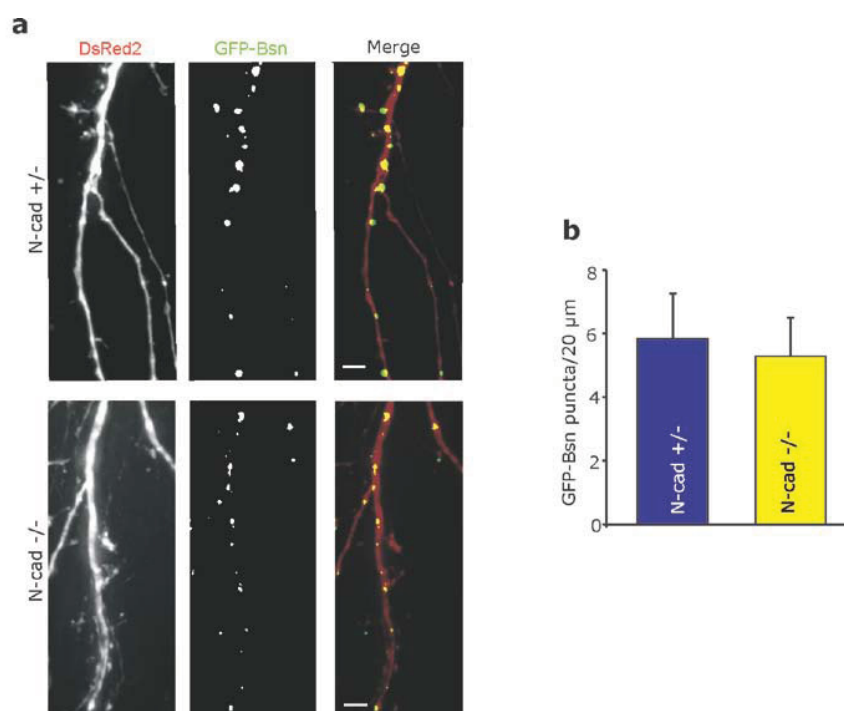


**Figure 3.16. Density of clusters of the active zone protein Bassoon is not affected in more mature N-cadherin deficient neurons**

(a) Fluorescence images of dendrites from ES cell-derived neurons at 14 days in microisland culture (DIV). Neurons were co-transfected with EGFP-Bassoon (green) and DsRed2 (red) using the lipofectamine technique. N-cad<sup>+/-</sup>: control neurons; N-cad<sup>-/-</sup>: homozygous N-cadherin knockout neurons. Scale bars represent 2 $\mu$ m. (b) Quantification of the density of EGFP-Bassoon puncta on dendrites at 10-14 DIV (N-cad<sup>+/-</sup>:  $n=8$ ; N-cad<sup>-/-</sup>:  $n=12$ ). Error bars, s.e.m.,  $n$  represents the number of neurons

### 3.2.2.2. Quantitative analysis of the fluorescence intensity of EGFP-Bassoon labeled active zones in mature neurons

As described for immature neurons, the transfection of EGFP tagged Bassoon protein not only allowed the visualization of vesicle clusters, but also the quantification of fluorescence intensity and size of labeled clusters. These parameters are potential indicators of the cytomatrix organization at active zones. Mean fluorescence intensity and area of the EGFP-Bassoon clusters were also analyzed in more mature N-cadherin heterozygous control and N-cadherin homozygous knockout neurons (10-14DIV). The results were similar to the ones obtained in immature neurons. A strong correlation between the mean fluorescence intensity of the EGFP-Bassoon signal in clusters and the mean fluorescence intensity of EGFP-Bassoon in the dendrite of individual neurons was found (Fig. 3.17a). The analysis of the mean fluorescence intensity of clustered EGFP-Bassoon in N-cadherin knockout neurons (Fig. 3.17b) revealed no significant difference as compared to control neurons (N-cad<sup>+/-</sup>:  $614.19 \pm 173.02$  a.u.,  $n=8$ ; N-cad<sup>-/-</sup>:  $392.47 \pm 57.93$  a.u.,  $n=12$ ). Similarly, the mean area of EGFP-Bassoon clusters showed no significant difference between the two genotypes (Fig. 3.17c, N-cad<sup>+/-</sup>:  $0.20 \pm 0.04 \mu\text{m}^2$ ,  $n=8$ ; N-cad<sup>-/-</sup>:  $0.17 \pm 0.02 \mu\text{m}^2$ ,  $n=12$ ).

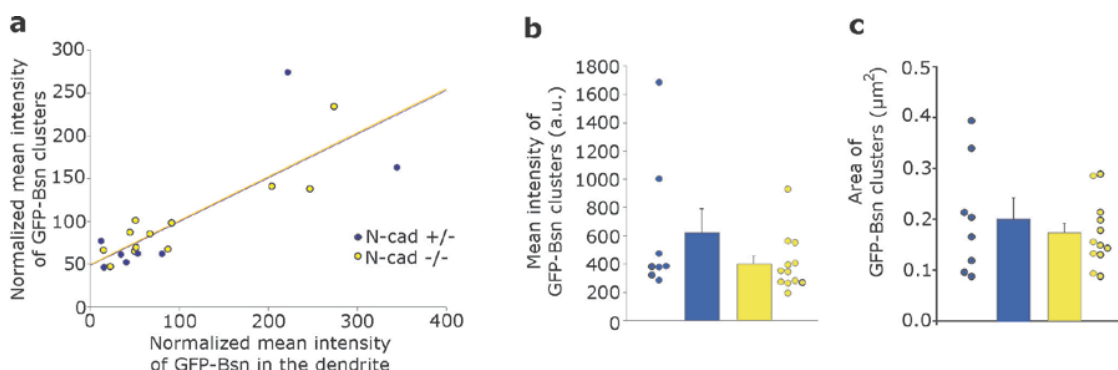


**Figure 3.17. Analysis of the fluorescence intensity and area of the EGFP-Bassoon clusters in mature neurons shows no differences between the two genotypes**

(a) Correlation of normalized mean fluorescence intensity of EGFP-Bassoon clusters versus normalized mean fluorescence intensity of diffusely distributed EGFP-Bassoon signal outside of the clusters for individual mature 10-14 DIV neurons. (N-cad<sup>+/-</sup>: control neurons, blue symbols,  $n=8$ ; N-cad<sup>-/-</sup>: homozygous N-cadherin knockout neurons, yellow symbols,  $n=12$ ). Each circle represents one neuron for which the mean fluorescence intensity of its EGFP-Bassoon signal in clusters was normalized to the mean fluorescence intensity of EGFP-Bassoon clusters present in

all neurons to visualize variability. Similarly, the mean fluorescence intensity of the EGFP-Bassoon signal outside of the clusters (in the dendrites) of a neuron was normalized to the mean fluorescence intensity of the EGFP-Bassoon signal in the dendrites of all neurons. **(b, c)** Quantification of **(b)** mean fluorescence intensity and **(c)** mean area of EGFP-Bassoon clusters in mature N-cad<sup>+/+</sup> and N-cad<sup>-/-</sup> neurons. Error bars, s.e.m., *n* represents number of neurons.

### **3.3. Co-localization of presynaptic specializations with the postsynaptic marker protein PSD-95 in cultured ES-cell derived neurons**

In the experiments described above, the role of N-cadherin in the formation of the presynaptic specialization of glutamatergic synapses was studied by investigating DsRed2-labeled presynaptic vesicle clusters and EGFP-labeled Bassoon protein accumulations. To confirm that indeed the presynaptic specializations studied here are part of excitatory glutamatergic synapses, N-cadherin heterozygous control and N-cadherin homozygous knockout neurons were co-transfected with DsRed2-VAMP2 for labeling presynaptic vesicle clusters and PSD95-EGFP for labeling post-synaptic densities of glutamatergic synapses. PSD95 is an important scaffolding protein of the postsynaptic density of excitatory synapses. Studies in neuronal cell cultures have shown that between 1 and 3 weeks in vitro, PSD95 localization shifts from mostly non-synaptic to a predominantly synaptic pattern (Rao et al., 1998). For this reason, only 10-14 DIV old neurons were used for the experiments. In immature neurons (6-7 DIV) PSD95-EGFP had a diffuse, non-synaptic distribution (data not shown).

#### **3.3.1. Digital image processing of the PSD95-EGFP signal**

To investigate the postsynaptic specializations in N-cadherin control and N-cadherin deficient neurons, PSD95-EGFP fluorescence images were acquired and processed under identical conditions for the two genotypes. For quantification of the PSD95-EGFP signal, digital images were analyzed after a threshold operation had been applied.

PSD95-EGFP expression had a punctate distribution (Fig. 3.18a), well corresponding to the postsynaptic density clusters. To visualize the fluorescence intensity of PSD95-EGFP clusters, a colour coded image was used (Fig. 3.18b), where high intensity pixels are depicted as hot colours whereas low intensity pixels are shown as cold colours. For simplification of the image presentation but also for all quantitative measurements, the

PSD95-EGFP signal was thresholded using an automatic threshold operation analogous to the DsRed2-VAMP2 signal. This threshold operation takes into account the histogram distribution of all pixels in the image and the pixels, which have a fluorescence intensity that is higher than two times the standard deviation of the background fluorescence, are shown in white whereas all the pixels whose fluorescence intensity is lower than this threshold value are shown in black (for more details see Threshold operation in Materials and Methods). Thus, GFP-labeled postsynaptic specializations appear as white puncta on a black background (Fig. 3.18c).

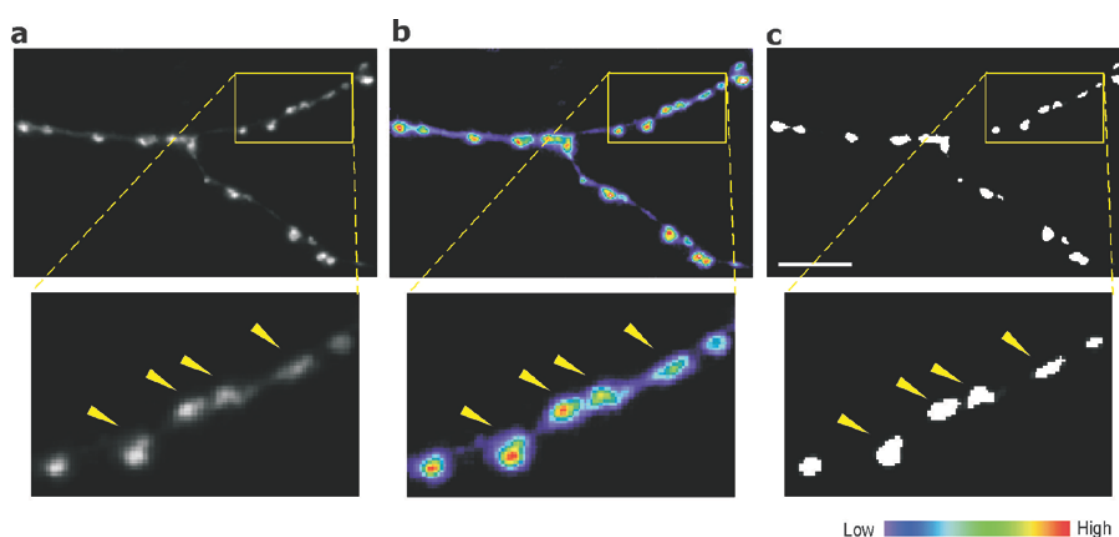


**Figure 3.18. Threshold operation used for analysis of the PSD95-EGFP clusters in ES cell-derived neurons**

Fluorescence images of dendrites from ES cell-derived neuron (13 DIV) co-transfected with PSD95-EGFP. Boxed areas in images a-c are magnified below the corresponding images for better visualization. **(a)** Raw image showing that PSD95-EGFP has a punctate distribution (arrows) corresponding to postsynaptic specializations. **(b)** Pseudocolour images of the same dendritic region indicating that PSD95 clusters have high fluorescence intensity whereas the fluorescence outside of the clusters has low intensity. PSD95-EGFP fluorescence intensity is colour-coded. **(c)** Threshold images showing that after the threshold operation GFP-labeled postsynaptic specializations appear as white puncta on a black background.

### 3.3.2. Analysis of colocalization between presynaptic vesicles and postsynaptic PSD-95 in N-cadherin deficient neurons

In the glial microisland culture system used throughout this study, 10-15 neurons are growing on a glial island in complete separation from other islands. Usually, only one neuron per glial island was co-transfected either with DsRed2-VAMP and EGFP or with EGFP-Bassoon and DsRed2. This was similar for co-transfections with DsRed2-VAMP2 and PSD95-EGFP (Fig. 3.19a). Quantitative analysis of co-localization of the DsRed2 signal and the GFP signal indicated that the fraction of autapses is very high in this culture system and not significantly different for N-cadherin control and N-cadherin deficient neurons (Fig. 3.19b, N-cad<sup>+/-</sup>:  $81.82 \pm 2.60\%$ ,  $n=20$ ; N-cad<sup>-/-</sup>:  $79.56 \pm 2.94\%$ ,  $n=18$ ). The DsRed2-VAMP2 clusters that do not have a PSD95-EGFP apposition (arrows in Fig. 3.19a) may represent either transport packages, which are recruited to nascent synapses to form the vesicle pool, presynaptic vesicle clusters of inhibitory synapses or presynaptic specializations of synapses made with a dendrite of a non-transfected neuron present on the island. PSD95-EGFP clusters that do not have a DsRed2-VAMP2 apposition (arrowheads in Fig. 3.19a) may represent post-synaptic specializations of synapses made by axons of non-transfected neurons with the dendrites of the transfected cell. The high percentage of co-localization between PSD95-EGFP and DsRed2VAMP2 found indicates that in our microisland system the majority of synapses are glutamatergic autapses and that the presynaptic vesicle accumulations and active zones analyzed represent presynaptic specialization of synapses.

## RESULTS

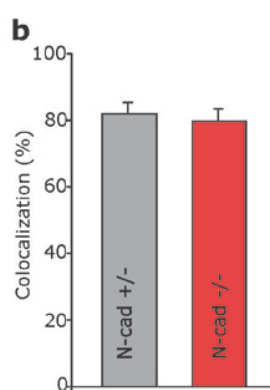
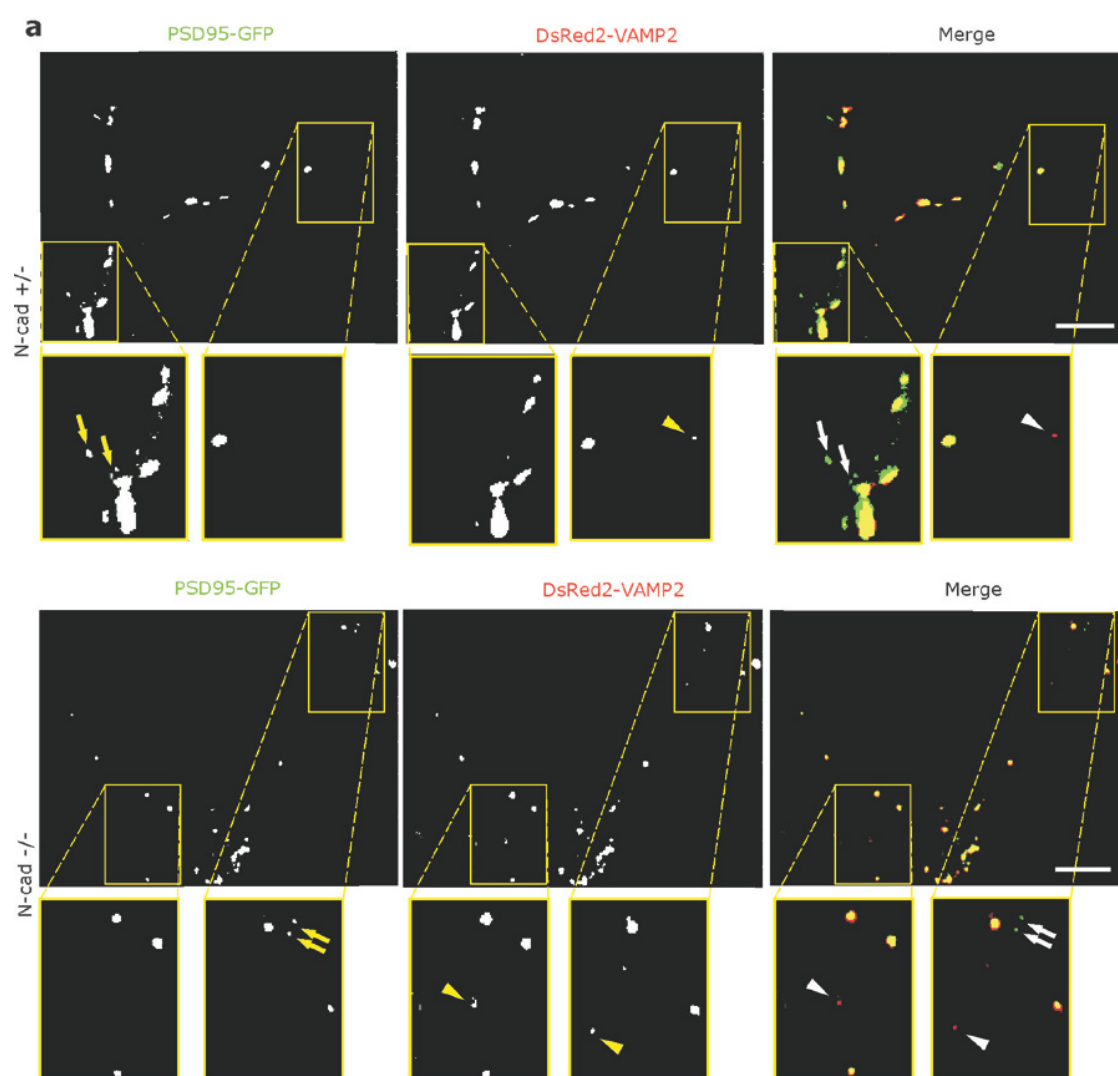


**Figure 3.19. DsRed2-VAMP2 labeled presynaptic vesicle clusters are largely co-localized with PSD95-EGFP labeled postsynaptic densities**

(a) Fluorescence images of dendrites from ES cell-derived neurons at 12 days in microisland culture (DIV). Boxed areas in images are magnified below the corresponding images for better visualization. PSD95-EGFP for labeling postsynaptic densities (green) and DsRed2-VAMP2 for labeling presynaptic vesicle clusters (red) were co-transfected using the lipofectamine technique and only one neuron was transfected on an individual glial microisland. N-cad<sup>+/-</sup>: control neurons; N-cad<sup>-/-</sup>: homozygous N-cadherin knockout neurons. Autapses appear yellow in the overlay image. Arrows (yellow in black and white images and white in merged image) indicate non-colocalized PSD95-EGFP puncta and arrowheads (yellow in black and white images and white in merged image) indicate non-colocalized DsRed2-VAMP2 puncta. Scale bars represent 5 $\mu$ m (b) Quantification of the level of co-localization of presynaptic vesicle clusters and postsynaptic densities confirming a highly autaptic culture system. Error bars, s.e.m., N-cad<sup>+/-</sup>:  $n = 20$  cells; N-cad<sup>-/-</sup>:  $n = 18$  cells.

### 3.3.3. Analysis of fluorescence intensity and area of PSD95-EGFP postsynaptic specializations

Overexpression of PSD95 in hippocampal neurons is known to drive maturation of glutamatergic synapses by enhancing postsynaptic clustering and activity of glutamate receptors but also enhances the maturation of the presynaptic terminals (El-Husseini et al., 2000). To investigate whether PSD95 overexpression has a similar effect in N-cadherin heterozygous control and homozygous N-cadherin knockout neurons, the relationship between the mean fluorescence intensity of PSD95-EGFP clusters and the mean fluorescence intensity of DsRed2-VAMP2 clusters was analyzed (Fig. 3.20a). No significant correlation between the fluorescence intensities of the pre- and postsynaptic markers was found, neither in N-cadherin heterozygous nor in homozygous N-cadherin knockout neurons. This result can again be explained by the independent and widely variable expression levels of DsRed2-VAMP2 and PSD95-EGFP vectors in individual neurons. As a next step, the mean fluorescence intensity (Fig. 3.20b) and area (Fig. 3.20c) of PSD95-EGFP clusters was analyzed and no significant differences between the two genotypes were found (mean fluorescence intensity: N-cad<sup>+/-</sup>:  $256.95 \pm 32.03$  a.u.,  $n=20$ ; N-cad<sup>-/-</sup>:  $276.58 \pm 36.42$  a.u.; Area: N-cad<sup>+/-</sup>:  $0.25 \pm 0.02 \mu\text{m}^2$ ; N-cad<sup>-/-</sup>:  $0.29 \pm 0.04 \mu\text{m}^2$ ,  $n=18$ ).



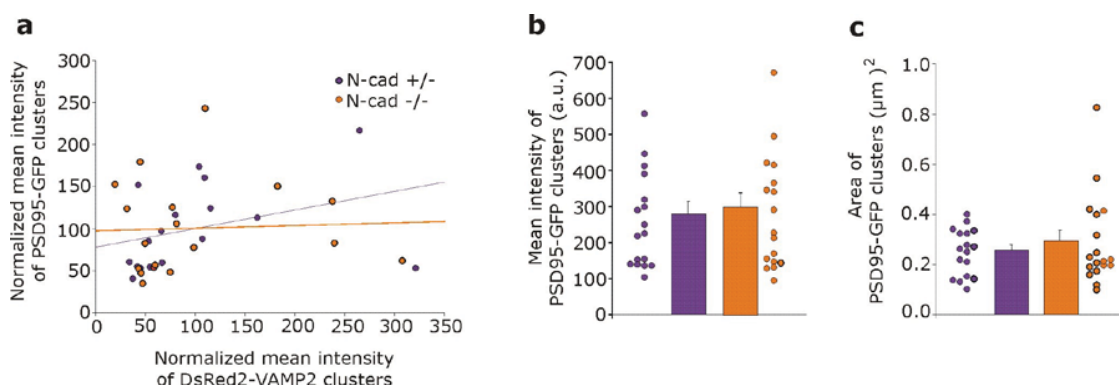


**Figure 3.20. Analysis of mean fluorescence intensity and area of the PSD95-EGFP clusters revealed no differences between the two genotypes**

(a) Correlation of normalized fluorescence intensity of PSD95-EGFP clusters versus normalized fluorescence of DsRed2-VAMP2 clusters for individual 10-14 DIV neurons. (N-cad<sup>+/-</sup>: control neurons, purple symbols,  $n=18$ ; N-cad<sup>-/-</sup>: homozygous N-cadherin knockout neurons, orange symbols,  $n=20$ ). Each circle represents one neuron for which the mean fluorescence intensity of its PSD95-EGFP clusters was normalized to the mean fluorescence intensity of the PSD95-EGFP signal present in all neurons. Similarly, the mean fluorescence intensity of DsRed2-VAMP2 clusters of a neuron was normalized to the mean fluorescence intensity of the DsRed2-VAMP2 signal in the clusters of all neurons. (b, c) Quantification of (b) mean fluorescence intensity and (c) area of PSD95-EGFP clusters in N-cad<sup>+/-</sup> and N-cad<sup>-/-</sup> neurons (Error bars, s.e.m.,  $n$  represents number of neurons).

### 3.4. Essential cooperation of N-cadherin and neuroligin1 during synapse formation in immature neurons

The major finding of the experiments described above was that N-cadherin is required for the accumulation of vesicles at immature synapses, whereas at later maturational stages N-cadherin becomes less important. To gain further insights into the mechanisms used by N-cadherin to control vesicle clustering at nascent synapses, neuroligin1 overexpression was used to trigger formation of new synapses (Sara et al., 2005; Scheiffele et al., 2000) in immature cultured neurons.

#### 3.4.1. Comparison of N-cadherin and neuroligin function in inducing presynaptic vesicle accumulation

The experiments described above firmly established that N-cadherin plays a crucial role in the regulation of vesicle accumulation during early synapse maturation. The density of DsRed2-labeled vesicle clusters is reduced in immature N-cadherin knockout neurons

and also the recruitment and accumulation of vesicles at individual synaptic sites is much slower in the absence of N-cadherin compared with control neurons.

However, using an assay involving co-culture of non-neuronal and neuronal cells to study the minimum molecular requirements for synapse induction, it has been shown that presentation of N-cadherin on the surface of non-neuronal cells is not able to induce accumulation of synaptic vesicles in contacting neurons, whereas another cell adhesion molecule, neuroligin1, is able to induce presynaptic vesicle clusters in axons contacting the transfected heterologous cells (Scheiffele et al., 2000). Additionally, overexpression of neuroligins has been reported by several groups to be also sufficient to induce synapse formation in cultured hippocampal neurons, but the effect of N-cadherin overexpression was in most cases not tested in these cultures. Because of these seemingly conflicting results, on one hand involvement of N-cadherin in the accumulation of presynaptic vesicles and on the other hand inability to induce vesicle clustering in contacting axons, the ability of neuroligin1 and N-cadherin to trigger vesicle accumulation was tested in immature primary cortical neurons.

Cortical neurons from E17 mouse fetuses (from C57Bl/6 pregnant mice) were cultured in a glial microisland system for 4-5 DIV similar to embryonic stem cell-derived neurons. At this immature stage, the neurons were co-transfected either with EGFP + DsRed2-VAMP2 (control), or neuroligin1-EGFP + DsRed2-VAMP2 or N-cadherin-EGFP + DsRed2-VAMP2, and analyzed for vesicle clusters after 2 days (Fig. 3.21a). As expected from previous studies, neuroligin1-EGFP expression induced the formation of significantly ( $P=0.027$ ) more presynaptic vesicle clusters (Fig. 3.21b,  $5.55 \pm 0.56$  DsRed2-VAMP2 clusters/  $20\mu\text{m}$  dendrite,  $n=27$ ) compared to the control EGFP expression ( $3.68 \pm 0.53$  DsRed2-VAMP2 clusters/  $20\mu\text{m}$ ,  $n=24$ ), whereas the expression of N-cadherin-EGFP did not have any significant effect on the number of vesicle clusters ( $3.89 \pm 0.42$  DsRed2-VAMP2 clusters/  $20\mu\text{m}$  dendrite,  $n=16$ ).

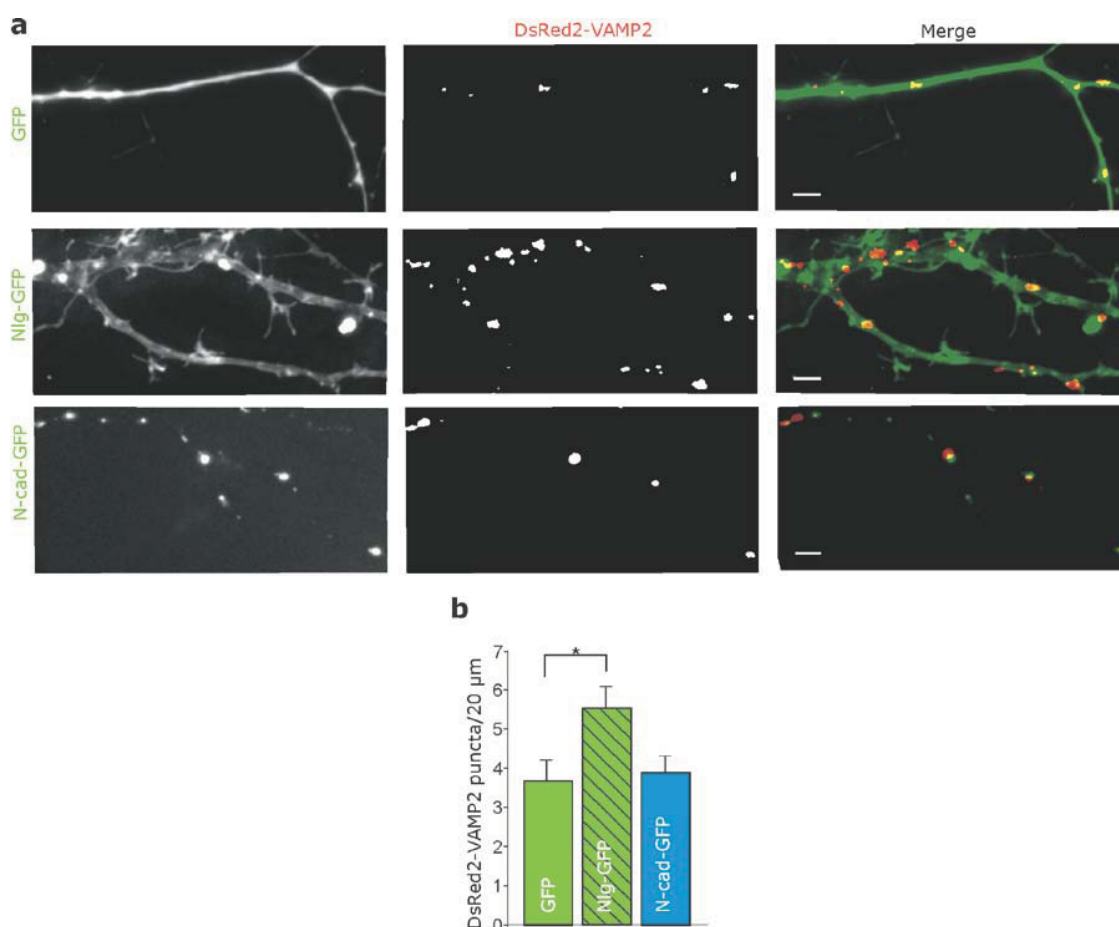


**Figure 3.21. Expression of neuroligin1-EGFP, but not N-cadherin-EGFP, resulted in an increase in the density of presynaptic vesicle clusters in primary cultured cortical neurons (7 DIV) as compared to EGFP expression (control)**

DsRed2-VAMP2 (to visualize vesicle clusters) was co-transfected with either EGFP (GFP) or neuroligin1-EGFP (Nlg-GFP) or N-cadherin-EGFP (N-cad-GFP). **(a)** Fluorescence images of dendrites. Left: EGFP fluorescence to visualize expressed proteins in dendrites. Middle: DsRed2 fluorescence to visualize presynaptic vesicle clusters. Right: Overlay of EGFP fluorescence (green) and DsRed2 fluorescence (red) to visualize vesicle clusters on dendrites. Scale bars represent 2μm. **(b)** Quantification of the density of presynaptic vesicle clusters. Type of co-transfection with DsRed2-VAMP2 is indicated on bars. GFP:  $n=24$ ; Nlg-GFP:  $n=27$ ; N-cad-GFP:  $n=16$ . Error bars represent s.e.m.\*  $P<0.05$ .  $n$  indicates number of cells

This puzzling result that N-cadherin seems to participate in the accumulation of presynaptic vesicles at nascent synapses but alone is not able to trigger *de novo* vesicle clustering in cortical neurons, suggested that N-cadherin might be involved in the maturation of already existing presynaptic specializations by filling them with vesicles. To test this idea, the mean fluorescence intensity of DsRed2-VAMP2 clusters in N-

cadherin-EGFP transfected neurons was analyzed and compared with the fluorescence intensity of vesicle clusters in control GFP transfected neurons. Interestingly, overexpression of N-cadherin-EGFP, but not of neuroligin1-EGFP, led to almost a doubling (93% increase,  $P=0.002$ ) of the mean fluorescence intensity of DsRed2-labeled presynaptic vesicle clusters compared to GFP-expressing neurons (Fig. 3.22a; EGFP transfection;  $191.27 \pm 20.56$  a.u.,  $n=24$ ; Nlg-EGFP transfection:  $169.43 \pm 13.94$  a.u.,  $n=27$ ; N-cad-EGFP transfection:  $369.52 \pm 58.71$  a.u.,  $n=16$ ). Similarly, the area occupied by the vesicle clusters was significantly increased ( $P=0.019$ ) upon N-cadherin-EGFP expression compared with control EGFP-expression (Fig. 3.22b; EGFP transfection;  $0.23 \pm 0.02$  a.u.,  $n=24$ ; Nlg-EGFP transfection:  $0.23 \pm 0.03$  a.u.,  $n=27$ ; N-cad-EGFP transfection:  $0.36 \pm 0.05$  a.u.,  $n=16$ ). These results strongly support the idea that N-cadherin is involved in the accumulation of synaptic vesicles at presynaptic terminals, but alone is not sufficient to trigger the formation of new vesicle clusters (a role attributed to neuroligins).

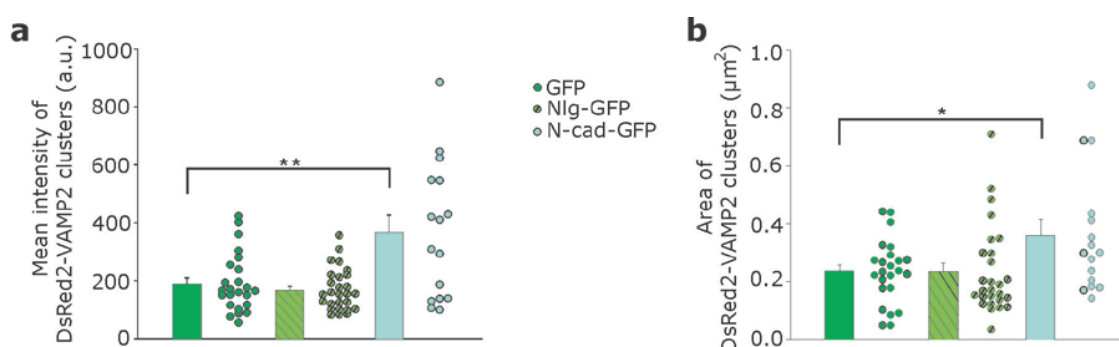


**Figure 3.22. N-cadherin-EGFP overexpression in immature primary cortical neurons increased the mean fluorescence intensity and area of DsRed2-VAMP2 clusters**

Quantification of (a) mean fluorescence intensity and (b) area of DsRed2-VAMP2 clusters in neurons co-transfected with DsRed2-VAMP2 and either control EGFP (GFP, green symbols,  $n=24$ ) Neuroligin1-EGFP (Nlg-GFP, striking green symbols,  $n=27$ ) or N-cadherin-EGFP (N-cad-GFP, blue symbols,  $n=16$ ). Each circle represents the mean fluorescence intensity (a) or mean area (b) of the DsRed2-VAMP2 clusters of a single neuron. Error bars represent s.e.m.\*  $P<0.05$ , \*\*  $P<0.01$ ;  $n$  indicates number of cells.

### 3.4.2. Vesicle-clustering activity of neuroligin1 requires N-cadherin expression

Based on the observations that both adhesion molecules, N-cadherin and neuroligin1, are involved in presynaptic vesicle accumulation at nascent synapses, it was hypothesized that N-cadherin might control presynaptic vesicle accumulation by regulating the function of the neuroligin/neurexin system, which has been shown to actively induce the formation of new presynaptic vesicle clusters. To address this potential mechanism experimentally, neuroligin1-EGFP was expressed together with DsRed2-VAMP2 in immature N-cadherin heterozygous control and N-cadherin knockout ES cell-derived neurons at 4-5 DIV and the density of presynaptic vesicle clusters was assessed 2 days later (Fig. 3.23a). In control neurons (N-cad<sup>+/-</sup>) co-expression of neuroligin1-EGFP and DsRed2-VAMP2 led to a highly significant ( $P=0.00003$ ) increase in the density of vesicle clusters on dendrites ( $5.7\pm0.3$  puncta/20 $\mu$ m dendrite,  $n=31$ ) as compared to EGFP-expressing N-cad<sup>+/-</sup> neurons (Fig. 3.23b,  $3.9\pm0.3$  puncta/20 $\mu$ m dendrite,  $n=45$ ). Most intriguingly, this vesicle cluster-inducing effect of neuroligin1 expression was completely absent upon expression of neuroligin1-EGFP in N-cadherin deficient neurons (Fig. 3.23b EGFP transfected:  $2.21\pm0.22$  puncta/20 $\mu$ m dendrite,  $n=38$ ; Nlg-EGFP transfected:  $1.73\pm0.14$  puncta/20 $\mu$ m dendrite,  $n=36$ ). This finding strongly indicates that in neuronal cells neuroligin can exert its effect of triggering presynaptic vesicle clustering only if N-cadherin is present.

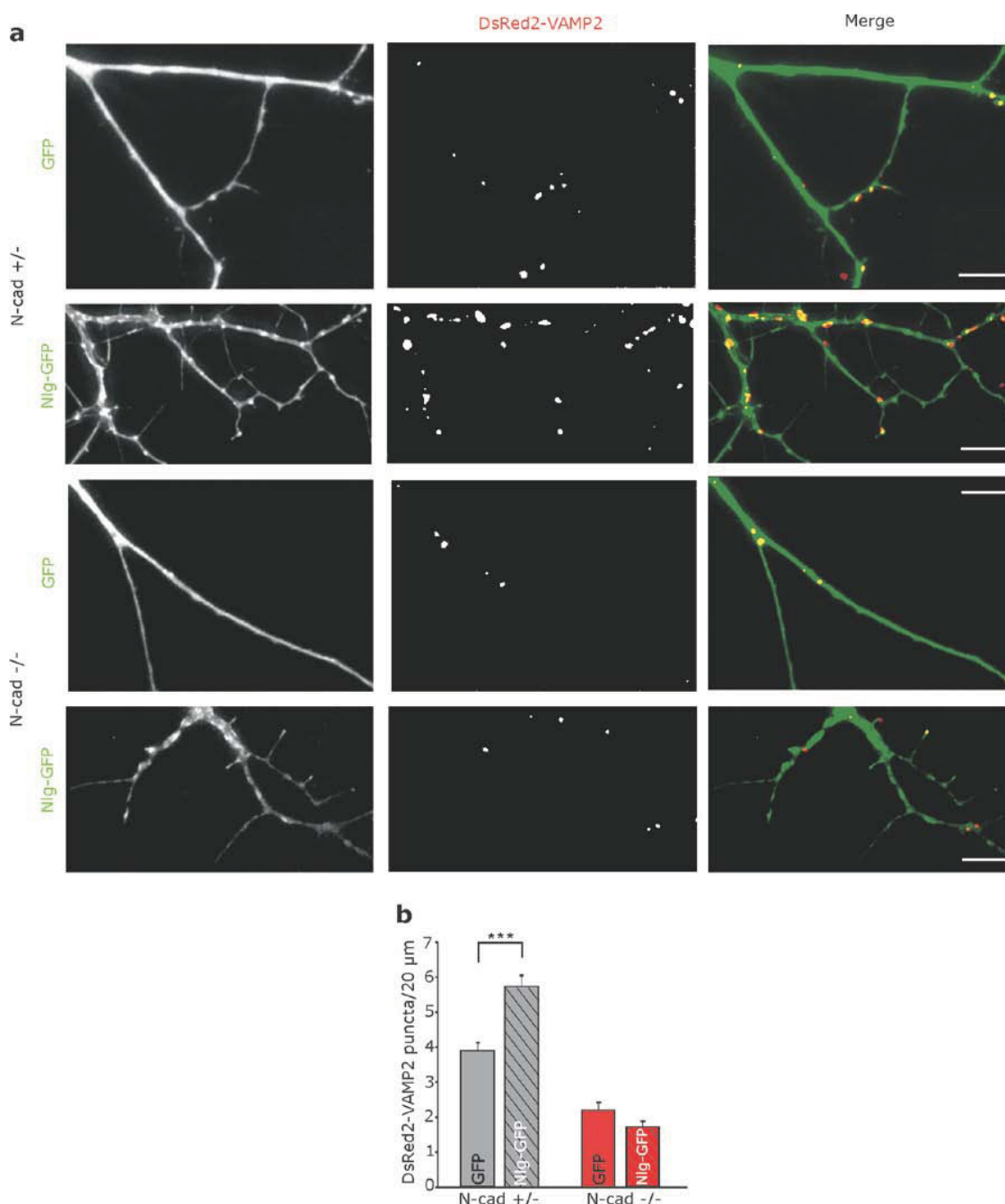


**Figure 3.23. N-cadherin is required for the induction of presynaptic vesicle clusters by overexpression of neuroligin1**

In immature N-cadherin-deficient neurons (N-cad $^{-/-}$ ) at 6-7 DIV neuroligin1-EGFP expression did not induce additional vesicle clusters (control neurons: N-cad $+/+$ ). **(a)** Images of dendrites of control and of N-cadherin knockout neurons co-transfected with DsRed2-VAMP2 (to label autaptic vesicle clusters) and either neuroligin1-EGFP (to induce vesicle clusters; Nlg-GFP) or EGFP (control transfection; GFP). Left: EGFP fluorescence (green) visualizing fluorescent proteins in dendrites. Middle: DsRed2 fluorescence (red) visualizing vesicle clusters. Right: Overlay of EGFP fluorescence and DsRed2 fluorescence visualizing vesicle clusters on dendrites.

Scale bars represent 5µm. **(b)** Quantification of the induction of presynaptic vesicle clusters by overexpression of neuroligin1. Co-expression of either neuroligin1-EGFP or EGFP with DsRed2-VAMP2 is indicated on bars. N-cad<sup>+/+</sup>: GFP *n*=45; Nlg-GFP *n*=31. N-cad<sup>-/-</sup>: GFP *n*=38; Nlg-GFP *n*=36 (*n* indicates number of cells). Error bars represent s.e.m. \*\*\* *P*<0.001.

### **3.4.3. Role of N-cadherin in synaptic localization of neuroligin1**

A potential molecular mechanism underlying the above finding that vesicle-clustering activity of neuroligin1 requires N-cadherin expression, is that N-cadherin may control the postsynaptic localization and clustering of neuroligin1. In a second step neuroligin would then heterophilically interact with presynaptic neurexins, which finally accumulate presynaptic vesicles. To begin to test this hypothetical mechanism, the clustering and synaptic localization of neuroligin1-EGFP was analyzed in control and N-cadherin deficient neurons.

#### **3.4.3.1. Digital image processing of neuroligin1-EGFP clusters**

To investigate the subcellular localization of the expressed neuroligin1-EGFP along dendrites of transfected N-cadherin control and N-cadherin deficient neurons, neuroligin1-EGFP images were acquired and processed using identical conditions for the two genotypes. For quantification of the neuroligin1-EGFP signal, digital images were analyzed after a threshold operation had been applied. Because neuroligin1-EGFP had only a partially clustered expression in immature neurons (Fig. 3.24a), the threshold was set manually, so that the diffuse neuroligin1-EGFP signal in the dendrite was removed and only the strong neuroligin1-EGFP signal in the clusters was above threshold. The analysis of the expression levels of neuroligin1-EGFP in individual N-cadherin heterozygous control and homozygous N-cadherin knockout neurons indicated a strong correlation between the neuroligin1-EGFP signal in the clusters and in the dendrite, with no significant differences between genotypes (Fig. 3.24b).



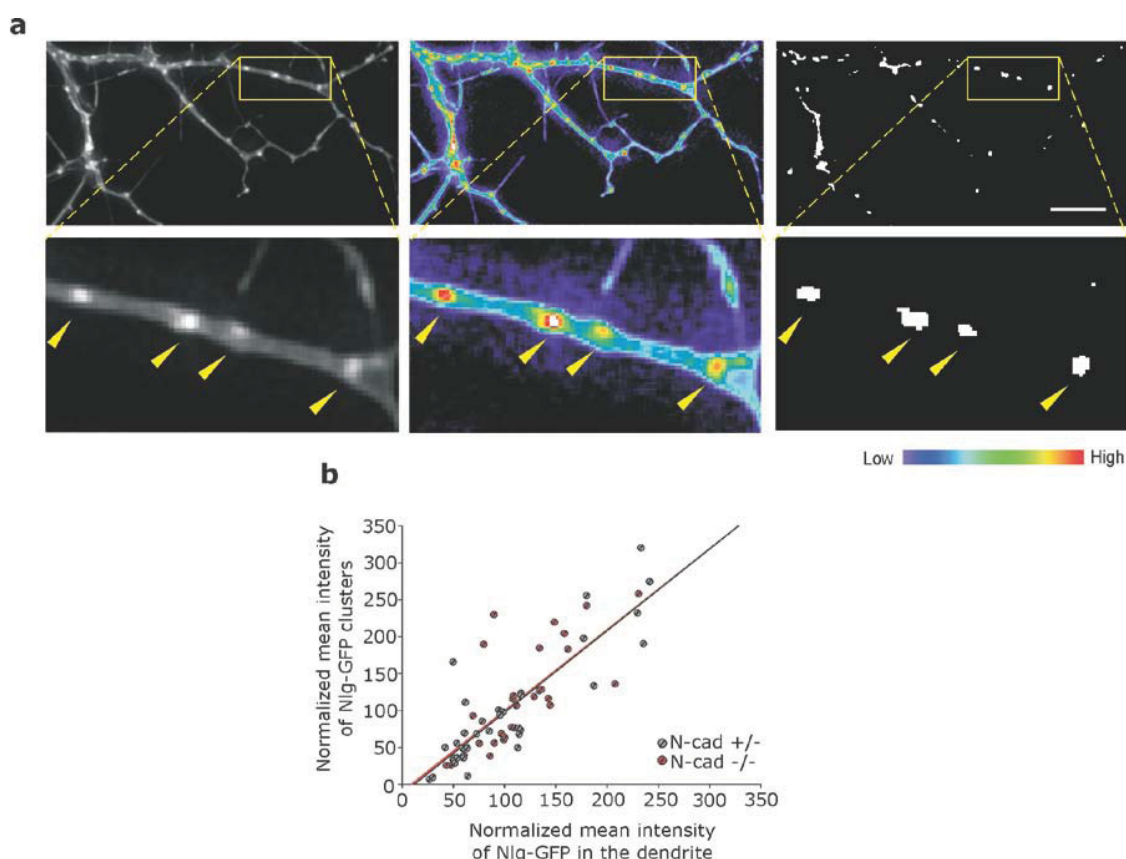


**Figure 3.24. Correlation analysis of mean Nlg-EGFP fluorescence intensity in clusters versus mean fluorescence intensity of diffusely distributed Nlg-EGFP signal in the dendrites of control and N-cadherin deficient neurons**

(a) Threshold operation used for analysis of the neuroligin1-EGFP clusters in ES cell-derived neurons. Fluorescence images of a dendrite from N-cadherin heterozygous ES cell-derived neuron (7 DIV) transfected with neuroligin1-EGFP. Boxed areas in the images are magnified below the corresponding images for better visualization. Left: raw image of a neuroligin1-EGFP (Nlg-GFP) expressing dendrite. Nlg-GFP has a punctate distribution (arrows) but there is also a diffuse Nlg-GFP signal outside of the clusters. Middle: Pseudocolour images of the same dendritic region indicating that Nlg-GFP clusters have high intensity, whereas the fluorescence outside of the clusters has lower intensity but still much above background levels. Nlg-GFP fluorescence intensity is colour-coded. Right: Threshold images showing that after the threshold operation Nlg-GFP clusters appear as white puncta on a black background. Scale bar represents 5  $\mu$ m. (b) Correlation of normalized mean fluorescence intensity of the Nlg-GFP signal in clusters versus normalized mean Nlg-GFP fluorescence of the diffusely distributed signal outside of the clusters for individual immature 6-7 DIV neurons. (N-cad<sup>+/−</sup>: control neurons transfected with Nlg-GFP, strikethrough grey symbols,  $n=31$ ; N-cad<sup>−/−</sup>: homozygous N-cadherin knockout neurons transfected with Nlg-GFP, strikethrough red symbols,  $n=36$ ). Each circle represents one neuron for which the mean fluorescence intensity of its Nlg-GFP signal in clusters was normalized to the mean fluorescence intensity of Nlg-GFP clusters present in all neurons. Similarly, the mean fluorescence intensity of Nlg-GFP signal outside of the clusters (in the dendrites) of a neuron was normalized to the mean fluorescence intensity of Nlg-GFP signal in the dendrites of all neurons.  $n$  represents number of neurons.



### 3.4.3.2. Analysis of the density and colocalization of postsynaptic neuroligin accumulations with presynaptic vesicles clusters

After the threshold operation was applied to the neuroligin1-EGFP signal and the DsRed2-VAMP2 signal in N-cadherin control and N-cadherin deficient neurons (Fig. 3.25a), the density and colocalization of postsynaptic neuroligin accumulations with presynaptic vesicle clusters was investigated. In the absence of N-cadherin a significant reduction ( $P=0.0032$ ) in the density of neuroligin1-EGFP clusters was observed (Fig. 3.25b; N-cad<sup>+/-</sup>:  $4.68 \pm 0.45$  /20 $\mu$ m dendrite,  $n=31$ ; N-cad<sup>-/-</sup>:  $3.02 \pm 0.32$  /20 $\mu$ m dendrite,  $n=36$ ), suggesting that N-cadherin is required for clustering of neuroligin1. Furthermore the co-localization of neuroligin1-EGFP puncta with presynaptic vesicle clusters was analyzed (Fig. 3.25c). In the absence of N-cadherin the fraction of neuroligin1-EGFP puncta co-localized with DsRed2-VAMP2 puncta ( $12 \pm 4\%$ ,  $n=36$ ) was strongly reduced ( $P=0.00003$ ) as compared to control N-cad<sup>+/-</sup> neurons ( $43 \pm 5\%$ ,  $n=31$ ) indicating that N-cadherin is important for alignment of postsynaptic neuroligin1 clusters with presynaptic vesicles. In summary, these findings strongly suggest a cooperation of the N-cadherin and the neuroligin/neurexin adhesion systems during early synapse maturation, where N-cadherin defines the postsynaptic localization of neuroligin1 and in turn neuroligin1 is actively accumulating the presynaptic vesicles by binding to  $\beta$ -neurexins localized on the presynaptic membranes.

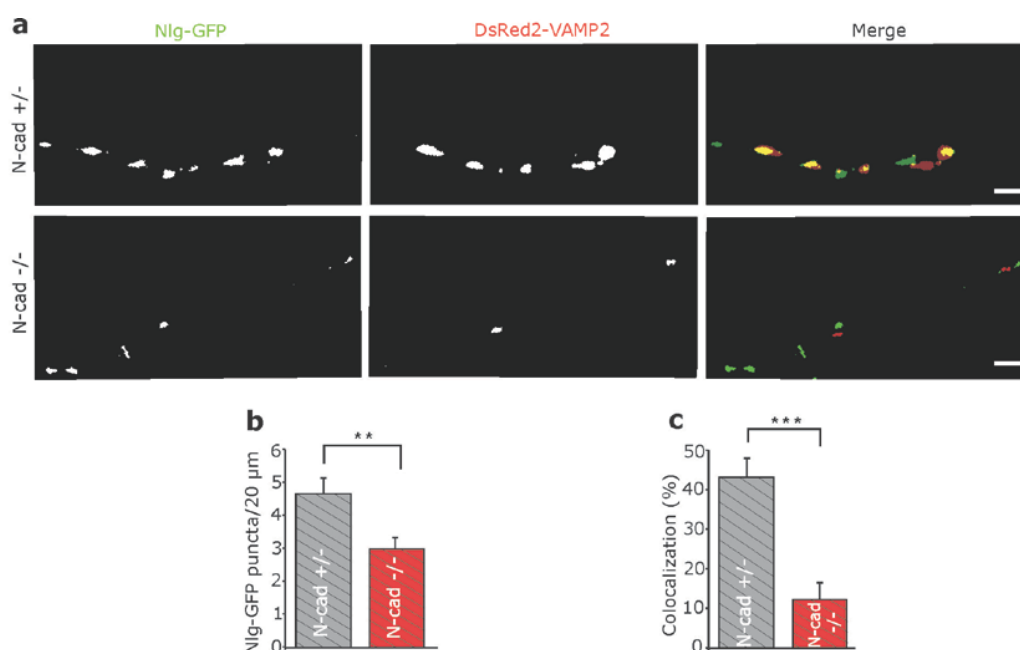


**Figure 3.25. Synaptic targeting of neuroligin1-EGFP is reduced in the absence of N-cadherin**

(a) Fluorescence images of dendrites of control (N-cad<sup>+/-</sup>) and of N-cadherin-deficient (N-cad<sup>-/-</sup>) neurons co-transfected with neuroligin1-EGFP and DsRed2-VAMP2. Left: EGFP fluorescence (Nlg-GFP) visualizing neuroligin1-EGFP puncta on dendrites (puncta were isolated from overall fluorescence in the dendrite by thresholding the image as in figure 3.24). Middle: DsRed2 fluorescence (DsRed2-VAMP2) visualizing presynaptic vesicle clusters. Right: Overlay of EGFP fluorescence (green) and DsRed2 fluorescence (red) visualizing co-localization of neuroligin1-EGFP with presynaptic vesicle clusters. Scale bars represent 1  $\mu$ m. (b) Quantification of the density of neuroligin1-EGFP puncta on dendrites. N-cad<sup>+/-</sup>: control neurons; N-cad<sup>-/-</sup>: homozygous N-cadherin knockout neurons. (c) Quantification of co-localization of neuroligin1-EGFP puncta with DsRed2-labeled presynaptic vesicle clusters. N-cad<sup>+/-</sup>:  $n=31$ ; N-cad<sup>-/-</sup>:  $n=36$  ( $n$  represents number of neurons). Error bars represent s.e.m. \*\*  $P<0.01$ ; \*\*\*  $P<0.001$ .

**3.4.4. Role of the postsynaptic scaffolding molecule S-SCAM in mediating the interaction of N-cadherin and neuroligin1**

In the above experiments, N-cadherin was required for effective postsynaptic targeting of expressed neuroligin1 and this cooperation was essential for the vesicle cluster-inducing activity of neuroligin1. Mechanistically, this interaction might be mediated by postsynaptic scaffolding molecules binding to both neuroligin1 and the  $\beta$ -catenin/N-cadherin adhesion system. A major candidate for such a connecting molecule is S-SCAM (a synaptic scaffolding molecules with multiple PDZ domains, also known as MAGI-2), because it has been shown to bind to  $\beta$ -catenin via its 5<sup>th</sup> PDZ domain (Nishimura et al., 2002) and to bind to neuroligin1 via its WW and 1<sup>st</sup> PDZ domains (Hirao et al., 1998; Iida et al., 2004).

To examine the potential role of S-SCAM as a connecting pathway, truncated, function-blocking forms of S-SCAM (Fig. 3.26b: S-SCAM with either PDZ5 or PDZ1 deleted) together with neuroligin1-EGFP and DsRed2-VAMP2 were co-expressed in primary cultured cortical neurons using the above described autaptic culture system (Fig 3.26a). As a control experiment, full-length S-SCAM together with neuroligin1-EGFP and DsRed2-VAMP2 were co-expressed in immature 6-7 DIV neurons. As expected, 2 days after transfection, expression of neuroligin1-EGFP resulted in a clear, significant ( $P=0.016$ ) vesicle cluster-inducing effect (Fig. 3.26c; EGFP and S-SCAM full:  $3.51\pm0.42$  clusters/20 $\mu$ m dendrite,  $n=21$ ; Nlg-EGFP and S-SCAM full:  $5.15\pm0.49$  clusters/20 $\mu$ m dendrite,  $n=16$ ). To test the functional role of S-SCAM, a truncated form of S-SCAM was co-expressed in which the  $\beta$ -catenin binding domain PDZ5 was deleted, while the

## RESULTS

other domains including the neuroligin1 binding domains were intact (Fig. 3.26a). Consistent with a crucial role of S-SCAM as a connecting molecule, the vesicle cluster-inducing effect of expressed neuroligin1-EGFP was completely inhibited (Fig. 3.26c; EGFP and S-SCAM PDZ5del:  $3.82 \pm 0.34$  clusters/20 $\mu$ m dendrite,  $n=18$ ; Nlg-EGFP and S-SCAM PDZ5del:  $2.12 \pm 0.23$  clusters/20 $\mu$ m dendrite,  $n=20$ ). The number of vesicle clusters was even reduced compared to controls ( $P=0.0001$ ) indicating a dominant negative effect. To further study the role of S-SCAM, we also co-expressed a truncated version of S-SCAM in which the neuroligin1 binding domains WW and PDZ1 were deleted, while the other PDZ domains including the  $\beta$ -catenin binding domain were intact (Fig. 3.26a). Similar to deleting the  $\beta$ -catenin binding domain, deletion of PDZ1 resulted in a complete inhibition of the vesicle cluster-inducing activity of expressed neuroligin1-EGFP (Fig. 3.26c; EGFP and S-SCAM PDZ1del:  $3.68 \pm 0.45$  clusters /20 $\mu$ m dendrite,  $n=18$ ; Nlg-EGFP and S-SCAM PDZ1del:  $3.90 \pm 0.44$  clusters/20 $\mu$ m dendrite,  $n=17$ ). In summary, the results with co-expression of truncated forms of S-SCAM lacking either the PDZ domain binding to  $\beta$ -catenin or the WW and PDZ domains binding to neuroligin1 suggest that the interaction of the N-cadherin/ $\beta$ -catenin and the neuroligin/neurexin transsynaptic adhesion systems is mediated by the postsynaptic scaffolding protein S-SCAM and that in the absence of cooperation between the cadherins and neuroligins system, the presynaptic vesicle accumulation process is strongly perturbed.

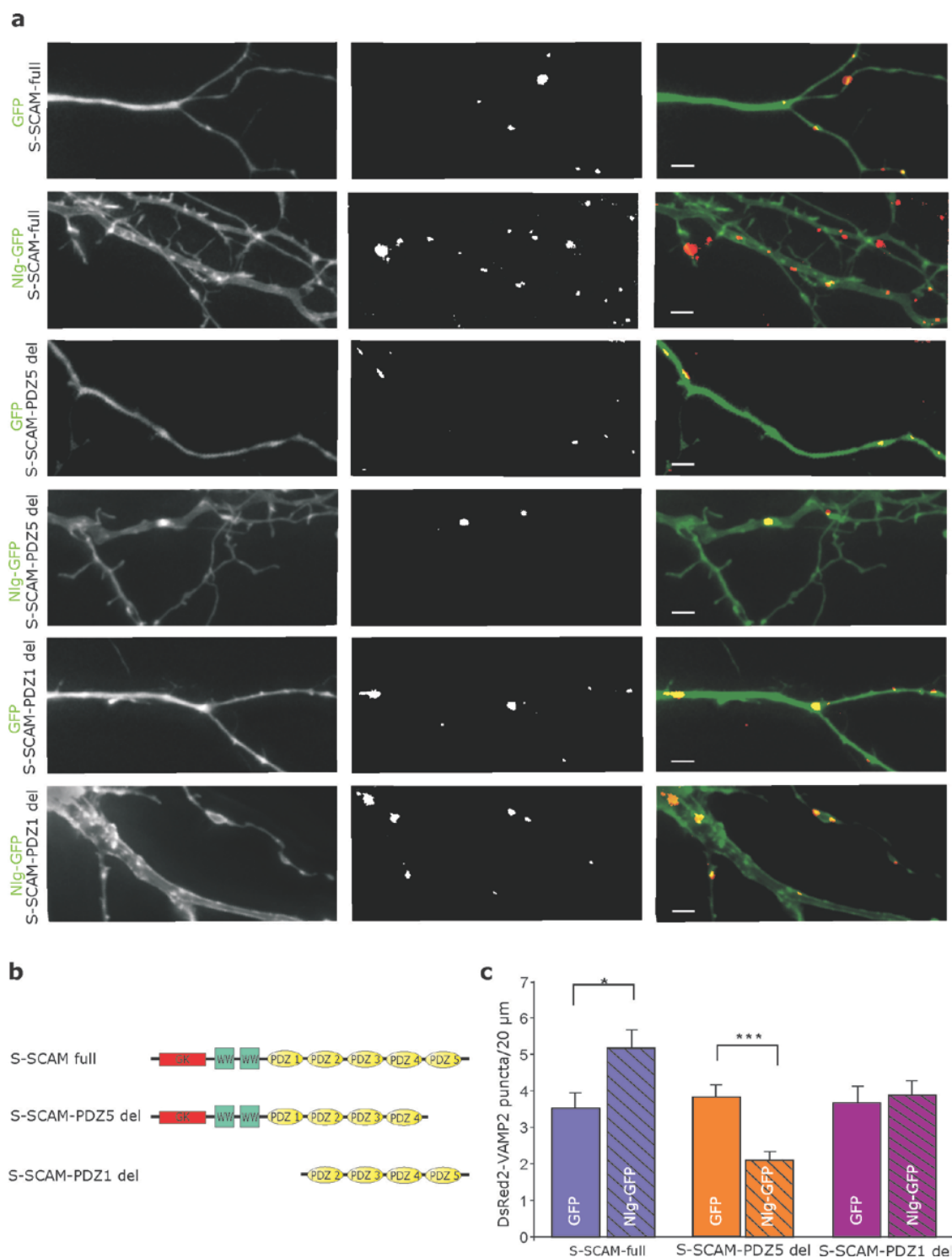


**Figure 3.26. Interaction of N-cadherin and neuroligin1 in the regulation of presynaptic vesicle accumulation is mediated by S-SCAM (MAGI2)**

(a) Inhibition of S-SCAM function by expression of truncated S-SCAM versions with either PDZ5 deleted or PDZ1 deleted blocks the induction of presynaptic vesicle accumulation by

neuroligin1-EGFP. DsRed2-VAMP2 (to visualize vesicle clusters) was co-transfected with either EGFP (GFP) or neuroligin1-EGFP (Nlg-EGFP) and either full-length S-SCAM (S-SCAM full) or S-SCAM with PDZ5 deleted (S-SCAM-PDZ5 del) or S-SCAM with PDZ1 deleted (S-SCAM-PDZ1 del). Fluorescence images of dendrites. Left: EGFP fluorescence to visualize dendrites. Middle: DsRed2 fluorescence to visualize presynaptic vesicle clusters. Right: Overlay of EGFP fluorescence (green) and DsRed2 fluorescence (red) to visualize vesicle clusters on dendrites. Scale bars represent 2 $\mu$ m. **(b)** Quantification of the density of presynaptic vesicle clusters. Type of co-transfection is indicated on and below bars. S-SCAM-full: EGFP  $n=21$ , Nlg-EGFP  $n=16$ ; S-SCAM-PDZ5del: GFP  $n=18$ , Nlg-EGFP  $n=20$ ; S-SCAM-PDZ1del: EGFP  $n=18$ , Nlg-EGFP  $n=17$  ( $n$  represents number of neurons) Error bars represent s.e.m. \* $P<0.05$ ; \*\*\* $P<0.001$ .

### 3.4.5. Role of S-SCAM in synaptic localization of neuroligin1

In the absence of N-cadherin an impaired postsynaptic localization of expressed neuroligin1-EGFP was observed (see Fig. 3.25) suggesting that N-cadherin is required for proper targeting of neuroligin at nascent synapses. If the interaction between the N-cadherin/ $\beta$ -catenin and the neuroligin/neurexin adhesion systems is mediated by S-SCAM on the postsynaptic side, then it is expected that S-SCAM is also involved in postsynaptic targeting of expressed neuroligin1-EGFP similar to N-cadherin. To confirm this experimentally, the density of neuroligin1-EGFP puncta was analyzed two days after co-transfection of truncated, function-blocking forms of S-SCAM (Fig. 26b: either PDZ5 domain or WW and PDZ1 domains deleted) together with neuroligin1-EGFP and DsRed2-VAMP2 (Fig. 3.27a) as described above. Deletion of the  $\beta$ -catenin binding domain PDZ5 resulted in a significantly reduced ( $P=0.0093$ ) density of neuroligin1-EGFP puncta (Fig. 3.27b: only Nlg-EGFP:  $5.26\pm0.36$  clusters /20 $\mu$ m dendrite,  $n=27$ ; Nlg-EGFP and S-SCAM full:  $5.31\pm0.53$  clusters/20 $\mu$ m dendrite,  $n=16$ ; Nlg-EGFP and S-SCAM PDZ5del:  $3.35\pm0.47$  clusters/20 $\mu$ m dendrite,  $n=20$ ) and in a significantly reduced ( $P=0.0001$ ) co-localization of neuroligin1-EGFP puncta with presynaptic vesicle clusters (Fig. 3.27c: only Nlg-EGFP:  $42.39\pm5.38\%$ ,  $n=27$ ; Nlg-EGFP and S-SCAM full:  $50.31\pm6.73\%$ ,  $n=16$ ; Nlg-EGFP and S-SCAM PDZ5del:  $19.80\pm3.44\%$ ,  $n=20$ ). Deletion of the neuroligin1 binding domain PDZ1 also resulted in a significantly reduced ( $P=0.012$ ) co-localization of neuroligin1-EGFP puncta with presynaptic vesicle clusters (Fig. 3.27c: Nlg-EGFP and S-SCAM PDZ1del:  $29.82\pm4.14\%$ ,  $n=17$ ), however, there was no significant effect on the density of neuroligin1-EGFP puncta (Fig. 3.27b: Nlg-EGFP and S-SCAM PDZ1del:  $4.88\pm0.72$  clusters /20 $\mu$ m dendrite,  $n=17$ ). Together, these results strongly indicate that S-SCAM mediates the interaction of N-cadherin and neuroligin1 by

postsynaptically targeting neuroligin1 to the N-cadherin/ $\beta$ -catenin adhesion system at nascent synapses and thus enables the vesicle cluster-inducing activity of expressed neuroligin1.

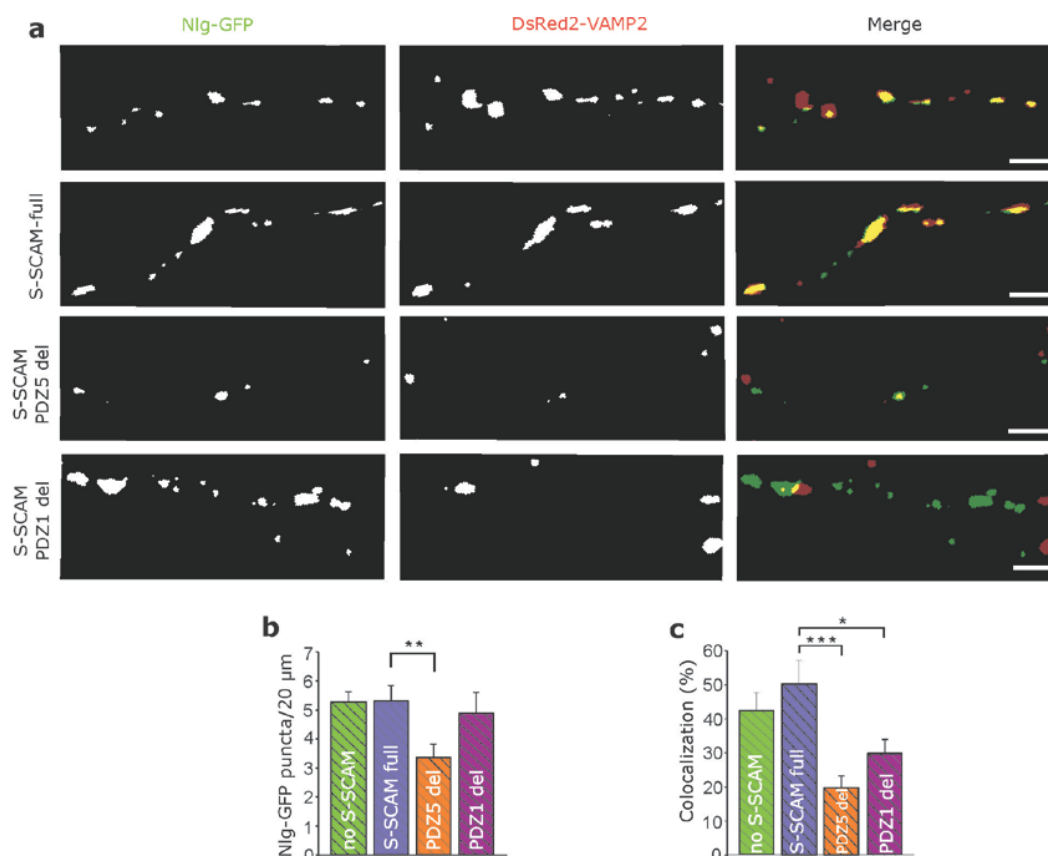


**Figure 3.27. Synaptic targeting of neuroligin1-EGFP is dependent on S-SCAM functional domains**

(a) Fluorescence images of dendrites of primary cultured cortical neurons co-transfected with neuroligin1-EGFP and DsRed2-VAMP2 and either no additional vector (no S-SCAM) or full-length S-SCAM (S-SCAM full) or S-SCAM with PDZ5 deleted (S-SCAM PDZ5del) or S-SCAM with PDZ1 deleted (S-SCAM PDZ1del). Left: EGFP fluorescence (Nlg-EGFP) visualizing neuroligin1-EGFP puncta on dendrites (puncta were isolated from overall fluorescence in the dendrite by thresholding the image). Middle: DsRed2 fluorescence (DsRed2-VAMP2) visualizing presynaptic vesicle clusters. Right: Overlay of EGFP fluorescence (green) and DsRed2 fluorescence (red) visualizing co-localization of neuroligin1-EGFP with presynaptic vesicle clusters. Scale bars represent 2  $\mu$ m. (b) Quantification of the density of neuroligin1-EGFP puncta on dendrites. (c) Quantification of co-localization of neuroligin1-EGFP puncta with DsRed2-labeled presynaptic vesicle clusters. No S-SCAM: n=27; S-SCAM full: n=16; S-SCAM PDZ5del: n=20; S-SCAM PDZ1del: n=17 (*n* represents number of neurons). Error bars represent s.e.m.\*  $P < 0.05$ ; \*\* $P < 0.01$ ; \*\*\* $P < 0.001$ .

### 3.4.6. Role of N-cadherin and neuroligin1 in filopodia formation

Upon neuroligin1-EGFP expression in N-cadherin heterozygous ES cell-derived neurons not only presynaptic vesicle clustering was triggered, but another interesting phenomenon was observed: the induction of dendritic filopodia. Dendritic filopodia are thought to actively participate in synaptogenesis by initiating physical contacts with nearby axons (Ziv and Smith, 1996). The formation of filopodia might represent a very early step in synapse formation preceeding the vesicle clustering activity of neuroligin1. To test whether neuroligin's function to induce filopodia requires also N-cadherin, immature N-cadherin heterozygous control and N-cadherin homozygous knockout neurons were transfected with neuroligin1-EGFP (Fig. 3.28a) and the density of dendritic filopodia was quantitatively analyzed. The density of filopodia was significantly increased ( $P=0.026$ ) not only in the control, N-cadherin heterozygous neurons upon neuroligin1-EGFP expression but also in the N-cadherin homozygous knockout neurons transfected with neuroligin1-EGFP ( $P=0.002$ ) (Fig. 3.28b, N-cad<sup>+/-</sup>: EGFP:  $1.25 \pm 0.20$  filopodia/20 $\mu$ m dendrite,  $n=45$ ; Nlg-EGFP:  $2.25 \pm 0.43$  filopodia/20 $\mu$ m dendrite,  $n=31$ ; N-cad<sup>-/-</sup>: EGFP:  $0.63 \pm 0.16$  filopodia/20 $\mu$ m dendrite,  $n=38$ ; Nlg-EGFP:  $1.66 \pm 0.28$  filopodia/20 $\mu$ m dendrite,  $n=36$ ). As a next step, it was tested whether N-cadherin has any direct effect on filopodia formation independent of neuroligin1-EGFP expression. For this, the density of filopodia in N-cadherin knockout neurons was compared with control N-cadherin heterozygous neurons and a significant reduction ( $P=0.022$ ) was observed in the absence of N-cadherin. These results suggest that N-cadherin deficient neurons show impaired filopodia formation but upon neuroligin1-EGFP expression they are able to initiate new filopodia at the same extent as control N-cadherin heterozygous neurons, contrary to the vesicle clustering behaviour. Intriguingly, the analysis of the length of filopodia indicated that filopodia extend the same distance independent on N-cadherin or neuroligin1-EGFP expression (Fig. 3.28c; N-cad<sup>+/-</sup>: EGFP:  $3.20 \pm 0.21 \mu$ m,  $n=45$ ; Nlg-EGFP:  $3.07 \pm 0.25 \mu$ m,  $n=31$ ; N-cad<sup>-/-</sup>: EGFP:  $3.05 \pm 0.18 \mu$ m,  $n=38$ ; Nlg-EGFP:  $2.83 \pm 0.20 \mu$ m,  $n=36$ ). Together, the above described results suggest that neuroligin1 is able to trigger the formation of new filopodia and in this way initiate new synaptic contacts in an N-cadherin independent manner but the accumulation of vesicles at these sites requires the presence of postsynaptic N-cadherin.



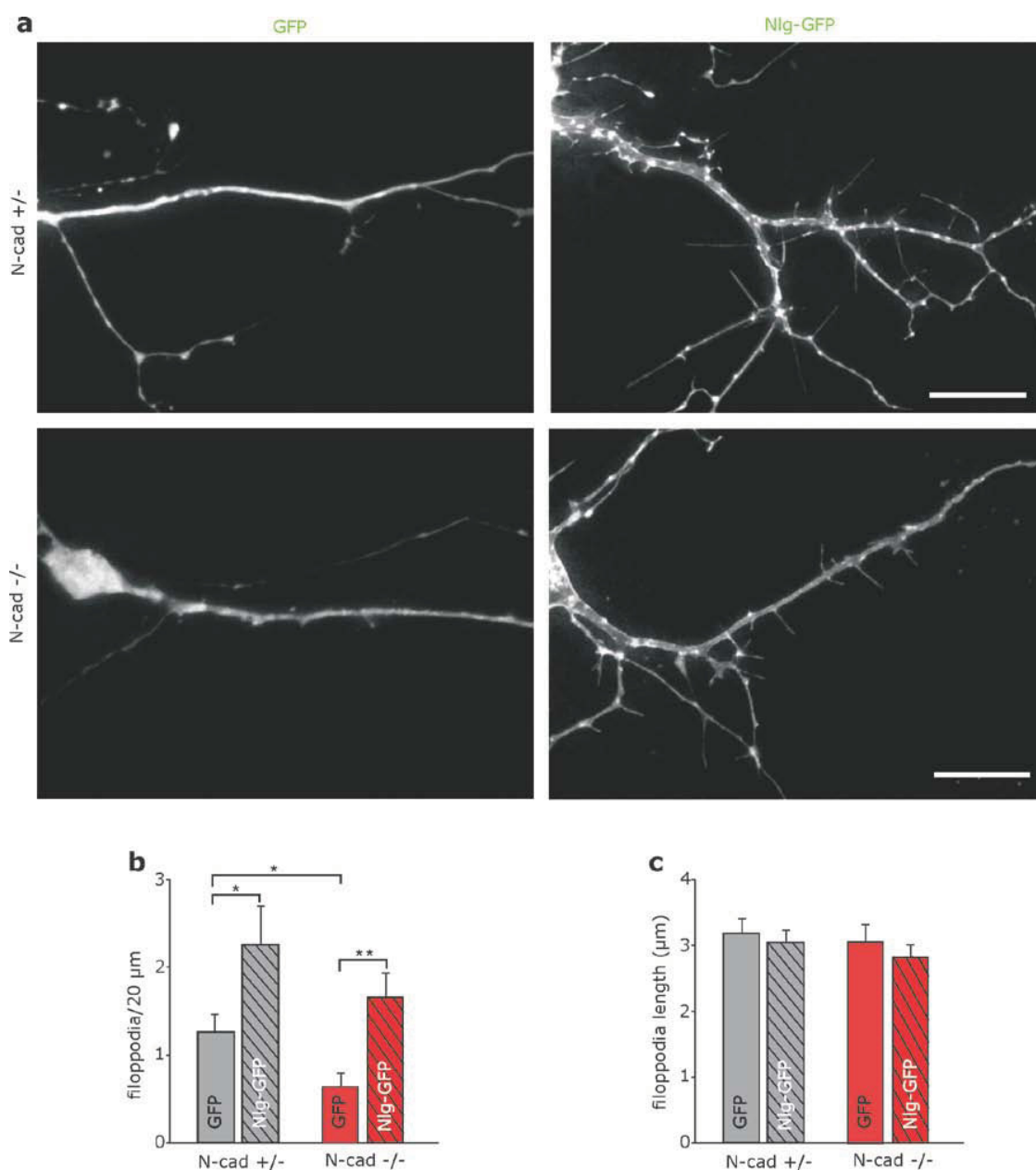


**Figure 3.28. Expression of neuroligin1-EGFP promotes filopodia formation in an N-cadherin independent manner**

(a) Images of dendrites of control (N-cad<sup>+/+</sup>) and homozygous N-cadherin knockout neurons (N-cad<sup>-/-</sup>) transfected with EGFP (left) or Nlg-EGFP (right). Scale bars represent 10 $\mu$ m (b, c) Quantification of (b) the density of filopodia and (c) the mean length of filopodia upon expression of neuroligin1-EGFP in immature N-cad<sup>+/+</sup> and N-cad<sup>-/-</sup> neurons. Expression of either neuroligin1-EGFP or EGFP is indicated on bars. N-cad<sup>+/+</sup>: EGFP  $n=45$ , Nlg-EGFP  $n=31$ . N-cad<sup>-/-</sup>: EGFP  $n=38$ ; Nlg-EGFP  $n=36$  ( $n$  indicates number of cells). Error bars represent s.e.m. \*  $P<0.05$  and \*\*  $P<0.01$



#### 4. Discussion

Synaptogenesis can be defined as the process of assembling pre- and postsynaptic proteins into the highly specialized subcellular structure of the synapse. The accumulation of transmitter-filled vesicles at presynaptic release sites represents a major step in this formation and early maturation of glutamatergic synapses during establishment of neuronal circuits in the brain (Dresbach et al., 2006; 2007; Mohrmann et al., 2003). In this study, the formation of presynaptic boutons consisting of presynaptic vesicles and active zone proteins like Bassoon was investigated by time-lapse live-cell imaging. Previous reports have described that presynaptic specializations of new synapses form within 30 minutes after the initial axodendritic contact was established, whereas clusters of the postsynaptic density molecule PSD-95 and glutamate receptors were found on average only approximately 45 minutes after presynaptic boutons were first detected (Friedman et al., 2000). For this reason, the accumulation of presynaptic vesicles and active zone proteins was used in this study as a morphological criterion for the detection of nascent synapses. Furthermore, presynaptic vesicles at these nascent synapses have been shown to undergo evoked vesicle recycling (a hallmark of functional presynapses) in less than one hour after stabilization of axodendritic contact (Ahmari et al., 2000). For synapses to form so quickly, specific contacts between axons and dendrites must initiate bidirectional signals that lead to the rapid accumulation of pre- and postsynaptic proteins. Trans-synaptic signaling molecules (cadherins, integrins, NCAM, nectins, neuroligins/neurexins, SynCAMs, ephrins/Eph receptors, etc.), secreted factors (BDNF, Wnt, FGF, glia derived molecules, etc.) and synapse limiting molecules (transcription factors of the myocyte enhancer factor 2 – MEF2- family) have all been shown to contribute to the formation of synapses (Akins and Biederer, 2006; Craig et al., 2006; McAllister, 2007). Furthermore, classical cadherins are among the first molecules to be detected at the axon-filopodial contact site (Jontes et al., 2004) and they have been shown to persist in mature synapses (Togashi et al., 2002), where they are thought to keep the pre- and postsynaptic specializations closely aligned (Bozdagi et al., 2004). However, the study of the functional role of neural (N)-cadherin in synapse formation and maturation has been largely hindered by the early embryonic lethality of mice genetically

null for N-cadherin (Radice et al., 1997). Therefore, the majority of researchers investigating the role of N-cadherin at synapses have used a pan-cadherin block of function by either expressing a dominant-negative truncated cadherin (Abe et al., 2004; Bozdagi et al., 2004; Togashi et al., 2002), or by application of antibodies and peptides that block the interaction of extracellular N-cadherin domains (Bozdagi et al., 2000; Tang et al., 1998). For this reason, the specific role that N-cadherin plays during synapse formation and maturation has remained largely elusive. For the present experiments, N-cadherin knockout neurons were differentiated *in vitro* from embryonic stem cell lines deficient for N-cadherin (Moore et al., 1999), in this way circumventing the early embryonic lethality of mice having no N-cadherin. An immunoisolation procedure was used to purify N-cadherin deficient neurons from *in vitro* differentiated mouse ES cells. This selective N-cadherin knockout approach combined with time lapse imaging and FRAP technology was employed to gain further insight into the role of N-cadherin in synapse formation and maturation.

#### **4.1. Characterization of presynaptic specializations of ES-cell derived neurons grown in glial microisland cultures**

In this study, all experiments were performed on cultured neurons grown in a glial microisland system. In this system, 10-15 neurons are present on an “island” formed by glial cells, growing in complete separation from the other glial islands. This leads to the formation of a high percentage of autapses (synaptic contacts made between the axon of a neuron with its own dendrites). Lipofectamine 2000 was used as a reagent to deliver the constructs into the cells leading to a low transfection efficacy, usually less than 1%. As a result, only one neuron per glial island was cotransfected. The microisland system was employed to increase the number of synapses visualized after cotransfection of fluorescence-tagged presynaptic proteins with GFP (or DsRed2) for labeling the dendrites (as shown in Fig. 3.1). Although some previous studies have indicated that in isolated hippocampal neurons grown in microisland culture mismatches of pre- and postsynaptic compartments are frequently present (Rao et al., 2000), autapses do not represent only a culture artifact, but they have also been described *in vivo*. Autapses have been shown to

occur in 80% of the layer 5 pyramidal neurons and they are formed, like synapses, either on dendritic spines or shafts. Although there is structural evidence for the existence of autapses in the brain, it is not clear whether and how they affect neuronal function. A recent study has shown that autapses in fast-spiking interneurons are used to shape inhibitory activity in the brain (Bacci and Huguenard, 2006). To identify the type of autapses present in the glial microisland system, neurons were cotransfected with DsRed2-VAMP2 for labeling the presynaptic vesicle clusters and PSD95-EGFP to visualize the postsynaptic densities of glutamatergic synapses. Interestingly, more than 80% of synapses made by the neurons on a glial island were glutamatergic autapses (similar for N-cadherin heterozygous control and N-cadherin deficient neurons; see Fig. 3.19), confirming that the glial microisland culture system employed in this study represents a reliable method for studying synapses *in vitro*.

#### **4.2. Role of N-cadherin in the formation of presynaptic specializations in immature neurons**

The above described results show that the accumulation of vesicles at nascent synapses is strongly dependent on the expression of N-cadherin. However, the accumulation of the active zone protein Bassoon does not require N-cadherin expression, suggesting that N-cadherin plays a rather specific role during synapse formation in controlling the filling of nascent release sites with vesicles. Previous studies in cultured hippocampal neurons using expression of a dominant-negative cadherin construct, that inhibits the function of all classical cadherins, also led to a reduced number of presynaptic vesicle clusters (Bozdagi et al., 2004; Togashi et al., 2002), however, active zone formation was not specifically addressed in these studies. Assembly of neurotransmitter-filled vesicle pools requires mobile cytoplasmic packets of synaptic vesicles which are associated with additional presynaptic molecules including synaptic vesicle proteins SV2 and synapsins (Ahmari et al., 2000). The cytomatrix of active zones (CAZ), however, is formed by fusion of vesicular structures, called Piccolo-Bassoon transport vesicles (PTVs), with the plasma membrane (Dresbach et al., 2006; Zhai et al., 2001). These different modalities used to assemble distinct parts of the presynaptic terminal may explain why N-cadherin

presence is critical in some but not all aspects of presynaptic differentiation. In line with our results,  $\beta$ -catenin knockout neurons, in which N-cadherin function should be strongly impaired, showed a reduced clustering of synaptic vesicles at presynaptic release sites whereas the punctuate distribution of bassoon was not affected (Bamji et al., 2003).

If N-cadherin is crucial for the accumulation of vesicle at nascent synaptic sites then the number of vesicles in the boutons should be smaller in the N-cadherin knockout neurons. The most straightforward way to show the size of vesicle pools at synapses is by means of electron microscopy. Unfortunately, nascent synapses are difficult to detect ultrastructurally, because of their immature structure with few of the hallmarks that characterize a mature synapse on electron micrographs (Ahmari and Smith, 2002). Because of this shortcoming, electron microscopic analysis was performed only in mature N-cadherin knockout neurons, but no significant difference in the overall number of vesicles was detectable (Jüngling et al., 2006). However, the authors did not study changes in the three-dimensional structure of vesicle pools and synapses in the absence of N-cadherin. The size of the recycling vesicle pool can be inferred also from the intensity of synaptic vesicle clusters upon loading with FM dye. This was shown to be lower in N-cadherin knockout neurons (Jüngling et al., 2006) as well as in hippocampal neurons transfected with a dominant-negative mutant cadherin (Bozdagi et al., 2004), suggesting a smaller pool size of recycling vesicles. In the present study, the initial fluorescence intensity of DsRed2-labeled presynaptic vesicle clusters did not show any differences between N-cadherin deficient and control synapses in young or in mature neurons. This may be due to the wide variation in the level of expression of the DsRed2-VAMP2 construct in different neurons (as indicated in Fig. 3.4 and 3.13). However, if the changes in fluorescence intensity of DsRed2-labeled clusters in individual neurons over time are analyzed (with the fluorescence intensity normalized to the individual expression level of the DsRed2-VAMP2 construct in each cell), a reduced recruitment of vesicles can be demonstrated at individual nascent synaptic sites in the absence of N-cadherin (see Fig. 3.5). Similarly, fluorescence recovery after photobleaching (FRAP) analysis indicated that the accumulation of synaptic vesicles at individual synaptic sites is much slower in N-cadherin deficient neurons than in control neurons (see Fig. 3.6). In FRAP experiments

individual EGFP-VAMP2 clusters on dendrites were locally photobleached using high intensity laser light and then the recovery of EGFP fluorescence was monitored with live-imaging. The recovery of fluorescence will take place as mobile vesicles from neighbouring axon regions will start to enter the bleached area over time. The rate of recovery depends on the vesicle mobility between the clusters but also on the capacity of presynaptic terminals to retain the incoming vesicles at the synaptic site. Recovery after 45 minutes was only 30% in N-cadherin knockout neurons, whereas in heterozygous N-cadherin control neurons the recovery was 60%.

Consistent with the proposed role of N-cadherin in synaptic vesicle clustering (Benson and Tanaka, 1998; Togashi et al., 2002), this study shows additional evidence that N-cadherin controls the integrity of the vesicle pool. An analysis of vesicle cluster stability in  $\beta$ -catenin deficient hippocampal neurons was performed by two previous studies (Bamji et al., 2006; Bamji et al., 2003) that showed an increased splitting of vesicle clusters and a dispersal of vesicles along the axons in the absence of  $\beta$ -catenin. In N-cadherin deficient neurons similar increased dynamics of vesicle clusters were observed, suggesting that the mechanism by which N-cadherin controls the stability of the vesicle pool may involve  $\beta$ -catenin, which is a major downstream signaling protein associated with N-cadherin (Uchida et al., 1996). Axonal transport of vesicle clusters has been considered to play a specific role in presynaptic assembly or disassembly in developing and more mature neurons (Ahmari et al., 2000; Hopf et al., 2002; Krueger et al., 2003). Aside from this, a recent study (Darcy et al., 2006) has indicated that exchange of mobile synaptic vesicle clusters between boutons is potentially involved in homeostatic mechanisms. This may enable neurons to redistribute synaptic weights across multiple release sites and in this way allow the coordinated regulation of neighboring recycling pools. From this perspective, the increased mobility of synaptic vesicle clusters observed in immature N-cadherin knockout neurons may represent a compensatory mechanism. This would allow more release sites to share vesicles with neighboring synaptic vesicle pools in an attempt to keep the synaptic activity at levels similar with control neurons. Indeed, the analysis of the active zone protein Bassoon has indicated that in N-cadherin deficient neurons at least the number of release sites is similar with control neurons, but

the density of presynaptic vesicle clusters is reduced. Accordingly, it has been shown that presynaptic functional impairment in N-cadherin knock out neurons becomes detectable only under high activity conditions when vesicle pools are used at their maximum capacity, indicating a defective vesicle pool function (Jungling et al., 2006). On the other hand, the increased mobility of synaptic vesicles in N-cadherin deficient neurons may reflect also an on-going process of elimination of defective synaptic structures. During development, more synapses are established than ultimately will be retained. Therefore, the elimination of excess synaptic inputs is a critical step in synaptic circuit maturation. It has been shown that elimination of a specific synapse type occurs during brain development *in vivo* to limit redundant connectivities, like in the case of climbing fiber-Purkinje cell synapses (Eccles et al., 1966; Mariani and Changeux, 1981) and in the segregation of neuronal populations in the visual cortex receiving inputs from the right or the left eye (Hubel et al., 1977). Synapse elimination is a competitive process that involves interactions between pre- and postsynaptic partners. Homophilic recognition between cadherins would lock in an interaction and thus support the accumulation of other synaptic proteins that would stabilize the intercellular junction. In support of this view, it has been shown *in vivo* that as soon as the levels of N-cadherin expression in the cortical barrels decrease, ventrobasal thalamocortical synapses are readily eliminated strongly suggesting that N-cadherin plays a critical role in maintenance of synapses (Huntley and Benson, 1999).

#### **4.3. Role of N-cadherin in maturation and maintenance of presynaptic specializations**

In this study, in addition the role of N-cadherin in further maturation of presynaptic vesicle pools was investigated. In more mature cultured neurons, in which the initial strong vesicle accumulation had ceased, N-cadherin loses its major role in controlling vesicle clustering (see Fig. 3.14). Accordingly, the density of vesicle clusters was not altered in the absence of N-cadherin as described previously in mature N-cadherin deficient neurons (Jungling et al., 2006; Kadowaki et al., 2007) and in mature neurons transfected with a dominant negative mutant cadherin (Bozdagi et al., 2004). Moreover,

the analysis of presynaptic active zone clusters in mature N-cadherin deficient neurons showed a similar density as in control neurons, confirming previous results carried out in  $\beta$ -catenin deficient neurons where the active zones were not altered either (Bamji et al., 2003). Together, these data suggest that N-cadherin appears to function in vesicle accumulation only at nascent synapses whereas later on during synapse maturation its function maybe taken over by other compensatory mechanisms. In line with this idea, the synaptic localization of N-cadherin has been described to change with synapse maturation, initially being present at all synaptic sites but at later stages becoming restricted to a subpopulation of excitatory synapses (Benson and Tanaka, 1998). Furthermore, it has been shown that at 5-6 days in culture, when most synapses are newly formed, cadherins are evenly distributed at the synaptic cleft throughout the active zone, whereas at 14 days, when the majority of synapses are rather mature, cadherin concentrates in discrete clusters surrounding the synaptic cleft (Elste and Benson, 2006). A recent study demonstrated that synapses, that formed on neurons transfected with a dominant-negative mutant N-cadherin, failed to acquire resistance to F-actin depolymerization, a hallmark of mature stable contacts (Bozdagi et al., 2004) strongly supporting the view that N-cadherin is involved in the maturation of synapses. Moreover, the role of N-cadherin appears to switch from regulation of structural properties, i.e. vesicle clustering at nascent synapses, to modulation of synaptic function, i.e. trans-synaptic regulation of the synaptic vesicle cycle at mature synapses (Gottmann, 2008; Jungling et al., 2006).

#### **4.4. Cooperation of N-cadherin and neuroligin1 during synapse formation in immature neurons**

Classical cadherins, such as N-cadherin, are well known to act on the actin cytoskeleton via  $\beta$ -catenin and  $\alpha$ -catenin. Thus, a direct presynaptic mechanism of action of N-cadherin on actin filaments that controls vesicle accumulation appears conceivable (Zhang and Benson, 2001) although the exact role of actin filaments in organizing presynaptic vesicle pools remains unclear (Colicos et al., 2001; Sankaranarayanan et al., 2003; Shupliakov et al., 2002). Moreover, if N-cadherin would control the presynaptic



organization through  $\alpha$ -catenin – actin cytoskeleton interaction, then one would expect that in the absence of  $\alpha$ -catenin from synapses, the distribution of synaptic vesicles would be altered. However,  $\alpha$ -catenin knockout neurons do not show any impairment in vesicle localization (Abe et al., 2004) and the loss of function of  $\alpha$ -catenin in hippocampal neurons (Togashi et al., 2002) or disruption of  $\alpha$ N-catenin/ $\beta$ -catenin interactions (Bamji et al., 2003) did not inhibit the clustering of synaptic vesicles. Nevertheless, cadherins might regulate the organization of the actin cytoskeleton in a number of different ways, for example by interacting with the p120 catenin family of proteins which in turn control the activity of Rho family of GTPases, molecules known as modulators of actin polymerization (Goodwin and Yap, 2004). p120 catenin gene deletion in hippocampal pyramidal neurons in vivo resulted in reduced spine and synapse densities along dendrites (Elia et al., 2006). The number of puncta that express the synaptic vesicle protein synaptophysin or the postsynaptic scaffolding protein PSD95 in the stratum radiatum of CA1 hippocampus were also reduced in the absence of p120 catenin. p120 catenin has been shown to promote spine maturation by controlling the activity of Rho and Rac, as well as levels of N-cadherin (Elia et al., 2006). In addition it has been shown that p120 catenin enhances cadherin function through stabilization of cadherin interactions with the cytoskeleton (Xu et al., 2004).

N-cadherin might also use a presynaptic signaling cascade via  $\beta$ -catenin and its PDZ domain-binding motif to control presynaptic PDZ domain-containing proteins like Veli and CASK (Bamji et al., 2003). In this way, intercellular cadherin interactions may provide  $\beta$ -catenin-rich nucleation sites for recruitment of synaptic PDZ proteins and other scaffold proteins, which in turn “trap” preassembled packets of synaptic vesicles at contact sites (Bamji, 2005).

Such direct presynaptic mechanisms of vesicle clustering would further predict that expression of N-cadherin on the postsynaptic side is able to induce *de novo* accumulation of vesicles presynaptically. However, expression of N-cadherin in cultured primary cortical neurons did not trigger the formation of additional vesicle clusters (see Fig. 3.21), whereas other adhesion molecules such as SynCAM (Biederer et al., 2002; Sara et al., 2005) and neuroligin-neurexins (Nam and Chen, 2005; Sara et al., 2005; Scheiffele et al.,



2000) readily induce presynaptic vesicle clusters in heterologous systems and in primary neuronal cultures (Dean et al., 2003; Prange et al., 2004; Sara et al., 2005; Scheiffele et al., 2000). Insights into a direct role of these two adhesion systems in synapse development came from an ingenious assay involving co-culture of non-neuronal and neuronal cells to study the minimum molecular requirements for synapse induction. In these experiments, presentation of only neuroligin or only Syn-CAM (but not N-cadherin) at the surface of heterologous cells was sufficient to induce functional presynaptic terminals in axons contacting these cells (Biederer et al., 2002; Sara et al., 2005; Scheiffele et al., 2000). Later it was shown that the postsynaptic expression of neuroligins in primary neurons triggers presynaptic vesicle clustering via interaction with presynaptically localized neurexins (Boucard et al., 2005; Chih et al., 2005; Chih et al., 2006; Chubykin et al., 2007; Dean et al., 2003; Graf et al., 2004; Prange et al., 2004). To this end, the inability of N-cadherin to induce vesicle clusters in these expression assays strongly argues against a direct presynaptic mechanism in the regulation of vesicle accumulation by N-cadherin.

Alternatively to a direct presynaptic mechanism, this study provides first evidence for a trans-synaptic retrograde mechanism of the control of presynaptic vesicle accumulation that is based on a postsynaptic interaction of the N-cadherin/ $\beta$ -catenin and the neurexin/neuroligin adhesion systems. The critical experiment to validate this model was the overexpression of neuroligin1 (in order to induce presynaptic vesicle clustering) in N-cadherin knock-out neurons. This test demonstrated a strict dependence of neuroligin's vesicle cluster-inducing activity on the expression of N-cadherin (see Fig. 3.23). Moreover, the analysis of the subcellular localization of neuroligin1-EGFP fusion protein indicated an impairment in the subsynaptic targeting of neuroligin in the absence of N-cadherin. The reduced colocalization of postsynaptic neuroligin1-EGFP with the DsRed2-labeled presynaptic vesicle clusters in N-cadherin deficient neurons (see Fig. 3.25) suggests that in the absence of transsynaptic signalling mediated by homophilic N-cadherin interactions, the pre- and postsynaptic specializations are mismatched. This result is in accordance with the proposed role of N-cadherin and other classical cadherins

in specific neuronal recognition processes (Benson et al., 2001; Fannon and Colman, 1996; Redies, 2000; Takeichi, 2007).

Synaptic targeting of postsynaptic membrane proteins such as ion channels and adhesion molecules is thought to be controlled by postsynaptic scaffolding molecules, like the MAGUK (membrane-associated guanylate kinase) superfamily of proteins. MAGUKs have one or more PDZ domains, which are protein-protein interaction modules that usually bind the C-terminal sequences of target proteins (Craven and Brecht, 1998), and include amongst others, members like PSD95, CASK and S-SCAM (Montgomery et al., 2004). Because a central role of these proteins is to organize heterogeneous ensembles of proteins through their PDZ domains, in the present study the interaction of the N-cadherin/ $\beta$ -catenin and the neuroligin/neurexin adhesion systems was hypothesized to be mediated by a connecting postsynaptic scaffolding protein that can bind to both  $\beta$ -catenin and the cytoplasmic domain of neuroligin.  $\beta$ -catenin (Perego et al., 2000) and neuroligin1 (Ichtchenko et al., 1995; Irie et al., 1997) have been shown to possess PDZ-binding domains at their C terminal end. The idea that the MAGI-type (membrane-associated guanylate kinase with inverted organization) postsynaptic scaffolding protein S-SCAM might link the two cell adhesion systems N-cadherin/ $\beta$ -catenin and neuroligin/neurexin was primarily inspired by two independent studies. The first described the interaction of S-SCAM and  $\beta$ -catenin (Nishimura et al., 2002) and the second showed the binding of neuroligin to S-SCAM (Iida et al., 2004) in cultured hippocampal neurons. S-SCAM has five PDZ domains (PDZ1 to PDZ5), one GK domain and two WW domains (Hirao et al., 1998), and it has been shown to bind  $\beta$ -catenin with its PDZ5 domain (Nishimura et al., 2002) and to interact with neuroligin1 via its PDZ1 domain (Hirao et al., 1998) and its WW domains (Iida et al., 2004). Additionally, S-SCAM interacts with NMDA receptor subunits and  $\gamma$ -catenin (Hirao et al., 1998; Ide et al., 1999) and also forms homodimers via the region containing PDZ4 and PDZ5 (Hirao et al., 2000). Based on these data from binding studies, S-SCAM might provide an interconnectivity platform for several postsynaptic proteins and cell adhesion molecules (like N-cadherin and neuroligin1), which eventually will act in concert to transsynaptically control vesicle accumulation at immature synapses. The present study shows using the vesicle cluster-inducing activity of

neuroligin1 as a functional assay, that indeed expression of mutant S-SCAM proteins leads to a functional block of the interaction between the N-cadherin/ $\beta$ -catenin and the neuroligin/neurexin systems, and as result inhibits presynaptic vesicle accumulation. Blocking either  $\beta$ -catenin/S-SCAM interaction by deleting PDZ5 of S-SCAM or S-SCAM/neuroligin1 binding by deleting PDZ1 and WW domains of S-SCAM were effective in suppressing neuroligin's vesicle clustering activity (see Fig. 3.26), strongly suggesting that S-SCAM functionally connects the N-cadherin/ $\beta$ -catenin and the neuroligin/neurexin adhesion systems. This finding provides also first evidence for a functional role of S-SCAM in controlling presynaptic vesicle accumulation as previous data have linked it only to postsynaptic functions, like recruitment of neuroligin1, PSD95 and NMDA receptors (Hirao et al., 1998; Iida et al., 2004).

The reason why the expression of N-cadherin is so crucial for the vesicle clustering activity of neuroligin1 appears to be that N-cadherin regulates the synaptic targeting of neuroligin1 via S-SCAM thus enabling its interaction with presynaptic neurexins. The co-localization analysis of this study strongly supported this mechanism. Both the number of postsynaptic neuroligin1-EGFP clusters and their co-localization with DsRed2-labeled presynaptic vesicles were reduced in the absence of N-cadherin (see Fig. 3.25) and at the same degree upon expression of mutant S-SCAM proteins (see Fig. 3.27). In line with these results, synaptic targeting of S-SCAM by  $\beta$ -catenin has been suggested (Nishimura et al., 2002). In addition, synaptic targeting of neuroligin1 has been proposed to be mediated by S-SCAM, but not by PSD95 (Dresbach et al., 2004; Iida et al., 2004). Binding of PSD95 to neuroligin1 (Ichtchenko et al., 1995; Irie et al., 1997) might instead modulate the interaction of the N-cadherin/ $\beta$ -catenin and the neuroligin/neurexin adhesion systems as a number of studies have described that postsynaptic expression of PSD95 enhances maturation of glutamatergic presynaptic terminals (El-Husseini et al., 2000; Han and Kim, 2008; Prange et al., 2004; Regalado et al., 2006).

However, the S-SCAM block of function studies revealed two interesting additional phenomena: i) the S-SCAM mutant constructs (S-SCAM with PDZ5 domain deleted and S-SCAM with WW and PDZ1 domains deleted) have an inhibiting effect on clustering of

presynaptic vesicles only under neuroligin1-EGFP overexpression conditions whereas in the control situation these mutants have no effect (see Fig 3.26) and ii) the deletion of the PDZ5 domain of S-SCAM seemed to have a more dramatic effect on vesicle accumulation and on synaptic localization of neuroligin1 compared to the deletion of WW and PDZ1 domains (see Fig. 3.26 and 3.27). The first finding that S-SCAM seems to connect the two cell adhesion systems only under high neuroligin1 expression levels may be caused by quantitatively different requirements for S-SCAM during a very intense period of synaptogenesis (triggered by neuroligin overexpression) as compared to the relatively slower synapse formation under normal culture conditions. The fraction of synapses formed during the relatively short (2 days) period of mutant S-SCAM expression is rather low without neuroligin1 overexpression. From this point of view it would be interesting to investigate the cooperation between endogenous neuroligin1 and endogenous N-cadherin in primary neurons after mutation of S-SCAM protein (deletion of PDZ domains) or after knocking down S-SCAM using siRNA technology. However, the interpretation of these experiments would be difficult as there are 3 different, alternatively spliced variants of S-SCAM present at the synapses: S-SCAM  $\alpha$ ,  $-\beta$  and  $-\gamma$ . (Hirao et al., 2000). Recently, a knockout mouse for S-SCAM  $\alpha$  has been described (Iida et al., 2007) having abnormally elongated dendritic spines but no significant alteration in excitatory and inhibitory synapse formation at the morphological level was found. This may be due to compensatory effects of S-SCAM  $\beta$  and  $\gamma$  that are still expressed in the S-SCAM  $\alpha$  knockout.

If N-cadherin/ $\beta$ -catenin and neuroligins/neurexins would cooperate to trigger new synapses only when the neurons undergo periods of high synapse formation, then this mechanism might play a very important role in new synapse formation during long term potentiation (LTP). Previous studies have suggested that both N-cadherin and neuroligin1 are involved in LTP. During late-phase LTP (L-LTP) a significant increase in numbers of synaptophysin and N-cadherin puncta has been reported, whereas after blocking the interaction of N-cadherin extracellular domains, the induction of L-LTP was prevented suggesting that N-cadherin is recruited to synaptic sites and required for potentiation (Bozdagi et al., 2000). Accordingly, synaptic N-cadherin has been shown to dimerize and

become protease resistant in response to synaptic activity, thus possibly enhancing adhesion (Tanaka et al., 2000). On the other hand, neuroligin1 has been shown to be required for normal expression of LTP in the amygdala, but interestingly not for the basal synaptic connectivity at the thalamo-amygdala pathway (Kim et al., 2008).

Another interesting result of the S-SCAM function block in this study was that deletion of the PDZ5 domain of S-SCAM had a more dramatic effect on vesicle accumulation (see Fig. 3.26) and on synaptic localization of neuroligin1 than deletion of WW and PDZ1 domains (see Fig. 3.27: WW and PDZ1 domains deletion does not alter the clustering of neuroligin1-EGFP but it slightly affects its synaptic localization, whereas the PDZ5 deletion has a strong dominant negative effect on both neuroligin1-EGFP clustering and localization at synapses). Several possible explanations can be proposed for interpreting these results. The C-terminal domain of neuroligin1 contains a PDZ domain binding motif (Ichtchenko et al., 1995) that interacts with PDZ domain-containing proteins, thus playing an instructive role in postsynaptic assembly. Using a two-yeast hybrid system, Meyer et al., 2004 have identified an abundant number of target proteins (13 postsynaptically localized proteins) that potentially could bind to the cytoplasmic domain of neuroligin1. Furthermore, the PDZ domain-containing proteins can interact with an even larger number of proteins, making neuroligin1 a postsynaptic protein entangled in a complex web of potential interactions (Meyer et al., 2004). From this perspective, deletion of PDZ domains might either drive interactions that do not occur under physiological conditions or might have far reaching effects by blocking not only the interaction with one protein but interfering with the binding of many others (similar to a domino effect). In this way, expression of dominant negative S-SCAM with WW and PDZ1 domains deleted might lead to either triggering interactions of neuroligin1 with other PDZ domains of the mutant S-SCAM or altering the binding properties of neuroligin1 to other PDZ domain-containing targets like PSD95, SAP102, Chapsyn/PSD93, Magi1 and Magi3, Shank1 and 3, Pick1, etc. thus enabling a large number of potential compensatory effects. On the other hand, deletion of the PDZ5 domain of S-SCAM may have a different, stronger effect on the the N-cadherin/neuroligin1 cooperation, as this mutant construct interferes not only with  $\beta$ -

catenin binding (Nishimura et al., 2002), but also with the S-SCAM capacity to form multimers (Hirao et al., 2000). This potentially affects the general organization of the postsynaptic scaffold and thus might strongly inhibit compensatory effects. In light of the promiscuity that exists among protein-protein interactions mediated by PDZ domains and PDZ domain binding motifs (Meyer et al., 2004), the interpretation of experiments addressing individual interactions of S-SCAM with either neuroligin1 or the N-cadherin/ $\beta$ -catenin complex becomes difficult but not less informative. In summary, the experiments performed in this study clearly point to S-SCAM as one molecular linker between the N-cadherin/ $\beta$ -catenin and the neuroligin/neurexin systems, although the exact role that each of the individual PDZ domains plays in this interaction remains largely elusive.

Based on the present and previous studies, a model is proposed assuming that the cooperation of the N-cadherin/ $\beta$ -catenin and the neuroligin/neurexin adhesion systems contributes to the formation, maturation and validation of glutamatergic synapses (Fig. 4.1). One scenario would be that axons express a single or a limited number of cadherins, and that the dendritic tree expresses several cadherins (Huntley and Benson, 1999; Yamagata et al., 1995). Axonal recognition of matching dendritic cadherins then triggers the initiation of a synaptic contact. Consistent with this, it has been shown that cadherins are among the first molecules to be detected at nascent synaptic sites (Jontes et al., 2004). After trans-synaptic recognition between matching cadherins has been established, a series of molecular events follows, among them the recruitment of the synaptic scaffolding molecule S-SCAM via  $\beta$ -catenin to the postsynaptic membrane. Subsequently, neuroligin1 is recruited to the contact site and by retrograde trans-synaptic interaction with neurexins the accumulation of presynaptic vesicles is triggered. From this perspective, cadherins would be the initiators of synapse formation, whereas the neuroligins would play a crucial role in validating immature synapses, i.e. filling them with vesicles. This idea is in good agreement with a recent study (Chubykin et al., 2007) indicating that neuroligin1 acts not as a “synaptogenic” molecule, but as an activity-dependent “validator” of transient synaptic contacts. In line with the observation that neuroligin mediates the stabilization of transient synaptic contacts only under activity of

NMDA receptors (Chubykin et al., 2007), S-SCAM also represents a scaffold for NMDA receptors at glutamatergic synapses (Hirao et al., 1998) thus possibly enabling neuroligin1 to exert its “stabilizer/ validator” function in an NMDA receptor dependent way.

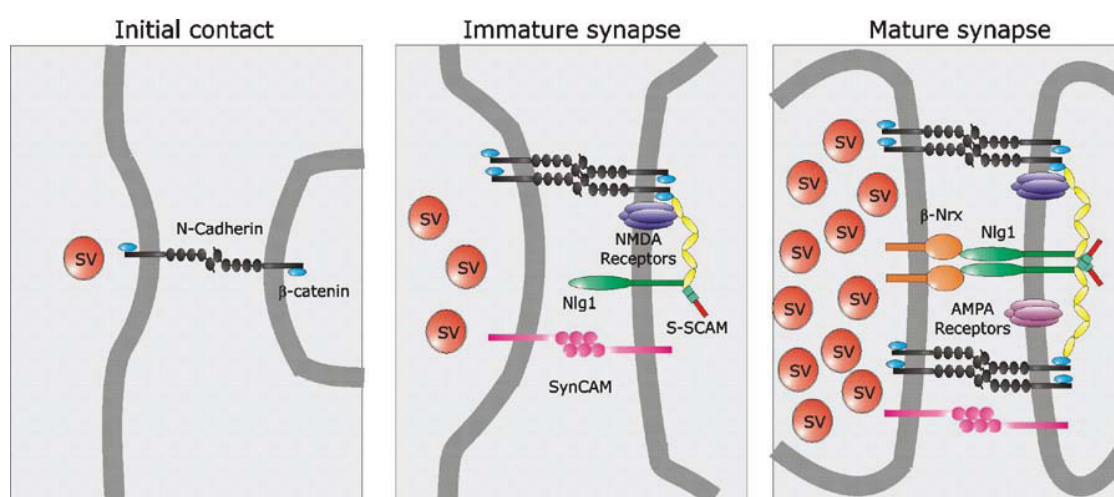


**Figure 4.1. Model of cooperation of the N-cadherin/β-catenin and the neuroligin/neurexin adhesion systems in synapse formation and maturation**

The initial axodendritic contact is established after recognition of matching pre- and postsynaptic cadherins (e.g. N-cadherin). SynCAMs together with cadherins may further specify the synaptic contact resulting in formation of immature synapses that can be functional but need to be further stabilized, as at this stage they can be easily eliminated. Postsynaptic N-cadherin recruits S-SCAM via β-catenin accumulation. S-SCAM scaffolding proteins recruit via PDZ1 domains neuroligin1 molecules and via PDZ5 domains NMDA receptors. Postsynaptic neuroligin clusters can then trigger the accumulation of presynaptic vesicles by interacting with β-neurexins, but this function of neuroligin depends on the activation of NMDA receptors.

The molecular interaction between the N-cadherin/β-catenin and the neuroligin/neurexin adhesion systems described in this study suggests that cadherins and neuroligins play different roles in synapse formation and their cooperation might be of general importance in the selective validation of nascent synapses. Their cooperative action would thus contribute to synapse specificity and neuronal circuit formation. In line with this model, an siRNA knockdown approach of neuroligins resulted in a reduced number of presynaptic vesicle clusters in cultured neurons (Chih et al., 2005). However, *in vivo* studies using neuroligin knockout mice have failed to show any morphological abnormalities of synapses (Varoqueaux et al., 2006), suggesting that *in vivo* other



synaptic adhesion systems with vesicle cluster-inducing activity like SynCAMs (Biederer et al., 2002) may be used to compensate for the loss of neuroligins (Chubykin et al., 2007).

#### **4.5. Role of N-cadherin in postsynaptic maturation: filopodia and spine formation, AMPA receptor regulation and LTP**

For synapses to form, contact must first be made between the axon and the dendrite. Synapses have been shown to be initiated by either filopodia from axonal growth cones (Meyer and Smith, 2006) or by dendritic filopodia (Sabo et al., 2006). Synapse formation at very early maturational stages is thought to be initiated by axonal growth cones, which are actively searching for the “correct” target dendrite to make synapses with. However, at later stages of development or during plasticity processes it has been shown that synaptogenesis is initiated mainly by dendritic filopodia (Luscher et al., 2000; Maletic-Savatic et al., 1999). Both axonal and dendritic filopodia are very dynamic structures which rapidly extend and retract surveying the extracellular matrix and surface of the other cells in order to identify appropriate targets for adhesion (Tessier-Lavigne and Goodman, 1996).

In the present study, the analysis of filopodia in N-cadherin deficient neurons indicated that N-cadherin is important for filopodia formation. In immature N-cadherin deficient neurons a significant reduction in the density of filopodia along the dendrites was observed (see Fig. 3.28). Filopodia formation and motility is thought to represent a mechanism of accelerating contact with axons and thus synapse formation. Previous studies have indicated that dendritic filopodia may initiate synaptogenic contacts with nearby axons and eventually they will develop into dendritic spines (Okabe et al., 2001; Ziv and Smith, 1996). Filopodia are thin protrusions that contain actin filaments cross-linked into bundles by actin-binding proteins such as cortactin, Arp2/3, formin1 and Rho family of GTPases (Hering and Sheng, 2003). Therefore, actin and regulators of actin polymerization are essential for filopodial and spine motility (Ackermann and Matus, 2003; Fischer et al., 1998). On the other side, the formation of cadherin-mediated cell-cell junctions in epithelial cells has been shown to induce a profound remodeling of the



actin cytoskeleton. The “core” mechanism of cadherin-based adhesion is thought to involve cadherin’s association with  $\beta$ -catenin, which in turn interacts with  $\alpha$ -catenin to tether cadherin to the actin cytoskeleton. However, the cadherin-catenin-actin cytoskeleton complex has been shown to be a more dynamic one, as  $\alpha$ -catenin seems to bind either to  $\beta$ -catenin or to F-actin in a mutually exclusive manner, with monomeric form preferentially binding  $\beta$ -catenin and dimeric form preferentially binding F-actin (Drees et al., 2005). There is evidence that  $\alpha$ N-catenin is an important regulator of spine motility. Deletion of  $\alpha$ N-catenin affected dendritic spine morphology leading to conversion of spines into filopodia like processes and the dendritic spines were highly motile. Conversely, overexpression of  $\alpha$ N-catenin in neurons results in the formation of excess spines along dendrites (Abe et al., 2004). Cadherins have been shown to modulate the actin cytoskeleton not only by direct structural association with the actin filaments via  $\alpha$ -catenin, but also by controlling the activity and localization of actin-binding molecules (Goodwin and Yap, 2004). It was demonstrated that p120catenin, a cadherin binding protein, affects the activity of Rho family GTPases. In addition, loss of p120catenin function in vivo resulted in reduced spine density and altered spine morphology (Elia et al., 2006). Cadherin-mediated adhesion has also been shown to affect the maturation and function of postsynaptic compartments. Previous studies indicated that blocking the cadherin-mediated intercellular contacts in hippocampal neurons delayed the maturation of dendritic spines, which tended to retain their long, immature filopodia morphology (Togashi et al., 2002).

It is well known that neuronal activity induces the remodeling of pre- and postsynaptic specializations. Strong activation of NMDA receptors by repetitive stimulation for induction of long-term potentiation (LTP) has been demonstrated to induce the growth of filopodia within minutes (Maletic-Savatic et al., 1999). Electron microscopic studies revealed a series of other morphological changes in response to synaptic activity, like enlargement and segmentation of the postsynaptic density, followed by the generation of multiple postsynaptic spines, which eventually leads to the increased number of synapses observed in the late-phase of LTP. Several studies have indicated that cadherin- and catenin-mediated control of synaptic stability plays a very important role in synaptic

plasticity. Blocking N-cadherin adhesion in hippocampal slices by application of anti-N-cadherin antibodies prevented the induction of late-phase LTP (L-LTP), which indicates that N-cadherin is required to maintain nascent synaptic contacts (Bozdagi et al., 2000). Similarly, it has been shown that N-cadherin is required for the spine expansion induced by neuronal activity (Okamura et al., 2004). However, N-cadherin plays an important role not only in the structural plasticity of synapses but also in their functional plasticity. A recent study has shown that N-cadherin regulates AMPA receptor trafficking in neurons (Nuriya and Haganir, 2006). N-cadherin and  $\beta$ -catenin were found to form a protein complex with the AMPA receptor subunits glutamate receptor 1 (GluR1) and 4 (GluR4) in vivo and this association was regulated by extracellular calcium (Nuriya and Haganir, 2006). Furthermore, it has been shown that N-cadherin can directly interact with GluR2 subunits via extracellular domains at excitatory synapses in hippocampal neurons and this complex promotes the growth and maintenance of spines (Saglietti et al., 2007).

The effect of neuroligin1 expression on filopodia formation was also investigated. In heterozygous N-cadherin control neurons, a significant increase in filopodia formation was found upon neuroligin1 overexpression (see Fig.3.28). Intriguingly, the same effect was also observed in N-cadherin deficient neurons indicating that neuroligin1 does not require N-cadherin to induce filopodia, contrary to its vesicle cluster-inducing activity. These results are intriguing and need to be further supported by more data as neuroligin's function in triggering filopodia has not yet been studied extensively. However, a possible role of neuroligin1 in filopodia formation can be associated with activity-dependent alterations in spine dynamics observed during changes in synaptic and structural plasticity (Bredt and Nicoll, 2003; Halpain et al., 1998). Indeed, neuroligin1 was shown to be required for normal LTP in the amygdala (Kim et al., 2008).

In line with these studies and the present data described above, it will be of major interest to further investigate the interplay between the N-cadherin/ $\beta$ -catenin and the neuroligin/neurexin adhesion systems at synapses expressing LTP or LTD, and gain additional insight into the mechanisms that these cell adhesion molecules employ to modulate pre- and postsynaptic changes under plasticity conditions.

## 5. References

- Abe, K., Chisaka, O., Van Roy, F., and Takeichi, M. (2004). Stability of dendritic spines and synaptic contacts is controlled by alpha N-catenin. *Nat Neurosci* 7, 357-363.
- Ackermann, M., and Matus, A. (2003). Activity-induced targeting of profilin and stabilization of dendritic spine morphology. *Nat Neurosci* 6, 1194-1200.
- Adam, G., and Matus, A. (1996). Role of actin in the organisation of brain postsynaptic densities. *Brain Res Mol Brain Res* 43, 246-250.
- Ahmari, S.E., Buchanan, J., and Smith, S.J. (2000). Assembly of presynaptic active zones from cytoplasmic transport packets. *Nat Neurosci* 3, 445-451.
- Ahmari, S.E., and Smith, S.J. (2002). Knowing a nascent synapse when you see it. *Neuron* 34, 333-336.
- Akins, M.R., and Biederer, T. (2006). Cell-cell interactions in synaptogenesis. *Curr Opin Neurobiol* 16, 83-89.
- Bacci, A., and Huguenard, J.R. (2006). Enhancement of spike-timing precision by autaptic transmission in neocortical inhibitory interneurons. *Neuron* 49, 119-130.
- Bamji, S.X. (2005). Cadherins: actin with the cytoskeleton to form synapses. *Neuron* 47, 175-178.
- Bamji, S.X., Rico, B., Kimes, N., and Reichardt, L.F. (2006). BDNF mobilizes synaptic vesicles and enhances synapse formation by disrupting cadherin-beta-catenin interactions. *J Cell Biol* 174, 289-299.
- Bamji, S.X., Shimazu, K., Kimes, N., Huelsken, J., Birchmeier, W., Lu, B., and Reichardt, L.F. (2003). Role of beta-catenin in synaptic vesicle localization and presynaptic assembly. *Neuron* 40, 719-731.
- Benson, D.L., Colman, D.R., and Huntley, G.W. (2001). Molecules, maps and synapse specificity. *Nat Rev Neurosci* 2, 899-909.
- Benson, D.L., and Tanaka, H. (1998). N-cadherin redistribution during synaptogenesis in hippocampal neurons. *J Neurosci* 18, 6892-6904.
- Biederer, T., Sara, Y., Mozhayeva, M., Atasoy, D., Liu, X., Kavalali, E.T., and Sudhof, T.C. (2002). SynCAM, a synaptic adhesion molecule that drives synapse assembly. *Science* 297, 1525-1531.
- Biederer, T., and Sudhof, T.C. (2001). CASK and protein 4.1 support F-actin nucleation on neuroligins. *J Biol Chem* 276, 47869-47876.

## REFERENCES

- Bouccard, A.A., Chubykin, A.A., Comoletti, D., Taylor, P., and Sudhof, T.C. (2005). A splice code for trans-synaptic cell adhesion mediated by binding of neuroligin 1 to alpha- and beta-neurexins. *Neuron* 48, 229-236.
- Bozdagi, O., Shan, W., Tanaka, H., Benson, D.L., and Huntley, G.W. (2000). Increasing numbers of synaptic puncta during late-phase LTP: N-cadherin is synthesized, recruited to synaptic sites, and required for potentiation. *Neuron* 28, 245-259.
- Bozdagi, O., Valcin, M., Poskanzer, K., Tanaka, H., and Benson, D.L. (2004). Temporally distinct demands for classic cadherins in synapse formation and maturation. *Mol Cell Neurosci* 27, 509-521.
- Bredt, D.S., and Nicoll, R.A. (2003). AMPA receptor trafficking at excitatory synapses. *Neuron* 40, 361-379.
- Bresler, T., Shapira, M., Boeckers, T., Dresbach, T., Futter, M., Garner, C.C., Rosenblum, K., Gundelfinger, E.D., and Ziv, N.E. (2004). Postsynaptic density assembly is fundamentally different from presynaptic active zone assembly. *J Neurosci* 24, 1507-1520.
- Butz, S., Okamoto, M., and Sudhof, T.C. (1998). A tripartite protein complex with the potential to couple synaptic vesicle exocytosis to cell adhesion in brain. *Cell* 94, 773-782.
- Chih, B., Engelman, H., and Scheiffele, P. (2005). Control of excitatory and inhibitory synapse formation by neuroligins. *Science* 307, 1324-1328.
- Chih, B., Gollan, L., and Scheiffele, P. (2006). Alternative splicing controls selective trans-synaptic interactions of the neuroligin-neurexin complex. *Neuron* 51, 171-178.
- Chubykin, A.A., Atasoy, D., Etherton, M.R., Brose, N., Kavalali, E.T., Gibson, J.R., and Sudhof, T.C. (2007). Activity-dependent validation of excitatory versus inhibitory synapses by neuroligin-1 versus neuroligin-2. *Neuron* 54, 919-931.
- Colicos, M.A., Collins, B.E., Sailor, M.J., and Goda, Y. (2001). Remodeling of synaptic actin induced by photoconductive stimulation. *Cell* 107, 605-616.
- Comoletti, D., Grishaev, A., Whitten, A.E., Tsigelny, I., Taylor, P., and Trewhella, J. (2007). Synaptic arrangement of the neuroligin/beta-neurexin complex revealed by X-ray and neutron scattering. *Structure* 15, 693-705.
- Craig, A.M., Graf, E.R., and Linhoff, M.W. (2006). How to build a central synapse: clues from cell culture. *Trends Neurosci* 29, 8-20.
- Craven, S.E., and Bredt, D.S. (1998). PDZ proteins organize synaptic signaling pathways. *Cell* 93, 495-498.

## REFERENCES

- Darcy, K.J., Staras, K., Collinson, L.M., and Goda, Y. (2006). Constitutive sharing of recycling synaptic vesicles between presynaptic boutons. *Nat Neurosci* 9, 315-321.
- Dean, C., and Dresbach, T. (2006). Neuroligins and neurexins: linking cell adhesion, synapse formation and cognitive function. *Trends Neurosci* 29, 21-29.
- Dean, C., Scholl, F.G., Choih, J., DeMaria, S., Berger, J., Isacoff, E., and Scheiffele, P. (2003). Neurexin mediates the assembly of presynaptic terminals. *Nat Neurosci* 6, 708-716.
- Dong, H., O'Brien, R.J., Fung, E.T., Lanahan, A.A., Worley, P.F., and Huganir, R.L. (1997). GRIP: a synaptic PDZ domain-containing protein that interacts with AMPA receptors. *Nature* 386, 279-284.
- Drees, F., Pokutta, S., Yamada, S., Nelson, W.J., and Weis, W.I. (2005). Alpha-catenin is a molecular switch that binds E-cadherin-beta-catenin and regulates actin-filament assembly. *Cell* 123, 903-915.
- Dresbach, T., Neeb, A., Meyer, G., Gundelfinger, E.D., and Brose, N. (2004). Synaptic targeting of neuroligin is independent of neurexin and SAP90/PSD95 binding. *Mol Cell Neurosci* 27, 227-235.
- Dresbach, T., Torres, V., Wittenmayer, N., Altroch, W.D., Zamorano, P., Zuschratter, W., Nawrothki, R., Ziv, N.E., Garner, C.C., and Gundelfinger, E.D. (2006). Assembly of active zone precursor vesicles: obligatory trafficking of presynaptic cytomatrix proteins Bassoon and Piccolo via a trans-Golgi compartment. *J Biol Chem* 281, 6038-6047.
- Eccles, J.C., Llinas, R., and Sasaki, K. (1966). The excitatory synaptic action of climbing fibres on the purinje cells of the cerebellum. *J Physiol* 182, 268-296.
- Elgersma, Y., and Silva, A.J. (1999). Molecular mechanisms of synaptic plasticity and memory. *Curr Opin Neurobiol* 9, 209-213.
- El-Husseini, A.E., Schnell, E., Chetkovich, D.M., Nicoll, R.A., and Brecht, D.S. (2000). PSD-95 involvement in maturation of excitatory synapses. *Science* 290, 1364-1368.
- Elia, L.P., Yamamoto, M., Zang, K., and Reichardt, L.F. (2006). p120 catenin regulates dendritic spine and synapse development through Rho-family GTPases and cadherins. *Neuron* 51, 43-56.
- Elias, G.M., Funke, L., Stein, V., Grant, S.G., Brecht, D.S., and Nicoll, R.A. (2006). Synapse-specific and developmentally regulated targeting of AMPA receptors by a family of MAGUK scaffolding proteins. *Neuron* 52, 307-320.

## REFERENCES

- Elste, A.M., and Benson, D.L. (2006). Structural basis for developmentally regulated changes in cadherin function at synapses. *J Comp Neurol* 495, 324-335.
- Fannon, A.M., and Colman, D.R. (1996). A model for central synaptic junctional complex formation based on the differential adhesive specificities of the cadherins. *Neuron* 17, 423-434.
- Fenster, S.D., Chung, W.J., Zhai, R., Cases-Langhoff, C., Voss, B., Garner, A.M., Kaempfer, U., Kindler, S., Gundelfinger, E.D., and Garner, C.C. (2000). Piccolo, a presynaptic zinc finger protein structurally related to bassoon. *Neuron* 25, 203-214.
- Fischer, M., Kaech, S., Knutti, D., and Matus, A. (1998). Rapid actin-based plasticity in dendritic spines. *Neuron* 20, 847-854.
- Friedman, H.V., Bresler, T., Garner, C.C., and Ziv, N.E. (2000). Assembly of new individual excitatory synapses: time course and temporal order of synaptic molecule recruitment. *Neuron* 27, 57-69.
- Garner, C.C., Waites, C.L., and Ziv, N.E. (2006). Synapse development: still looking for the forest, still lost in the trees. *Cell Tissue Res* 326, 249-262.
- Gerrow, K., Romorini, S., Nabi, S.M., Colicos, M.A., Sala, C., and El-Husseini, A. (2006). A preformed complex of postsynaptic proteins is involved in excitatory synapse development. *Neuron* 49, 547-562.
- Goodwin, M., and Yap, A.S. (2004). Classical cadherin adhesion molecules: coordinating cell adhesion, signaling and the cytoskeleton. *J Mol Histol* 35, 839-844.
- Gottmann, K. (2008). Transsynaptic modulation of the synaptic vesicle cycle by cell-adhesion molecules. *J Neurosci Res* 86, 223-232.
- Graf, E.R., Zhang, X., Jin, S.X., Linhoff, M.W., and Craig, A.M. (2004). Neurexins induce differentiation of GABA and glutamate postsynaptic specializations via neuroligins. *Cell* 119, 1013-1026.
- Halpain, S., Hipolito, A., and Saffer, L. (1998). Regulation of F-actin stability in dendritic spines by glutamate receptors and calcineurin. *J Neurosci* 18, 9835-9844.
- Han, K., and Kim, E. (2008). Synaptic adhesion molecules and PSD-95. *Prog Neurobiol* 84, 263-283.
- Hata, Y., Butz, S., and Sudhof, T.C. (1996). CASK: a novel dlg/PSD95 homolog with an N-terminal calmodulin-dependent protein kinase domain identified by interaction with neurexins. *J Neurosci* 16, 2488-2494.

## REFERENCES

- Hering, H., and Sheng, M. (2003). Activity-dependent redistribution and essential role of cortactin in dendritic spine morphogenesis. *J Neurosci* 23, 11759-11769.
- Hilfiker, S., Pieribone, V.A., Czernik, A.J., Kao, H.T., Augustine, G.J., and Greengard, P. (1999). Synapsins as regulators of neurotransmitter release. *Philos Trans R Soc Lond B Biol Sci* 354, 269-279.
- Hirao, K., Hata, Y., Ide, N., Takeuchi, M., Irie, M., Yao, I., Deguchi, M., Toyoda, A., Sudhof, T.C., and Takai, Y. (1998). A novel multiple PDZ domain-containing molecule interacting with N-methyl-D-aspartate receptors and neuronal cell adhesion proteins. *J Biol Chem* 273, 21105-21110.
- Hirao, K., Hata, Y., Yao, I., Deguchi, M., Kawabe, H., Mizoguchi, A., and Takai, Y. (2000). Three isoforms of synaptic scaffolding molecule and their characterization. Multimerization between the isoforms and their interaction with N-methyl-D-aspartate receptors and SAP90/PSD-95-associated protein. *J Biol Chem* 275, 2966-2972.
- Hollmann, M., Boulter, J., Maron, C., and Heinemann, S. (1994). Molecular biology of glutamate receptors. Potentiation of N-methyl-D-aspartate receptor splice variants by zinc. *Ren Physiol Biochem* 17, 182-183.
- Hopf, F.W., Waters, J., Mehta, S., and Smith, S.J. (2002). Stability and plasticity of developing synapses in hippocampal neuronal cultures. *J Neurosci* 22, 775-781.
- Hsueh, Y.P., Yang, F.C., Kharazia, V., Naisbitt, S., Cohen, A.R., Weinberg, R.J., and Sheng, M. (1998). Direct interaction of CASK/LIN-2 and syndecan heparan sulfate proteoglycan and their overlapping distribution in neuronal synapses. *J Cell Biol* 142, 139-151.
- Hubel, D.H., Wiesel, T.N., and LeVay, S. (1977). Plasticity of ocular dominance columns in monkey striate cortex. *Philos Trans R Soc Lond B Biol Sci* 278, 377-409.
- Huntley, G.W., and Benson, D.L. (1999). Neural (N)-cadherin at developing thalamocortical synapses provides an adhesion mechanism for the formation of somatopically organized connections. *J Comp Neurol* 407, 453-471.
- Ichtchenko, K., Hata, Y., Nguyen, T., Ullrich, B., Missler, M., Moomaw, C., and Sudhof, T.C. (1995). Neuroligin 1: a splice site-specific ligand for beta-neurexins. *Cell* 81, 435-443.
- Ichtchenko, K., Nguyen, T., and Sudhof, T.C. (1996). Structures, alternative splicing, and neurexin binding of multiple neuroligins. *J Biol Chem* 271, 2676-2682.
- Ide, N., Hata, Y., Deguchi, M., Hirao, K., Yao, I., and Takai, Y. (1999). Interaction of S-SCAM with neural plakophilin-related Armadillo-repeat protein/delta-catenin. *Biochem Biophys Res Commun* 256, 456-461.



## REFERENCES

- Iida, J., Hirabayashi, S., Sato, Y., and Hata, Y. (2004). Synaptic scaffolding molecule is involved in the synaptic clustering of neuroligin. *Mol Cell Neurosci* 27, 497-508.
- Iida, J., Ishizaki, H., Okamoto-Tanaka, M., Kawata, A., Sumita, K., Ohgake, S., Sato, Y., Yorifuji, H., Nukina, N., Ohashi, K., *et al.* (2007). Synaptic scaffolding molecule alpha is a scaffold to mediate N-methyl-D-aspartate receptor-dependent RhoA activation in dendrites. *Mol Cell Biol* 27, 4388-4405.
- Irie, M., Hata, Y., Takeuchi, M., Ichtchenko, K., Toyoda, A., Hirao, K., Takai, Y., Rosahl, T.W., and Sudhof, T.C. (1997). Binding of neuroligins to PSD-95. *Science* 277, 1511-1515.
- Jontes, J.D., Emond, M.R., and Smith, S.J. (2004). In vivo trafficking and targeting of N-cadherin to nascent presynaptic terminals. *J Neurosci* 24, 9027-9034.
- Jungling, K., Eulenburg, V., Moore, R., Kemler, R., Lessmann, V., and Gottmann, K. (2006). N-cadherin transsynaptically regulates short-term plasticity at glutamatergic synapses in embryonic stem cell-derived neurons. *J Neurosci* 26, 6968-6978.
- Kadowaki, M., Nakamura, S., Machon, O., Krauss, S., Radice, G.L., and Takeichi, M. (2007). N-cadherin mediates cortical organization in the mouse brain. *Dev Biol* 304, 22-33.
- Kennedy, M.B. (2000). Signal-processing machines at the postsynaptic density. *Science* 290, 750-754.
- Kim, J., Jung, S.Y., Lee, Y.K., Park, S., Choi, J.S., Lee, C.J., Kim, H.S., Choi, Y.B., Scheiffele, P., Bailey, C.H., *et al.* (2008). Neuroligin-1 is required for normal expression of LTP and associative fear memory in the amygdala of adult animals. *Proc Natl Acad Sci U S A* 105, 9087-9092.
- Kim, E., and Sheng, M. (2004). PDZ domain proteins of synapses. *Nat Rev Neurosci* 5, 771-781.
- Kornau, H.C., and Seeburg, P.H. (1997). Partner selection by PDZ domains. *Nat Biotechnol* 15, 319.
- Kraszewski, K., Mundigl, O., Daniell, L., Verderio, C., Matteoli, M., and De Camilli, P. (1995). Synaptic vesicle dynamics in living cultured hippocampal neurons visualized with CY3-conjugated antibodies directed against the luminal domain of synaptotagmin. *J Neurosci* 15, 4328-4342.
- Krueger, S.R., Kolar, A., and Fitzsimonds, R.M. (2003). The presynaptic release apparatus is functional in the absence of dendritic contact and highly mobile within isolated axons. *Neuron* 40, 945-957.



## REFERENCES

- Leonard, A.S., Davare, M.A., Horne, M.C., Garner, C.C., and Hell, J.W. (1998). SAP97 is associated with the alpha-amino-3-hydroxy-5-methylisoxazole-4-propionic acid receptor GluR1 subunit. *J Biol Chem* 273, 19518-19524.
- Lessmann, V., and Heumann, R. (1997). Cyclic AMP endogenously enhances synaptic strength of developing glutamatergic synapses in serum-free microcultures of rat hippocampal neurons. *Brain Res* 763, 111-122.
- Luscher, C., Nicoll, R.A., Malenka, R.C., and Muller, D. (2000). Synaptic plasticity and dynamic modulation of the postsynaptic membrane. *Nat Neurosci* 3, 545-550.
- Maletic-Savatic, M., Malinow, R., and Svoboda, K. (1999). Rapid dendritic morphogenesis in CA1 hippocampal dendrites induced by synaptic activity. *Science* 283, 1923-1927.
- Mariani, J., and Changeux, J.P. (1981). Ontogenesis of olivocerebellar relationships. I. Studies by intracellular recordings of the multiple innervation of Purkinje cells by climbing fibers in the developing rat cerebellum. *J Neurosci* 1, 696-702.
- Matteoli, M., Takei, K., Perin, M.S., Sudhof, T.C., and De Camilli, P. (1992). Exo-endocytotic recycling of synaptic vesicles in developing processes of cultured hippocampal neurons. *J Cell Biol* 117, 849-861.
- McAllister, A.K. (2007). Dynamic aspects of CNS synapse formation. *Annu Rev Neurosci* 30, 425-450.
- McNally, J.G., Karpova, T., Cooper, J., and Conchello, J.A. (1999). Three-dimensional imaging by deconvolution microscopy. *Methods* 19, 373-385.
- Menuz, K., O'Brien, J.L., Karmizadegan, S., Bredt, D.S., and Nicoll, R.A. (2008). TARP redundancy is critical for maintaining AMPA receptor function. *J Neurosci* 28, 8740-8746.
- Meyer, G., Varoqueaux, F., Neeb, A., Oschlies, M., and Brose, N. (2004). The complexity of PDZ domain-mediated interactions at glutamatergic synapses: a case study on neuroligin. *Neuropharmacology* 47, 724-733.
- Meyer, M.P., and Smith, S.J. (2006). Evidence from in vivo imaging that synaptogenesis guides the growth and branching of axonal arbors by two distinct mechanisms. *J Neurosci* 26, 3604-3614.
- Missler, M., Fernandez-Chacon, R., and Sudhof, T.C. (1998). The making of neurexins. *J Neurochem* 71, 1339-1347.

## REFERENCES

- Miyatani, S., Copeland, N.G., Gilbert, D.J., Jenkins, N.A., and Takeichi, M. (1992). Genomic structure and chromosomal mapping of the mouse N-cadherin gene. *Proc Natl Acad Sci U S A* 89, 8443-8447.
- Mohrmann, R., Lessmann, V., and Gottmann, K. (2003). Developmental maturation of synaptic vesicle cycling as a distinctive feature of central glutamatergic synapses. *Neuroscience* 117, 7-18.
- Moore, R., Radice, G.L., Dominis, M., and Kemler, R. (1999). The generation and in vivo differentiation of murine embryonal stem cells genetically null for either N-cadherin or N- and P-cadherin. *Int J Dev Biol* 43, 831-834.
- Montgomery, J.M., Zamorano, P.L., and Garner, C.C. (2004). MAGUKs in synapse assembly and function: an emerging view. *Cell Mol Life Sci* 61, 911-929.
- Mozhayeva, M.G., Sara, Y., Liu, X., and Kavalali, E.T. (2002). Development of vesicle pools during maturation of hippocampal synapses. *J Neurosci* 22, 654-665.
- Nam, C.I., and Chen, L. (2005). Postsynaptic assembly induced by neurexin-neurologin interaction and neurotransmitter. *Proc Natl Acad Sci U S A* 102, 6137-6142.
- Niethammer, M., Kim, E., and Sheng, M. (1996). Interaction between the C terminus of NMDA receptor subunits and multiple members of the PSD-95 family of membrane-associated guanylate kinases. *J Neurosci* 16, 2157-2163.
- Nishimura, W., Yao, I., Iida, J., Tanaka, N., and Hata, Y. (2002). Interaction of synaptic scaffolding molecule and Beta -catenin. *J Neurosci* 22, 757-765.
- Nuriya, M., and Huganir, R.L. (2006). Regulation of AMPA receptor trafficking by N-cadherin. *J Neurochem* 97, 652-661.
- O'Brien, R.J., Xu, D., Petralia, R.S., Steward, O., Huganir, R.L., and Worley, P. (1999). Synaptic clustering of AMPA receptors by the extracellular immediate-early gene product Narp. *Neuron* 23, 309-323.
- Okabe, S., Miwa, A., and Okado, H. (2001). Spine formation and correlated assembly of presynaptic and postsynaptic molecules. *J Neurosci* 21, 6105-6114.
- Okabe, S., Urushido, T., Konno, D., Okado, H., and Sobue, K. (2001b). Rapid redistribution of the postsynaptic density protein PSD-45 (Homer 1c) and its differential regulation by NMDA receptors and calcium channels. *J Neurosci* 21, 9561-9571.
- Okamura, K., Tanaka, H., Yagita, Y., Saeki, Y., Taguchi, A., Hiraoka, Y., Zeng, L.H., Colman, D.R., and Miki, N. (2004). Cadherin activity is required for activity-induced spine remodeling. *J Cell Biol* 167, 961-972.

## REFERENCES

- Perego, C., Vanoni, C., Massari, S., Longhi, R., and Pietrini, G. (2000). Mammalian LIN-7 PDZ proteins associate with beta-catenin at the cell-cell junctions of epithelia and neurons. *EMBO J* 19, 3978-3989.
- Phillips, G.R., Huang, J.K., Wang, Y., Tanaka, H., Shapiro, L., Zhang, W., Shan, W.S., Arndt, K., Frank, M., Gordon, R.E., *et al.* (2001). The presynaptic particle web: ultrastructure, composition, dissolution, and reconstitution. *Neuron* 32, 63-77.
- Pokutta, S., and Weis, W.I. (2007). Structure and mechanism of cadherins and catenins in cell-cell contacts. *Annu Rev Cell Dev Biol* 23, 237-261.
- Prange, O., and Murphy, T.H. (2001). Modular transport of postsynaptic density-95 clusters and association with stable spine precursors during early development of cortical neurons. *J Neurosci* 21, 9325-9333.
- Prange, O., Wong, T.P., Gerrow, K., Wang, Y.T., and El-Husseini, A. (2004). A balance between excitatory and inhibitory synapses is controlled by PSD-95 and neuroligin. *Proc Natl Acad Sci U S A* 101, 13915-13920.
- Radice, G.L., Rayburn, H., Matsunami, H., Knudsen, K.A., Takeichi, M., and Hynes, R.O. (1997). Developmental defects in mouse embryos lacking N-cadherin. *Dev Biol* 181, 64-78.
- Rao, A., Cha, E.M., and Craig, A.M. (2000). Mismatched appositions of presynaptic and postsynaptic components in isolated hippocampal neurons. *J Neurosci* 20, 8344-8353.
- Redies, C. (1997). Cadherins and the formation of neural circuitry in the vertebrate CNS. *Cell Tissue Res* 290, 405-413.
- Redies, C. (2000). Cadherins in the central nervous system. *Prog Neurobiol* 61, 611-648.
- Regalado, M.P., Terry-Lorenzo, R.T., Waites, C.L., Garner, C.C., and Malenka, R.C. (2006). Transsynaptic signaling by postsynaptic synapse-associated protein 97. *J Neurosci* 26, 2343-2357.
- Rizzoli, S.O., and Betz, W.J. (2005). Synaptic vesicle pools. *Nat Rev Neurosci* 6, 57-69.
- Sabo, S.L., Gomes, R.A., and McAllister, A.K. (2006). Formation of presynaptic terminals at predefined sites along axons. *J Neurosci* 26, 10813-10825.
- Saglietti, L., Dequidt, C., Kamieniarz, K., Rousset, M.C., Valnegri, P., Thoumine, O., Beretta, F., Fagni, L., Choquet, D., Sala, C., *et al.* (2007). Extracellular interactions between GluR2 and N-cadherin in spine regulation. *Neuron* 54, 461-477.

## REFERENCES

- Sambrook, J., and Russell D.W. (2000). *Molecular Cloning: A Laboratory Manual*, Published by CSHL Press
- Sankaranarayanan, S., Atluri, P.P., and Ryan, T.A. (2003). Actin has a molecular scaffolding, not propulsive, role in presynaptic function. *Nat Neurosci* 6, 127-135.
- Sara, Y., Biederer, T., Atasoy, D., Chubykin, A., Mozhayeva, M.G., Sudhof, T.C., and Kavalali, E.T. (2005). Selective capability of SynCAM and neuroligin for functional synapse assembly. *J Neurosci* 25, 260-270.
- Scheiffele, P., Fan, J., Choih, J., Fetter, R., and Serafini, T. (2000). Neuroligin expressed in nonneuronal cells triggers presynaptic development in contacting axons. *Cell* 101, 657-669.
- Shapira, M., Zhai, R.G., Dresbach, T., Bresler, T., Torres, V.I., Gundelfinger, E.D., Ziv, N.E., and Garner, C.C. (2003). Unitary assembly of presynaptic active zones from Piccolo-Bassoon transport vesicles. *Neuron* 38, 237-252.
- Sharma, K., Fong, D.K., and Craig, A.M. (2006). Postsynaptic protein mobility in dendritic spines: long-term regulation by synaptic NMDA receptor activation. *Mol Cell Neurosci* 31, 702-712.
- Shi, S.H., Hayashi, Y., Petralia, R.S., Zaman, S.H., Wenthold, R.J., Svoboda, K., and Malinow, R. (1999). Rapid spine delivery and redistribution of AMPA receptors after synaptic NMDA receptor activation. *Science* 284, 1811-1816.
- Shupliakov, O., Bloom, O., Gustafsson, J.S., Kjaerulff, O., Low, P., Tomilin, N., Pieribone, V.A., Greengard, P., and Brodin, L. (2002). Impaired recycling of synaptic vesicles after acute perturbation of the presynaptic actin cytoskeleton. *Proc Natl Acad Sci U S A* 99, 14476-14481.
- Song, J.Y., Ichtchenko, K., Sudhof, T.C., and Brose, N. (1999). Neuroligin 1 is a postsynaptic cell-adhesion molecule of excitatory synapses. *Proc Natl Acad Sci U S A* 96, 1100-1105.
- Sprengel, R., Suchanek, B., Amico, C., Brusa, R., Burnashev, N., Rozov, A., Hvalby, O., Jensen, V., Paulsen, O., Andersen, P., *et al.* (1998). Importance of the intracellular domain of NR2 subunits for NMDA receptor function in vivo. *Cell* 92, 279-289.
- Sytnyk, V., Leshchyns'ka, I., Delling, M., Dityateva, G., Dityatev, A., and Schachner, M. (2002). Neural cell adhesion molecule promotes accumulation of TGN organelles at sites of neuron-to-neuron contacts. *J Cell Biol* 159, 649-661.
- Takeichi, M. (2007). The cadherin superfamily in neuronal connections and interactions. *Nat Rev Neurosci* 8, 11-20.

## REFERENCES

- Takumi, Y., Ramirez-Leon, V., Laake, P., Rinvik, E., and Ottersen, O.P. (1999). Different modes of expression of AMPA and NMDA receptors in hippocampal synapses. *Nat Neurosci* 2, 618-624.
- Tanaka, H., Shan, W., Phillips, G.R., Arndt, K., Bozdagi, O., Shapiro, L., Huntley, G.W., Benson, D.L., and Colman, D.R. (2000). Molecular modification of N-cadherin in response to synaptic activity. *Neuron* 25, 93-107.
- Tang, L., Hung, C.P., and Schuman, E.M. (1998). A role for the cadherin family of cell adhesion molecules in hippocampal long-term potentiation. *Neuron* 20, 1165-1175.
- Tessier-Lavigne, M., and Goodman, C.S. (1996). The molecular biology of axon guidance. *Science* 274, 1123-1133.
- Togashi, H., Abe, K., Mizoguchi, A., Takaoka, K., Chisaka, O., and Takeichi, M. (2002). Cadherin regulates dendritic spine morphogenesis. *Neuron* 35, 77-89.
- Tomita, S., Adesnik, H., Sekiguchi, M., Zhang, W., Wada, K., Howe, J.R., Nicoll, R.A., and Brecht, D.S. (2005). Stargazin modulates AMPA receptor gating and trafficking by distinct domains. *Nature* 435, 1052-1058.
- Uchida, N., Honjo, Y., Johnson, K.R., Wheelock, M.J., and Takeichi, M. (1996). The catenin/cadherin adhesion system is localized in synaptic junctions bordering transmitter release zones. *J Cell Biol* 135, 767-779.
- Ushkaryov, Y.A., Hata, Y., Ichtchenko, K., Moomaw, C., Afendis, S., Slaughter, C.A., and Sudhof, T.C. (1994). Conserved domain structure of beta-neurexins. Unusual cleaved signal sequences in receptor-like neuronal cell-surface proteins. *J Biol Chem* 269, 11987-11992.
- Ushkaryov, Y.A., Petrenko, A.G., Geppert, M., and Sudhof, T.C. (1992). Neurexins: synaptic cell surface proteins related to the alpha-latrotoxin receptor and laminin. *Science* 257, 50-56.
- Varoqueaux, F., Aramuni, G., Rawson, R.L., Mohrmann, R., Missler, M., Gottmann, K., Zhang, W., Sudhof, T.C., and Brose, N. (2006). Neuroligins determine synapse maturation and function. *Neuron* 51, 741-754.
- Varoqueaux, F., Jamain, S., and Brose, N. (2004). Neuroligin 2 is exclusively localized to inhibitory synapses. *Eur J Cell Biol* 83, 449-456.
- Vaughn, J.E. (1989). Fine structure of synaptogenesis in the vertebrate central nervous system. *Synapse* 3, 255-285.
- Washbourne, P., Bennett, J.E., and McAllister, A.K. (2002). Rapid recruitment of NMDA receptor transport packets to nascent synapses. *Nat Neurosci* 5, 751-759.

## REFERENCES

- Xu, G., Craig, A.W., Greer, P., Miller, M., Anastasiadis, P.Z., Lilien, J., and Balsamo, J. (2004). Continuous association of cadherin with beta-catenin requires the non-receptor tyrosine-kinase Fer. *J Cell Sci* 117, 3207-3219.
- Yamada, A., Irie, K., Deguchi-Tawarada, M., Ohtsuka, T., and Takai, Y. (2003). Nectin-dependent localization of synaptic scaffolding molecule (S-SCAM) at the puncta adherentia junctions formed between the mossy fibre terminals and the dendrites of pyramidal cells in the CA3 area of the mouse hippocampus. *Genes Cells* 8, 985-994.
- Yamagata, M., Herman, J.P., and Sanes, J.R. (1995). Lamina-specific expression of adhesion molecules in developing chick optic tectum. *J Neurosci* 15, 4556-4571.
- Zhai, R.G., Vardinon-Friedman, H., Cases-Langhoff, C., Becker, B., Gundelfinger, E.D., Ziv, N.E., and Garner, C.C. (2001). Assembling the presynaptic active zone: a characterization of an active one precursor vesicle. *Neuron* 29, 131-143.
- Zhang, W., and Benson, D.L. (2001). Stages of synapse development defined by dependence on F-actin. *J Neurosci* 21, 5169-5181.
- Ziv, N.E., and Garner, C.C. (2001). Principles of glutamatergic synapse formation: seeing the forest for the trees. *Curr Opin Neurobiol* 11, 536-543.
- Ziv, N.E., and Garner, C.C. (2004). Cellular and molecular mechanisms of presynaptic assembly. *Nat Rev Neurosci* 5, 385-399.
- Ziv, N.E., and Smith, S.J. (1996). Evidence for a role of dendritic filopodia in synaptogenesis and spine formation. *Neuron* 17, 91-102.
- Zuo, Y., Lin, A., Chang, P., and Gan, W.B. (2005). Development of long-term dendritic spine stability in diverse regions of cerebral cortex. *Neuron* 46, 181-189.

## 6. Appendix

### 6.1. Abbreviations

AMPA	$\alpha$ -amino-3-hydroxy-5-methylisoxazol-4-propionacid
BDNF	Brain-derived neurotrophic factor"
BME	Basal medium Eagle
BSA	Bovine serum albumine
(X)°C	(X) degree Celsius
CAMs	Cell adhesion molecules
CAZ	Cytomatrix assembled at active zones
CNS	Central nervous system
CO <sub>2</sub>	Carbon dioxide
DIV	Days in vitro
DMEM	Dulbecco's Modified Eagle's Medium
DMSO	Dimethyl sulfoxide
DsRed	Discosoma sp. red fluorescent protein
EBs	Embryoid bodies
EDTA	Ethylenediamine-tetraacetic acid
EF cells	Embryonic feeder cells
EGFP	Enhanced green fluorescent protein
ES cells	Embryonic stem cells
FCS	Fetal calf serum
FRAP	Fluorescence recovery after photobleaching
GK domain	Guanylate kinase domain,
GRIP	Glutamate receptor interacting protein
h	Hour
HEPES	N-2-hydroxyethylpiperazin-N'-2-ethansulfonacid
kb	Kilobase
KO ES media	Knock out embryonic stem cell media
LB media	Luria-Bertani media
LIF	Leukemia inhibitory factor
L-LTP	Late-phase LTP
LNS	Laminin-neurexin-sex hormone-binding domain
LTP	Long term potentiation
PDZ	Postsynaptic density 95; discs large; zonula occludens-1
PSD	Postsynaptic density
MAGI	MAGUK with inverted domain structure
MAGUK	Membrane-associated guanylate kinase
mGluRs	Metabotropic glutamate receptors
min	Minutes
NB media	Neurobasal media
N-cad <sup>+/+</sup>	N-cadherin wild type
N-cad <sup>+/-</sup>	N-cadherin heterozygous deletion mutant
N-cad <sup>-/-</sup>	N-cadherin homozygous deletion mutant
NMDA	N-Methyl-D-Aspartat
PBS	Phosphate buffered saline
PCR	Polymerase Chain Reaction

PSF	Point-spread function
PTVs	Piccolo transport vesicles
RIMs	Rab3-interacting molecules
RRP	Readily releasable pool
RT	Room temperature
SEM	Standard error of means
SNARE	Soluble N-ethylmaleimide sensitive factor attachment receptor
SNAP-25	Soluble N-ethylmaleimide sensitive factor attachment protein 25
SR media	Serum replacement media
S-SCAM	Synaptic scaffolding molecule
STVs	Synaptic vesicle transport protein vesicles
SV	Synaptic vesicle
TAE	Tris-acetate-EDTA
TARPs	Transmembrane AMPA receptor regulatory proteins
UV	Ultraviolet
VAMP	Vesicle-associated membrane protein
WW domains	Domains with conserved Trp (W) residues

## 6.2. List of figures

Fig. 1.1.	Model of excitatory synapse formation .....	13
Fig. 1.2.	Model of the homophilic N-cadherin complex at the synapse .....	15
Fig. 1.3.	Model of the heterophilic neuroligin1/ $\beta$ -neurexin complex at the synapse .....	18
Fig. 2.1.	Full-length mouse MAGI-2 $\beta$ /S-SCAM cDNA sequence .....	29
Fig. 2.2.	Generation of mutant S-SCAM constructs .....	32
Fig. 2.3.	Targeted disruption of the N-cadherin gene .....	34
Fig. 2.4.	Schematic representation of the neuronal differentiation procedure .....	37
Fig. 2.5.	Schematic representation of purification of ES cell-derived neurons .....	39
Fig. 2.6.	Time lapse imaging set-up and fluorescence image acquisition .....	41
Fig. 2.7.	Example of sequential focal planes through a theoretically or experimentally determined point-spread function of a 100X, 1.35 NA Olympus UplanApo objective .....	44
Fig. 2.8.	Autothreshold and Low Pass Filter operation .....	46
Fig. 3.1.	Co-transfection of EGFP and DsRed2-VAMP2 in the same neuron .....	49



Fig. 3.2.	Threshold operation used for analysis of the DsRed2-VAMP2 clusters in ES cell-derived neurons .....	51
Fig. 3.3.	The density of presynaptic vesicle clusters is reduced in the absence of N-cadherin in immature neurons .....	53
Fig. 3.4.	Analysis of mean fluorescence intensity and size (area) of the DsRed2-VAMP2 clusters in immature neurons revealed no differences between the two genotypes .....	54
Fig. 3.5.	Presynaptic vesicle accumulation during early synapse maturation requires N-cadherin expression .....	56
Fig. 3.6.	FRAP experiments revealed slower recovery of vesicle cluster-associated fluorescence in the absence of N-cadherin .....	58
Fig. 3.7.	Spontaneous splitting of vesicle clusters is increased in the absence of N-cadherin (7DIV) .....	60
Fig. 3.8.	The total dynamics (fusion and splitting) of vesicle clusters is increased in the absence of N-cadherin (6-7DIV) .....	61
Fig. 3.9.	Threshold operation used for the analysis of the EGFP-Bassoon clusters in ES cell-derived neurons .....	63
Fig. 3.10.	Density of EGFP-Bassoon clusters is unaltered in N-cadherin deficient neurons indicating that formation of active zones does not require N-cadherin .....	64
Fig. 3.11.	Analysis of fluorescence intensity and area of the EGFP-Bassoon clusters in immature neurons shows no differences between the two genotypes .....	65
Fig. 3.12.	The density of presynaptic vesicle clusters is not different between the two genotypes in mature ES cell-derived neurons .....	67
Fig. 3.13.	Analysis of average fluorescence intensity and size of the DsRed2-VAMP2 clusters in more mature neurons revealed no differences between the two genotypes .....	68
Fig. 3.14.	Ongoing presynaptic vesicle accumulation is strongly reduced in more mature neurons (14 DIV) and is unaffected in N-cadherin knockout neurons .....	70

Fig. 3.15.	At late maturational stages (10-14 DIV) the total dynamics (fusion and splitting) of vesicle clusters is similar in the absence of N-cadherin .....	72
Fig. 3.16.	Density of clusters of the active zone protein Bassoon is not affected in more mature N-cadherin deficient neurons .....	73
Fig. 3.17.	Analysis of the fluorescence intensity and area of the EGFP-Bassoon clusters in mature neurons shows no differences between the two genotypes .....	74
Fig. 3.18.	Threshold operation used for analysis of the PSD95-EGFP clusters in ES cell-derived neurons .....	76
Fig. 3.19.	DsRed2-VAMP2 labeled presynaptic vesicle clusters are largely co-localized with PSD95-EGFP labeled postsynaptic densities .....	79
Fig. 3.20.	Analysis of mean fluorescence intensity and area of the PSD95-EGFP clusters revealed no differences between the two genotypes .....	80
Fig. 3.21.	Expression of neuroligin1-EGFP, but not N-cadherin-EGFP, resulted in an increase in the density of presynaptic vesicle clusters in primary cultured cortical neurons (7 DIV) as compared to EGFP expression (control) .....	82
Fig. 3.22.	N-cadherin-EGFP overexpression in immature primary cortical neurons increased the mean fluorescence intensity and area of DsRed2-VAMP2 clusters .....	83
Fig. 3.23.	N-cadherin is required for the induction of presynaptic vesicle clusters by overexpression of neuroligin1 .....	85
Fig. 3.24.	Correlation analysis of mean Nlg-EGFP fluorescence intensity in clusters versus mean fluorescence intensity of diffusely distributed Nlg-EGFP signal in the dendrites of control and N-cadherin deficient neurons .....	87
Fig. 3.25.	Synaptic targeting of neuroligin1-EGFP is reduced in the absence of N-cadherin .....	89

Fig. 3.26.	Interaction of N-cadherin and neuroligin1 in the regulation of presynaptic vesicle accumulation is mediated by S-SCAM (MAGI2) .....	91
Fig. 3.27.	Synaptic targeting of neuroligin1-EGFP is dependent on S-SCAM functional domains .....	93
Fig. 3.28.	Expression of neuroligin1-EGFP promotes filopodia formation in an N-cadherin independent manner .....	95
Fig. 4.1.	Model of cooperation of the N-cadherin/ $\beta$ -catenin and the neuroligin/neurexin adhesion systems in synapse formation and maturation .....	110

### 6.3. Curriculum vitae

Name	Adriana Stan
Date of birth	24.03.1980
Place of birth	Bucharest, Romania
2004-2008	PhD at the Institute of Neuro- and Sensory Physiology, University of Düsseldorf, Germany
2003-2004	Erasmus fellowship at the Centre for Molecular Neurobiology Hamburg (ZMNH), Germany
2002-2004	Master of Science in Neurobiology, Faculty of Biology, University of Bucharest, Romania
2001-2002	Research at the department of Epidemiology and Molecular Genetics, Cantacuzino Institute, Bucharest, Romania
1998-2002	Bachelor of Science, Faculty of Biology, University of Bucharest, Romania

### 6.4. Publications and conferences attended

Stan A., Fedorchenko O., Gohla A., Dresbach T. and Gottmann K., Essential cooperation of N-cadherin and neuroligin in the transsynaptic control of vesicle accumulation at nascent synapses (article in preparation)

Stan A., and Gottmann K., The adhesion molecule N-cadherin regulates the accumulation of presynaptic vesicles, (oral presentation), *87th Annual Meeting of the DPG Köln, Germany, 2008*

Stan A., and Gottmann K., N-cadherin is required for the accumulation of presynaptic vesicles at nascent synapses, (poster presentation), *6th FENS Forum of European Neuroscience, Geneva, Switzerland, 2008*

Stan A., and Gottmann K., Presynaptic vesicle accumulation is impaired in N-cadherin deficient ES-derived neurons, (poster presentation), *SfN 37th Annual Meeting, San Diego, USA, 2007*

Stan A., and Gottmann K., Role of N-cadherin in dynamics of presynaptic vesicles accumulations in mouse ES cell-derived neurons, (poster presentation), *5th FENS Forum of European Neuroscience, Vienna, Austria, 2006*

Stan A., and Gottmann K., Live imaging of presynaptic vesicle accumulation in mouse ES cell-derived neurons deficient for N-cadherin, (poster presentation award), *Joint Meeting of The German Physiological Society and The Federation of European Physiological Societies (FEPS), Munich, Germany, 2006*

## 7. Acknowledgements

I am indebted to many people for their long lasting-support and encouragement provided during completion of this research work. In the following lines only some of them are gratefully acknowledged. However, there are many more who contributed to the success of this work and these words can not express the gratitude and respect I feel for all of those.

First of all, I like to take this opportunity to thank the people who provided scientific and financial support. I am especially grateful to Prof. Dr. Kurt Gottmann for excellent supervision, for providing a big source of ideas and for the efforts, patience and constant support during the past years. Furthermore, I would like to acknowledge Prof. Dr. Christine R. Rose for her excellent support. I want to thank Dr. Volkmar Lessmann and Dr. Thomas Dresbach for scientific and experimental support.

My sincere thanks go to many friends and colleagues for scientific discussions, advice and continuous support always so greatly appreciated, among them Dipl.-Biol. Kim Pielarski for her outstanding help and encouragement in overcoming all kinds of problems, Dr. Corinna Walz and Dr. Kay Jüngling for introducing me in the new methods. I like to express further greatest thanks to Martina Bohndorf for cell culture help and creating a great working environment and Dipl.-Biol. Oleg Fedorchenko for providing help with the confocal microscop. For excellent technical assistance I would like to thank Stefan Schätz. I would like to thank all my present and former colleagues for the nice and inspiring atmosphere in the lab: Cand. Biol. Jörg Müller ("Mr. J."), Cand. Biol. Jessica Johnen, Cand. Biol. Bernd van Steegen, Cand. Med. Roman Ewert, Cand. Med. Andreas Fiederling, Cand. Med. Sebastian Flerus, Dipl.-Biol. Anne Boehlen and Dipl.-Biol. Jeanette Niestroy. For very funny breaks and creating a relaxed working ambiance I like to thank Kim, Boris, Thomas, Regis and David.

Last but by no means least, I like to thank my family and close friends for general support in my career in science and life in general. I am particularly indebted to my parents for their never-ending encouragement, understanding and confidence. I would also like to thank Roberto for his unrestricted support and friendship. I gratefully acknowledge also few of my friends, Foxy, Ame, Aparna, Anselm, Eka, Vassu, Julia, Wolfgang and Marcel, who continuously kept on asking about my work and future plans.

Thank you!